AD-A096 363 NAVAL POSTGRADUATE SCHOOL MONTEREY CA F/G 4/2
EVAPORATION DUCT OCCURRENCES IN THE NORTHEAST ATLANTIC DURING L--ETC(U)
SEP 80 T E CALLAHAM

UNCLASSIFIED NL

1 OF 2
AD A
096163

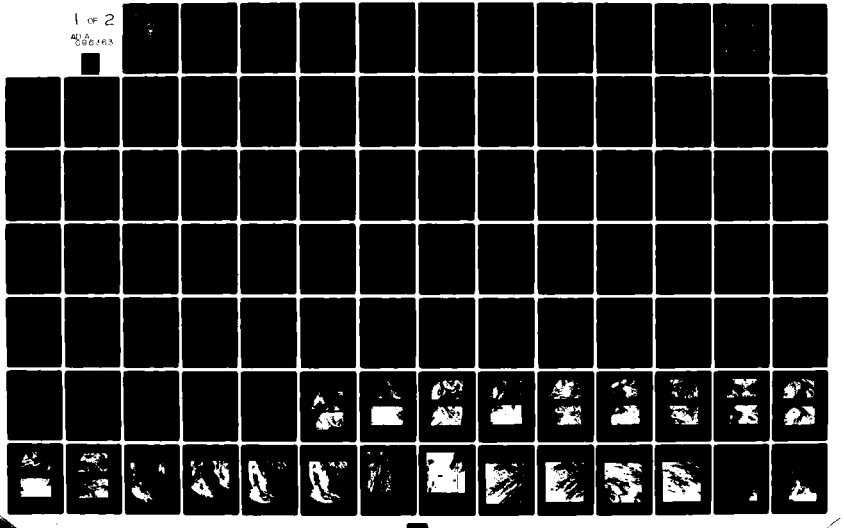

NAVAL POSTGRADUATE SCHOOL
Monterey, California

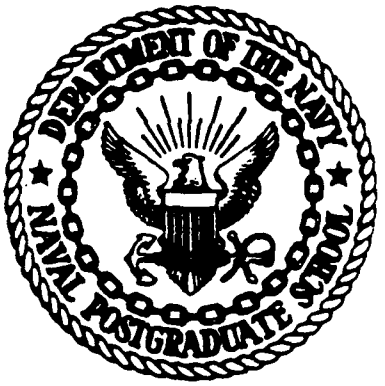

THESIS

EVAPORATION DUCT OCCURRENCES IN THE NORTHEAST ATLANTIC DURING LATE SUMMER,

by

Thomas Edwin Callaham

September 1980

Thesis Advisor: K. L. Davidson

Approved for public release; distribution unlimited

Unclassified

SECURITY CLASSIFICATION OF THIS PAGE (When Data Entered)

REPORT DOCUMENTATION PAGE		READ INSTRUCTIONS BEFORE COMPLETING FORM
1. REPORT NUMBER	2. GOVT ACCESSION NO. AD-A096363	3. RECIPIENT'S CATALOG NUMBER
4. TITLE (and Subtitle) Evaporation Duct Occurrences in the Northeast Atlantic During Late Summer		5. TYPE OF REPORT & PERIOD COVERED Master's Thesis; September 1980
		6. PERFORMING ORG. REPORT NUMBER
7. AUTHOR(s) Thomas Edwin Callaham		8. CONTRACT OR GRANT NUMBER(s)
9. PERFORMING ORGANIZATION NAME AND ADDRESS Naval Postgraduate School Monterey, California 1980		10. PROGRAM ELEMENT, PROJECT, TASK AREA & WORK UNIT NUMBERS
11. CONTROLLING OFFICE NAME AND ADDRESS Naval Postgraduate School Monterey, California 1980		12. REPORT DATE September 1980
		13. NUMBER OF PAGES 104
14. MONITORING AGENCY NAME & ADDRESS(if different from Controlling Office) Naval Postgraduate School Monterey, California 1980		15. SECURITY CLASS. (of this report) Unclassified
		15a. DECLASSIFICATION/DOWNGRADING SCHEDULE

16. DISTRIBUTION STATEMENT (of this Report)

Approved for public release; distribution umlimited

17. DISTRIBUTION STATEMENT (of the abstract entered in Block 20, if different from Report)

18. SUPPLEMENTARY NOTES

19. KEY WORDS (Continue on reverse side if necessary and identify by block number)

Evaporation Duct
Air-Sea Interaction
Joint Air-Sea Interaction Project (JASIN)

20. ABSTRACT (Continue on reverse side if necessary and identify by block number)

Analyses and interpretation of surface layer and synoptic-scale data obtained in the Northeast Atlantic were performed to obtain descriptions of the evaporation duct and associated atmospheric and oceanic synoptic features. The surface layer data were quite unique because they were obtained from high quality measurements from ships spatially separated in a fixed array. Magnitudes and horizontal homogeneity of duct heights were compared to air-mass trajectories and weather patterns. The mean duct height was 4-5m and higher values (8-13m) occurred with North and Northwest

DD FORM 1 JAN 73 1473 (Page 1)

EDITION OF 1 NOV 65 IS OBSOLETE

S/N 0102-014-6601

Unclassified

SECURITY CLASSIFICATION OF THIS PAGE (When Data Entered)

trajectories. During times when the heights were 8-13m, horizontal homogeneity occurred 35% of the time with a maximum duration of 12 hours. This was established on the basis of a two hundred kilometer separation between locations of duct height estimates.

Significant features of the duct height and its temporal and spatial variations were related to synoptic scale descriptions. Satellite imagery used in conjunction with point observations appears to provide the most useful information in describing the intensity and areal distribution of the evaporation duct.

Approved for public release; distribution unlimited.

Evaporation Duct Occurrences in the

Northeast Atlantic During Late Summer

by

Thomas Edwin Callaham
Lieutenant Commander, United States Navy
B.S., University of Utah, 1968
M.A., University of Oklahoma, 1975

Submitted in partial fulfillment of the
requirements for the degree of

MASTER OF SCIENCE IN METEOROLOGY AND OCEANOGRAPHY

from the

NAVAL POSTGRADUATE SCHOOL

September 1980

Author _____

Approved by: _____
Thesis Advisor

_____
Second Reader

_____
Chairman, Department of Meteorology

_____
Dean of Science and Engineering

ABSTRACT

Analyses and interpretation of surface layer and synoptic-scale data obtained in the Northeast Atlantic were performed to obtain descriptions of the evaporation duct and associated atmospheric and oceanic synoptic features. The surface layer data were quite unique because they were obtained from high quality measurements from ships spatially separated in a fixed array. Magnitudes and horizontal homogeneity of duct heights were compared to air-mass trajectories and weather patterns. The mean duct height was 4-5m and higher values (8-13m) occurred with North and Northwest trajectories. During times when the heights were 8-13m, horizontal homogeneity occurred 35% of the time with a maximum duration of 12 hours. This was established on the basis of a two hundred kilometer separation between locations of duct height estimates.

Significant features of the duct height and its temporal and spatial variations were related to synoptic scale descriptions. Satellite imagery used in conjunction with point observations appears to provide the most useful information in describing the intensity and areal distribution of the evaporation duct.

TABLE OF CONTENTS

ACKNOWLEDGEMENTS

I wish to express my deep appreciation to Dr. Kenneth L. Davidson for his encouragement, guidance and assistance throughout the course of this research.

My appreciation is also extended to Dr. Gordon Schacher for providing constructive criticism on my scientific method and Dr. Chris Fairall for graciously providing guidance in numerical methods used in this study. Additionally, for the many hours spent in editing and compiling the final manuscript, I express my deepest gratitude to my mother, Drusilla Keller.

Finally, I wish to thank my family, Mary, Lauren and Tim, for their interest in my research and their willingness to allow me the time to pursue it.

I. INTRODUCTION

Over the surface of the ocean there exists a phenomenon described as the evaporation duct. The military significance of its existence has been known for many years. Attempts have been made to quantify the evaporation duct height and determine its effect on electromagnetic propagation. Assessment of evaporation duct characteristics in tactical military applications should only require routine shipboard measurements and simple calculations; hence, a great deal of study has been performed to parameterize the duct on the basis of simple observational measurements of surface and near-surface parameters. Also, as the use of low-flying supersonic aircraft and missiles become increasing threats to Naval surface combatants, timely and precise descriptions of the nature of the evaporation duct will be required to permit its exploitation.

It has been expected that in an area in the high latitudes, well away from large land-mass influences, and where frequent migratory weather systems disturb the nature of the atmosphere near the surface, the height of the evaporation duct is likely to be small and its occurrence highly localized. Past research has been primarily limited to regions where ducts are known to be both strong (high) and persistent (e.g. tropics, southeast portion of subtropical high, coastal regions of warm offshore winds) with relatively little examination of higher latitude, open oceanic regions. This study will examine the occurrence and nature of the evaporation duct over the North Atlantic

Ocean subject to highly varying atmospheric conditions. This examination will focus on determining significant ducts and their 1) frequency of occurrence and duration; 2) temporal and spatial nature, and 3) sensitivity to atmospheric conditions.

The results reported here were made utilizing a unique set of data acquired from the Joint Air-Sea Interaction Project (JASIN) conducted in the Northeast Atlantic during the late summer of 1978. The results were analyzed and comparisons were made between several ships, synoptic analyses and high resolution satellite imagery. The resultant examination yielded a description of an evaporation duct characteristic of the region as it was affected by frequently changing weather patterns.

This study was on data collected from four research vessels engaged in the JASIN experiment from mid-July to early September, 1978 under open ocean conditions. The quantity of data and the large area of study permitted an examination to determine the nature of the duct and the atmospheric disturbances most likely to influence it. An important aspect of the experiment was the positioning of four ships in a triangle (180 x 180 x 200 km) during periods of intensive meteorological measurements. This constant spatial separation permitted accurate assessments of spatial as well as temporal variations over a large horizontal region as weather systems moved through the area. The data were used with expressions presented by Fairall et al [1978] to compute the associated oceanic evaporation duct height.

II. BACKGROUND

It has been long recognized that distributions of temperature and humidity in the lower atmosphere are responsible for anomalous electromagnetic (EM) wave propagation [Katzin, 1947 and Kerr, 1951] resulting in either enhancement or degradation of Naval sensors and weapons systems. In particular, propagation between terminals reasonably close to the sea surface has been observed to exhibit significant variation of signal strength at ranges far in excess of the radar horizon. (Fig. 1) Such anomalous propagation effects were first seriously studied during and immediately following World War II. In recent years, advances in mixed-layer theory have led to numerous computational approaches for real-time assessment of atmospheric refractive effects.

Often relatively cool moist marine air extends vertically from the ocean surface to altitudes of a few hundred meters. Above these heights the air becomes much warmer and drier for a variety of reasons. Therefore, a transition layer exists in which the air temperature increases and moisture rapidly decreases with increasing height. The resulting gradients can cause the EM refractive index to decrease rapidly enough to refract low incident angle radio waves downward relative to the earth and create ducting conditions. If the decrease in refractive index is great enough a surface-based duct occurs which will trap surface-originated radar signals and give greatly extended ranges for detection of near surface targets.

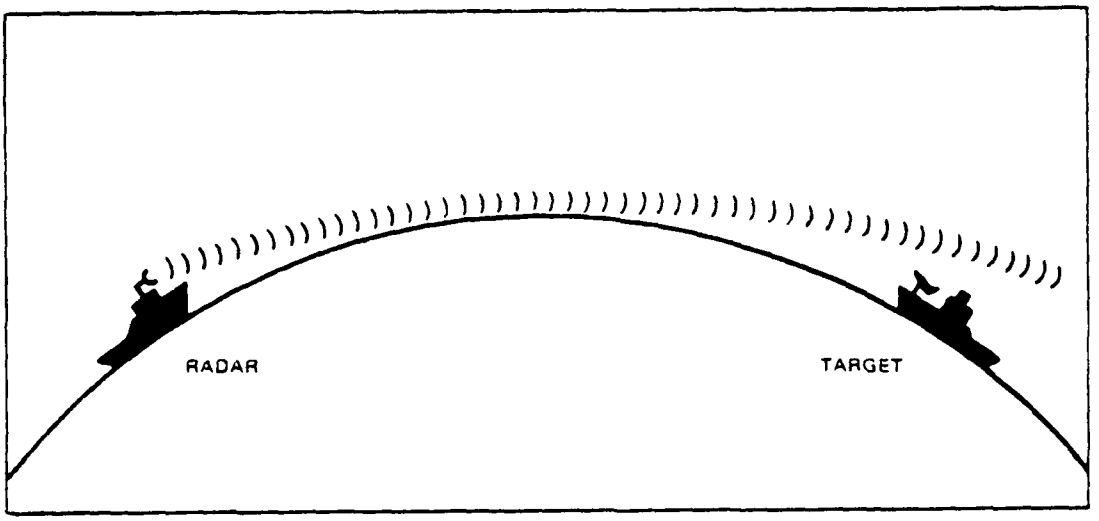

Figure 1a. Radar wave path under "standard" atmospheric conditions. Note path curves downward but at a rate less than the earth's curvature. Beyond-the-horizon target detection is not possible.

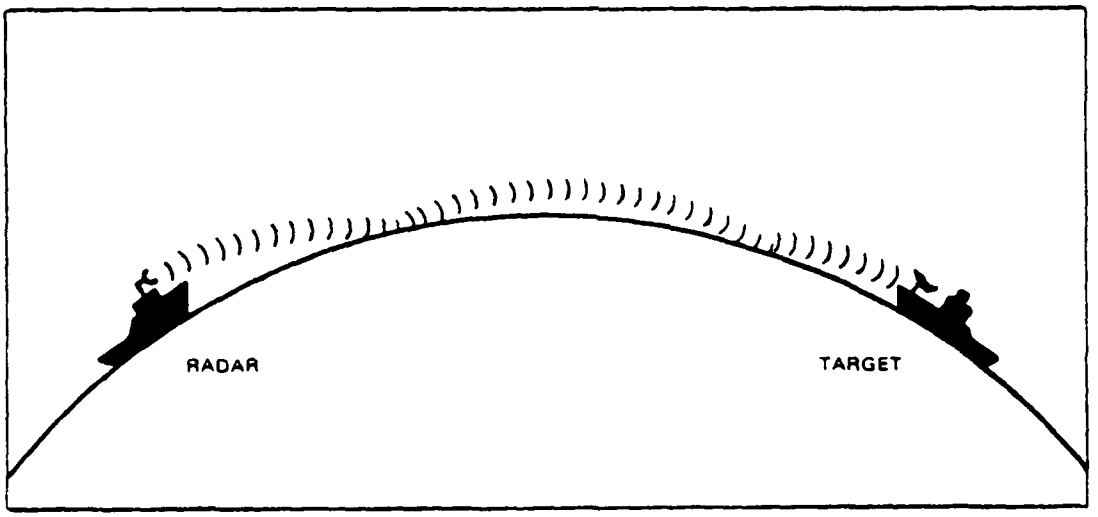

Figure 1b. Radar wave path under ducting conditions. Path curves downward at a rate exceeding the earth's curvature resulting in beyond-the-horizon target detection.

The air adjacent to the ocean is saturated and the relative humidity is near 100%, decreasing rapidly in the first few meters to ambient values which depend on varying meteorological conditions. The decrease of humidity causes the modified refractive index (M) to decrease with height initially. At greater heights, the humidity gradient decreases which will cause M to reach a minimum and thereafter increase with height (Fig. 2). The height at which M reaches a minimum value is called the evaporation duct height (Z*) and is a measure of the strength of the evaporation duct.

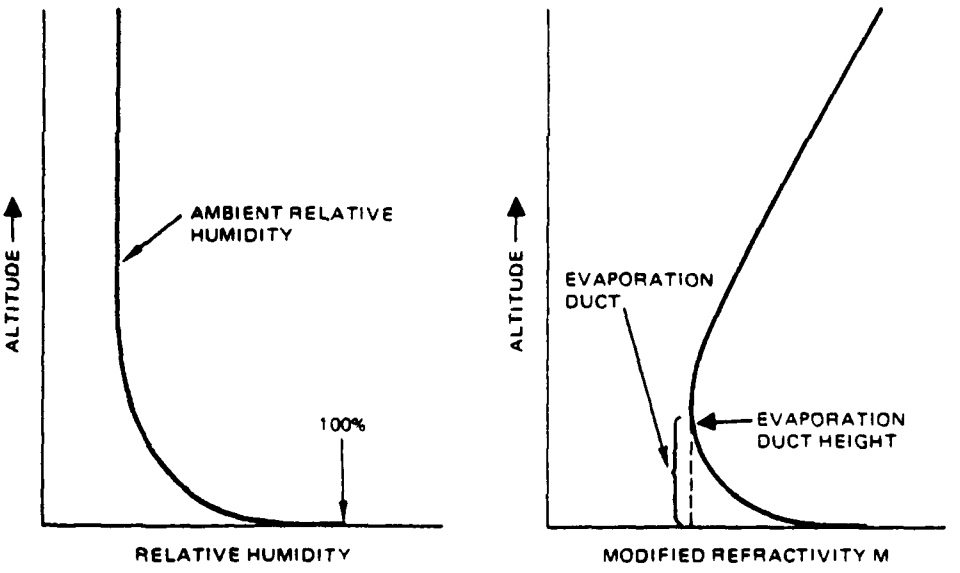

Figure 2. Relative humidity and modified refractivity M versus altitude for an evaporation duct.

The probability of occurrence of duct heights large enough to cause beyond-the-horizon detection capability for a particular radar varies according to geographic location, season and the time of day. The strongest ducts are generally found at tropical latitudes, during the summer season, and during daylight hours.

III. EVAPORATION DUCT MODEL

Flux-profile relationships in the atmospheric surface layer ($Z<50m$) above the ocean surface have been studied extensively and are well understood. Bulk methods can be used to determine surface flux scaling parameters from routine shipboard measurements. These scaling parameters can be applied to refractive equations to determine Z^*. The method requires only mean meteorological conditions as input parameters and is well suited to assessments using routine shipboard observations.

A. EM PROPAGATION CONSIDERATIONS

The refractivity N (in N units) of the atmosphere for EM waves is given by Battan [1959]

$$N = 77.6\ P/T + 3.73 \times 10^5\ e/T^2 \qquad (1)$$

where P is the atmospheric pressure, T is the absolute temperature and e is the partial pressure of water vapor. An expression for the vertical gradient in N is given by

$$dN/dZ = C1\ \delta P/\delta Z + C2\ \delta q/\delta Z + C3\ \delta T/\delta Z \qquad (2)$$

where q is the water vapor mixing ratio ($q=.625e/P$ in gm/kg, P in mb, T in °K, and $C1=.3$, $C2=7.2$ and $C3=-1.3$). A negative gradient in refractivity at height Z causes a horizontally propagating EM wave to be bent toward the surface and if the gradient is large enough, the amount of bending exceeds the curvature of the earth and the wave becomes ducted. Since magnitudes of specific humidity gradients decrease with increasing height in the near-surface layer, the gradient is no longer strong

enough for ducting at some height Z*. This height is termed the evaporative duct height and is defined by the critical gradient necessary for EM trapping.

$$dN/dZ = -.157 \ (m^{-1})$$

using Equation (2) and noting $dP/dZ = -\rho q$ (the hydrostatic balance for the atmosphere), Z* is then defined by the following equation.

$$-.157 = -.032 + C2 \ \delta q/\delta Z + C3 \ \delta T/\delta Z \qquad (3)$$

Since $\delta q/\delta Z$ and $\delta T/\delta Z$ are height dependent (approximately $1/Z$) there exists a value of $Z=Z^*$ such that Equation (3) is satisfied. The bulk method allows one to relate $\delta q/\delta Z$ and $\delta T/\delta Z$, which are needed to determine Z*, to the surface layer fluxes and, hence, to mean parameters.

B. BULK METHOD

The theoretical framework for determining the evaporation duct height comes from knowledge of surface layer scaling parameters using the Monin-Obukhov similarity (MOS) theory. The theory relates the surface layer profiles of temperature, wind speed, water vapor and turbulence to the surface fluxes of momentum, sensible and latent heat. Vertical gradients of wind speed (U), potential temperature (T) or water vapor mixing ratio (q) are given by the following general expression

$$\delta X/\delta Z = (X^*/\alpha\kappa Z) \ \phi_X(Z/L) \qquad (4)$$

Where X = U, T or q, κ = Von Karman's constant (0.35), α is a diffusivity constant, X* is the scaling parameter and $\phi(Z/L)$ is the MOS stability correction. The surface fluxes define the scaling parameters within the flux-profile relationships. Scaling parameters for

velocity, potential temperature and specific humidity are related to the normalized fluxes by:

$$U^* = (-\overline{u'w'})^{\frac{1}{2}} \quad (m/s)$$

$$T^* = (-\overline{T'w'})/U^* \quad (^\circ K)$$

$$q^* = (-\overline{q'w'})/U^* \quad (g/Kg)$$

where $\overline{u'w'}$, $\overline{T'w'}$ and $\overline{q'w'}$ are the mean turbulent fluxes of momentum, heat and moisture respectively. A scaling length, the Monin-Obukhov length (L), is used to account for stability influences. Stability magnitudes are based on the height scaled by L, i.e. Z/L. Negative and positive Z/L values corresponded to unstable and stable conditions. L is defined by the scaling parameters as

$$L = TU^{*2}/(\kappa g(T^* + .61q^*T)) \qquad (5)$$

The bulk method is based on integral forms of Equation (4). Integrating Equation (4) from $Z = Z_{oX}$ to some reference height, Z, an expression for the value of a parameter at the measurement height is obtained [Businger, 1973].

$$X(Z) = X(Z_{oX}) + X^*/\alpha\kappa(\ln Z/Z_{oX} - \psi(Z/L)) \qquad (6)$$

where $\psi(Z/L)$ is the profile stability function and subscript

X = U, T, or q. (Note: α and ψ depend on X)

Utilizing Equation (6), a method of estimating surfaces fluxes involves the scaling parameters and roughness lengths, Z_{oX}. Appropriate values of temperature, relative humidity and wind speed are obtained at both the sea surface and at some reference height, Z. Equation (6) can be used to determine scaling as a function of the differences.

$$U^* = (\kappa U) \; / \; (\ln (Z/Z_o) - \psi_1 \; (Z/L))$$

$$T^* = (T-Ts)\, \alpha\kappa / \; (\ln(Z/Z_{oT}) \; -\psi_2 \; (Z/L))$$

$$q^* = (q-qs)\, \alpha\kappa / \; (\ln(Z/Z_{oT}) \; -\psi_2 \; (Z/L))$$

α was set equal to 1.35 for T and q from Businger et al [1971]. The quantities Z_o and Z_{oT} are roughness lengths for velocity and temperature profiles. It is convenient to rewrite these equations in the generalized drag coefficient form

$$X^* = C_X^{\frac{1}{2}} \; (X(Z) - X(0)) \tag{7}$$

The neutral stability drag coefficient can be defined as

$$C_{XN}^{\frac{1}{2}} = \alpha\kappa / \ln(Z/Z_{oX}) \tag{8}$$

then the drag coefficient becomes

$$C_X = C_{XN} \; / \; (1 - ((C_{XN}^{\frac{1}{2}}) \; /\alpha\kappa) \; \; (\psi \; (Z/L)))^2 \tag{9}$$

In this form, Z_{oX} is related to the neutral drag coefficient by

$$C_{XN}^{\frac{1}{2}} = \alpha\kappa / \; \ln(Z/Z_{oX}) \tag{10}$$

where roughness length

$$Z_{oX} = Z \exp \; (\alpha\kappa \; / C_{XN}^{\;2}) \tag{11}$$

Equation (5) can be rewritten to give the MOS stability parameter, Z/L, as

$$Z/L = (Z/L)_o \; \frac{(1 - (C_{UN}^{\frac{1}{2}}) \; /\kappa \; (\psi_1(Z/L)))^2}{(1 - (C_{TN}^{\frac{1}{2}}) \; /\alpha\kappa \; (\psi_2 \; (Z/L)))} \tag{12}$$

where

$$(Z/L)_o = \frac{\kappa g Z}{T} \; \frac{C_{TN}^{\frac{1}{2}} \; \; ((T(Z)-T(0)) + .18(q(Z)-q(0)))}{C_{UN} \; \; \; \; \; \; \; \; U(Z)^2} \tag{13}$$

Note that $(Z/L)_o$ is an initial estimate of stability in terms of differences and neutral drag coefficient. Final values of Z/L and scaling parameters can be found from a simple iteration process. Stability correction functions used were:

Velocity profile:

$$\psi_1(Z/L) = 2 \ln ((1 + X)/2) + \ln ((1 + X^2)/2)$$
$$-2 \text{ ARCTAN } (X) + \pi/2 \qquad Z/L<0$$
$$X = (1 - 15\ Z/L)^{\frac{1}{4}}$$
$$\psi_1(Z/L) = -4.7(Z/L) \qquad Z/L>0$$

Temperature profile:

$$\psi_2(Z/L) = 2 \ln ((1 + X)/2) \qquad Z/L<0$$
$$X = (1 - 9\ Z/L)^{\frac{1}{2}}$$
$$\psi_2(Z/L) = -6.5(Z/L) \qquad Z/L>0$$

The velocity drag coefficient, C_{UN}, in a near-neutral atmosphere was calculated from the wind-speed dependent formulation given by Kondo [1975]. A typical value of C_{UN} at Z=10 m was 1.3×10^{-3} m/s which yielded $Z_o = 6 \times 10^{-4}$ m. Wind speeds and drag coefficients are given in Table I.

TABLE I

C_{UN} VERSUS WIND SPEED AT 10m [KONDO, 1975]

U(m/s)	$C_{DN} \times 10^3$
.3-2.2	$1.08 \times U^{-.15}$
2.2-5.0	.77 + .086 x U
5.0-8.0	.87 + .067 x U
8.0-25.0	1.2 + .025 x U

The temperature and moisture drag coefficients, C_{TN} and C_{qN}, at Z=10m were estimated as 1.3×10^{-3} [Davidson et al, 1978]. For α_T=1.35 [Businger, et al, 1971], a roughness length of $Z_{oT}=2.0 \times 10^{-5}$ m, was obtained, which is assumed to be independent of wind speed.

C. Z* EQUATION IN MDS FORM

In the surface layer, the gradient of N can be written in terms of T* and q* as

$$dN/dZ = -.032 = \phi(Z/L)/(\alpha\kappa Z)\ (7.2q^* - 1.3T^*) \qquad (14)$$

which arises from Equation (3). The duct height, Z*, is obtained from Equation (14) by setting dN/dZ = -.157, the critical gradient for ducting.

$$Z^* = \frac{-(7.2q^* - 1.3T^*)}{\alpha\kappa(.125)}\ \phi(Z^*/L) \qquad (15)$$

Given q*, T* and L, Equation (15) was solved iteratively to obtain Z*. No ducting occurs unless

$$7.2q^* - 1.3T^* < 0$$

IV. DATA ACQUISITION

The data used in this analysis were unique in that they represented accurate measurements of the atmospheric surface boundary layer on a horizontal scale of 1-200 km. All data were gathered from scientific research vessels whose primary cruise objectives were to observe, distinguish and quantify fluxes and mixing in atmospheric and oceanic boundary layers. The following are descriptions of the measurement platforms, their locations, the data accuracy and the intercomparison of data between ships.

A. PLATFORMS AND LOCATION

Data for this analysis were taken during the JASIN experiment in the summer of 1978. Data from four ships involved in this experiment were selected on the basis of two objectives:

1. Examine as much of the period as possible.
2. Examine variation over nearly fixed spatial separation.

The four ships selected were the METEOR, the JOHN MURRAY, the GARDLINE ENDURER and the HECLA. Figure 3 illustrates the profile and sensor locations for each ship. Hourly observations were made of air temperature (T), wet bulb temperature (Tw), sea (bucket) surface temperature (Ts) and wind speed (U). The triangle configuration of the ship locations, depicted in Figure 4, provided quite good areal coverage. The ships were positioned approximately 200 km apart at each corner of the

R.R.S. JOHN MURRAY

A = 11m
B = 6m

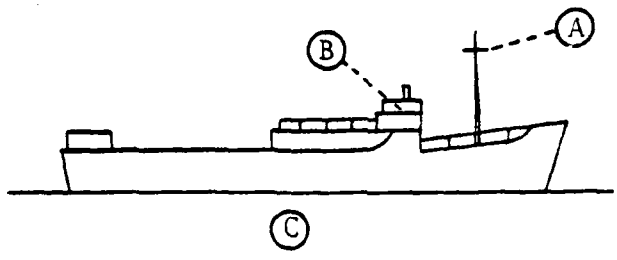

R.V. METEOR

A = 23m
B = 11m

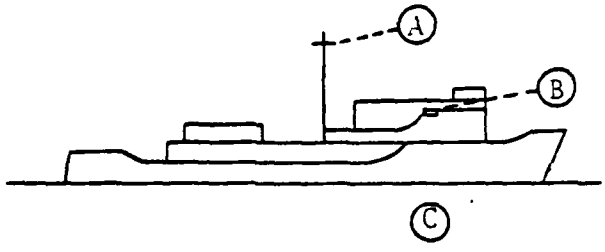

M.V. GARDLINE ENDURER

A = 15m
B = 4m

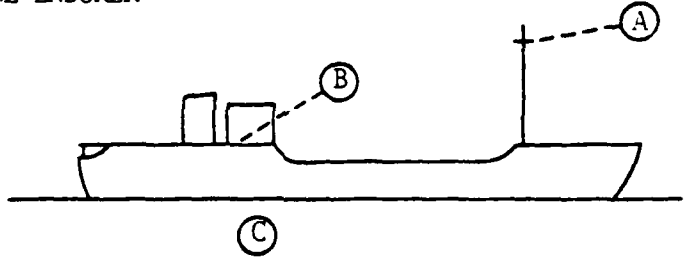

H.M.S. HECLA

A = 20m
B = 11m

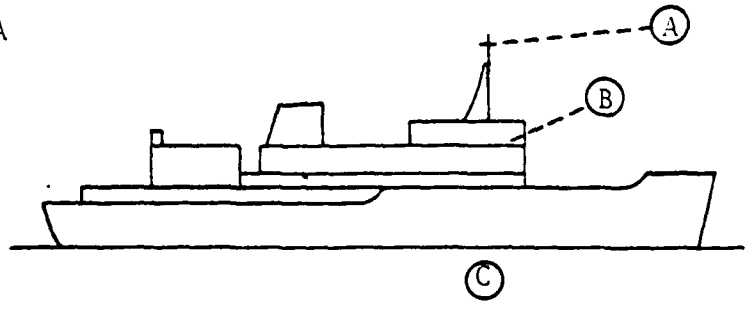

Figure 3. Ship profiles and sensor locations: (A)- U, (B) - T,Tw and (C) - Ts.

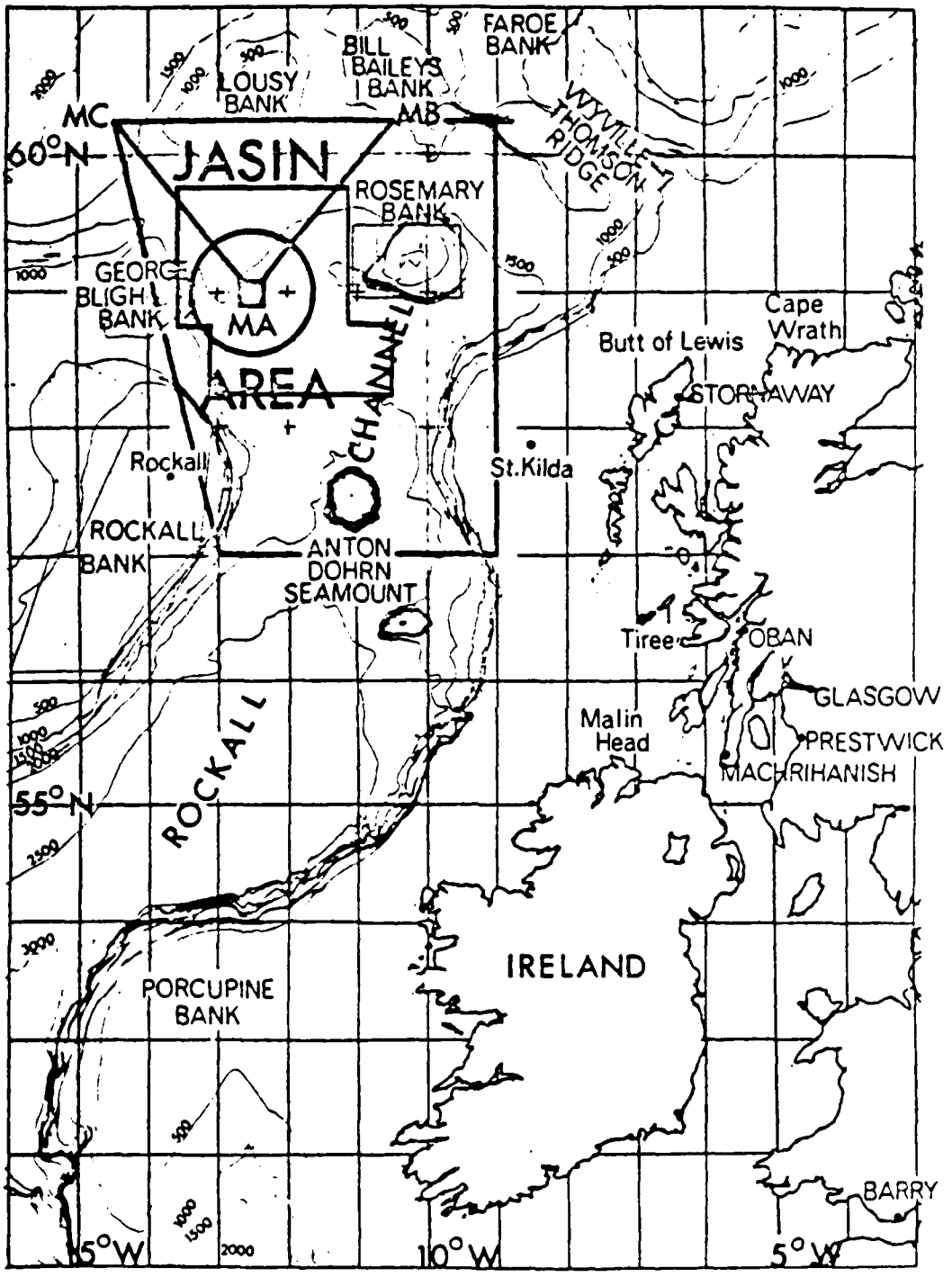

Figure 4. The JASIN area in relation to the British Isles.

triangle and one ship was located at the center. Nominal positions were:

MA	59.00 N	12.5 W
MB	60.25 N	10.5 W
MC	60.25 N	14.5 W
CENTER	59.77 N	12.5 W

B. DATA COLLECTION

The subject observations were recorded on log sheets and plots of three-hourly values were prepared by JASIN participants. The plots from the GARDLINE ENDURER, JOHN MURRAY and HECLA, were the primary source of data used in this study. Air temperature, wet bulb temperature, sea surface temperature were accurate to 0.2 °C, pressure to 1 mb and wind speed to 1 kt. Additionally, data used from the METEOR were available in computer printout.

C. DATA QUALITY AND INTERCOMPARISON

During the period 15-22 July, on 19 and 20 August, and on 5 September, the four ships were positioned for an intercomparison of meteorological measurements. Hourly (half-hourly during formal intercomparisons) values of wind speed, atmospheric pressure, dry and wet bulb air temperatures and sea surface temperature were compared between vessels approximately one kilometer apart. These data were initially evaluated for coding errors and inconsistencies resulting from position changes. Mean and standard deviations of each variable were calculated for each participating vessel. Time-series of inter-platform sensor disagreements were produced from mathematical differences between

observed variables. Interplatform means and standard deviations of these differences were calculated and, assuming the disagreements to be normally distributed, the 90% confidence interval of the estimates of differences were calculated.

Results derived from this procedure were time records of interplatform sensor differences. Constant disagreement throughout JASIN implied the sensor performed in a consistent manner and it remained only to explain these errors in terms of known disparities, such as non-uniform sensor heights or instrument bias. A variation of the interplatform corrections required further analyses either in terms of atmospheric stability or in terms of trends of sensor drifts. The latter were established by regression techniques. Inconsistencies unexplained or uncorrected by these considerations remained as errors in the four-ship system.

The METEOR data were selected as the standard to which data from the other vessels were adjusted. However, the METEOR's sea surface temperature values were corrected with data from the other three ships. The METEOR was chosen because it was involved in more intercomparisons, because it had a preferred method for station-keeping, and because of its proximity to other JASIN ships and buoys. The corrections according to measured parameters and individual ships are summarized below [Macklin and Guymer, 1980].

1. Wind speed (m/s)

METEOR = METEOR
HECLA = 0.89 (HECLA) + 0.3
MURRAY = MURRAY
ENDURER = ENDURER

2. Pressure (mb)

```
METEOR = METEOR
HECLA = HECLA + .08  To 0600, July 28
      = HECLA + .40  From 0900, July 28
MURRAY = 1.00640 (MURRAY) - 6.23
ENDURER = ENDURER + .38 To 1700, August 19
        = ENDURER + .38 After 1700, August 19   (P less than 1000)
        = ENDURER + .48 After 1700, August 19   (P greater than 1000)
```

3. Dry Bulb Temperature (°C)

```
METEOR = METEOR
HECLA = HECLA - 0.3
MURRAY = MURRAY - 0.5
ENDURER = ENDURER - 0.5
```

4. Wet Bulb Temperature (°C)

```
METEOR = METEOR
HECLA = HECLA - 0.3
MURRAY = MURRAY - 0.3
ENDURER = ENDURER - 0.1
```

5. Sea Bucket Temperature (°C)

```
METEOR = METEOR + 0.3 To 1300, July 27
       = METEOR       1300, July 27 to 0100, August 3
       = METEOR - 0.4 0100, August 3 to 1200, August 9
       = METEOR       From 1200, August 9
HECLA = HECLA
MURRAY = MURRAY
ENDURER = ENDURER
```

V. ANALYSIS PROCEDURES

Data analysis procedures were designed to determine 1) the representative Z* values for the summer regime, 2) meteorological factors which most affected Z*, 3) the frequency of occurrence and duration of ducts, and 4) the extent of horizontal homogeneity of the duct. To achieve this, the data were first corrected, then used as input to bulk formulae to compute Z*.

A data file was constructed of the most representative Z* values and corrected Ts-T, U and RH at three-hour intervals. Winds were reduced from anemometer height to temperature sensor heights using the stability-corrected logarithmic wind profile [Businger et al, 1971]. The periods examined and sensor heights are summarized in Table II. (Dates are in year-month-day-hour format)

TABLE II

SHIP DATA PERIODS AND MEASUREMENT HEIGHTS

SHIP	STARTING	ENDING	ANEMOMETER HGT (m)	Z(m)
MURRAY	78071312	78072103	11	6
METEOR	78072106	78080912	23	11
MURRAY	78080915	78081012	11	6
METEOR	78081709	78090506	23	11
ENDURER	78090509	78090606	15	4

Statistical and time-series analyses of Z* were performed along with subjective analyses of influencing meteorological conditions. The latter were performed with individual observations, synoptic weather maps, and satellite imagery (visual and infrared). These descriptions were correlated to the time-series of Z* values. Joint probability

density distribution and conditional mean function results were chosen to examine correlations of at least two weather parameters to Z* values. Finally, comparisons were made of Z* and all atmospheric measurements to assess the horizontal homogeneity of the duct for periods when ships were spatially separated and at fixed locations.

VI. PRESENTATION AND INTERPRETATION OF RESULTS

A. GENERAL ANALYSIS OF SUMMER PERIOD (13 July - 6 September)

Figure 5 is a time-series comparison of evaporation duct height (Z*), air-sea temperature difference (Ts-T), wind speed (U), and relative humidity (RH) for the period of study, 13 July to 6 September, with the exception of the interval between 1200 GMT, 10 August and 0900 GMT, 17 August. This time series was formulated from at least one ship located in the JASIN array and provided a near-continuous analysis of the evaporation duct height (Z*) at three-hour intervals. General conditions during the period will be described in the following sections.

1. Synoptic Conditions in JASIN Area

Daily weather maps for the Northeast Atlantic are shown in Appendix A. Julian day and date (day of the month) are shown on each map (see also Table A-I). Studies of the daily surface pressure charts and hourly observations [Guymer and Taylor, 1978] showed that there were essentially four synoptic situations affecting the JASIN area during the entire period.

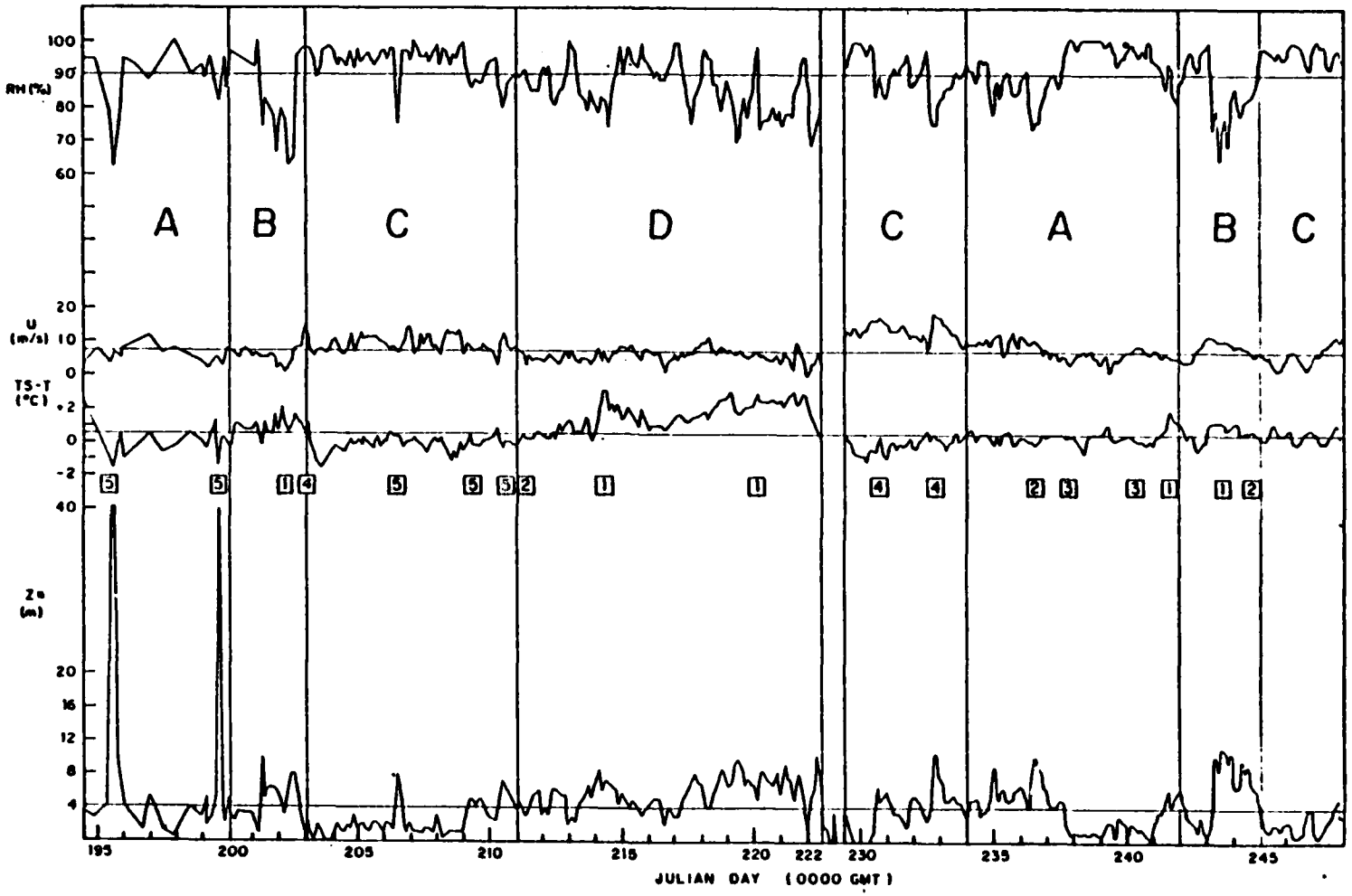

Figure 5. Time-Series (13 Jul-6 Sep) analysis of Z*, Ts-T, U and RH with synoptic weather types, special atmospheric events and mean values indicated.

a. Moist Anticyclonic (A)

The periods of 14-18 July and 22-30 August were affected by moist westerlies or northwesterlies on the northern flank of an anticyclone to the west of Ireland. Weak frontal waves were embedded in this flow and occasional incursions of drier air took place. Winds varied between 3 and 12 m/s.

b. Mobile Westerly Conditions (B)

The periods of 19-21 July and 30 August - 2 September were characterized by depressions moving through the area bringing cold and dry air. The disturbances were very weak.

c. Cyclonic Southwesterly (C)

During the periods 22-29 July; 11-21 August and 2-5 September the depressions became slow moving to the south of Iceland and fronts or troughs from the southwest affected the region. Generally, the fronts were occluded and slow moving by the time they reached the area, with only moderate winds. However, winds which were the strongest experienced during the entire JASIN period reached speeds in excess of 15 m/s on 22/26 July, 18/20 August and 5 September. The air was significantly warmer than the sea.

d. Blocked (D)

During the period 30 July - 10 August a blocking low formed over northwest France and moved very slowly northeast; to the west a ridge persisted. Low level northeasterlies were colder than the sea surface but convection was inhibited by warm air aloft associated with weak, slow moving occlusions which also produced occasional drizzle.

Towards the end of the period, the ridge intensified and moved eastward.

e. Special Events

Some interesting atmospheric occurrences were noted as events (refer to events marked on Figure 5) and are listed below.

1. Relatively cold, dry air (14, 20 July; overnight 1-2 August; 7-9, 29, 31 August).

2. Significant moisture flux in near-neutral conditions (30 July; 23-25 August; 1 September).

3. A warm frontal wave on 25 August and a cold front preceded by convective instability on 28 August. Surface fluxes were very small.

4. Winds in excess of 15 m/s (22 July; 18, 19 August).

5. Incursions of warm, dry air (14, 18, 25, 28, 29 July).

The following are descriptions of events which caused warm, dry air (not a normal occurrence over the open ocean) to occur.

(1) Afternoon Heating. On 14 July, both the MURRAY and HECLA reported increasing air temperature but MURRAY reported three consecutive wet bulb temperature readings markedly lower than HECLA. On 18 July, MURRAY and METEOR had similar air temperature readings while HECLA was 1.4°C lower. All three measured similar values for wet bulb temperature. On both occasions, winds were light under prevailing high pressure.

(2) Subsidence and Continental Trajectory. On 25 July, a weak ridge moved over the area as a low west of Ireland moved northeast. Winds backed from the northwest to the east-southeast. Warm,dry air, a result of subsidence from earlier ridging, flowed from the British Isles and influenced the area for six hours before the approaching

occlusion became dominant.

(3) Short Wave Troughs. Throughout 28 and 29 July, a long wave trough was oriented north-south from Iceland. Weak short wave impulses on both days provided surges of dry air, each lasting nine hours, while generally maintaining warm southerly flow.

2. Sea Surface Temperature (TS)

Surface water characteristics were associated with the North Atlantic Drift, an extension of the warm waters of the Gulf Stream. The mean water temperature in the vicinity of the JASIN triangle was 12.2°C. The general areal distribution of the surface temperature for the sampled periods is depicted in Figure 6 [Liu & Katsaros, 1978]. The Northeast corner of the triangle was always the coldest position (11.2°C). The Northwest and South corners of the triangle were always the warmest (between 12 and 13°C). A large tongue of cool water (11.8°C) from the north, intruded south and south-southeast through the center of the triangle. It persisted for the entire period resulting in minimal temperature variations at the center position (about 0.2°C). The most pronounced Ts gradients occurred along a line between the NW and NE stations.

3. Representative Z* Values

A statistical analysis of observed parameters and calculated values from 714 independent observations was performed to determine a representative Z* value (Table III). The mean evaporation duct height

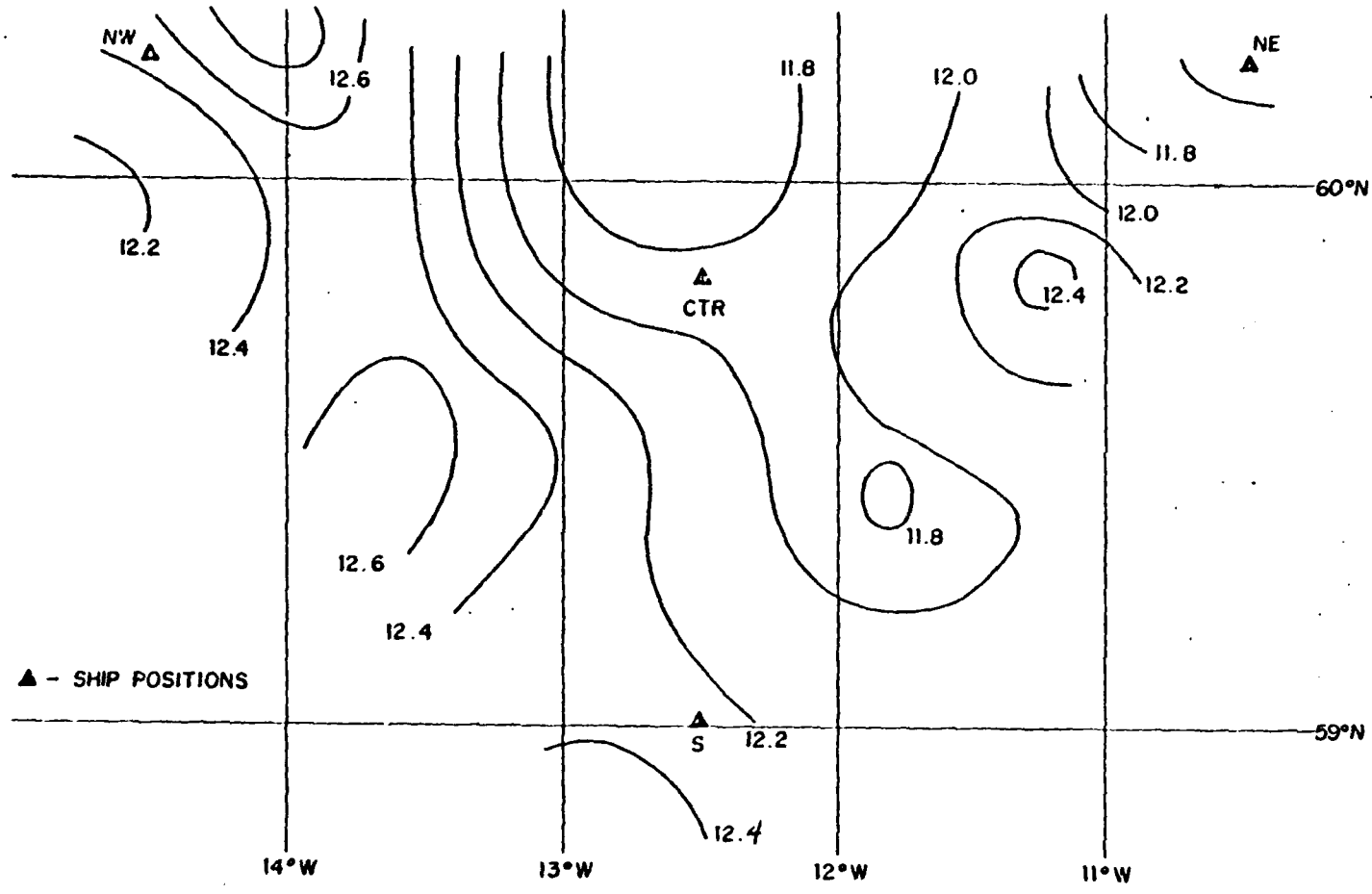

Figure 6. Composite Sea Surface Temperature Analysis

was 4.2 meters with a standard deviation of 3.9 meters. This height appears low when compared with the climatology of the region. Sweet [1979] determined an evaporation duct climatology at Ocean Station ALFA (62N/33W), 1100 km upstream of the JASIN array, and Ocean Station INDIA (58N/19W), 400 km southwest of the JASIN array. The following statistics are a comparison of the JASIN evaporation duct, using the method previously described and climatology which used bulk aerodynamic formulae and a method originated by Jeske [1971] and modified by Hitney [1975].

	ALFA	JASIN	INDIA
MEAN (m)	5.8	4.2	7
MEDIAN (m)	5.7	3.8	7
IQR (m)	3.4-8.3	1.9-5.7	4.1-9.8
# OBS	7058	714	6758

The interquartile range (IQR) represents the lower and upper bounds for the middle duct heights (25% of the ducts have heights below the lower number and 75% have heights below the upper number) and can be viewed as an indicator of the spread or variation of the duct height.

TABLE III

STATISTICS FOR JASIN PERIOD 13 JULY - 6 SEP 1978

(714 OBSERVATIONS)

	TS (°C)	T (°C)	TS-T (°C)	U (m/s)	RH (%)	Z/L	T* (°C)	U* (m/s)	q* (g/kg)	Z* (m)
MEAN	12.2	11.8	.5	6.6	90	-.1	-.02	.27	-.05	4.2
SIGMA	.6	.8	.9	2.9	8	1.0	.9	.13	.03	2.9

4. Atmospheric Factors Affecting Z*

Since Z* is a computational artifact determined by four meteorological parameters, Z* (Ts-T, Rh, U, Z/L), multivariable analyses were used to determine the degree to which individual variables affected duct strength. Joint probability density distributions were computed for each of the parametric interrelationships to examine the pattern of atmospheric factors as they are related to the occurrence of Z* values.

Based on probability theory [Batchelor, 1953] and utilizing a technique described by Holland [1968], the distribution of Z* was analyzed statistically against the distribution occurrence of a combination of meteorological variable such as Ts-T versus U, (Figures 7-12). Individual moments and distributions for each variable were also computed in the analysis. The following data were tabulated:

1. Mean
2. Variance
3. Standard Deviation (Sigma)
4. Skewness
5. Kurtosis
6. Dimensional Class Limits by Sigma/4 Intervals From -4.0 Sigma to +4.0 Sigma
7. Density of Observations for Each Occurrence by Sigma/4 Class Interval

Individual class and joint class intervals were computed for each observation set. Two indices were computed for each data pair representing its position in an array (18 x 18) of joint class intervals (Sigma/2 x Sigma/2) centered on the mean values of the two variables. Class intervals were determined by dividing the standard value of one of the joint variables by 0.5. Pairs of independent variables were then used to compute joint probability density functions

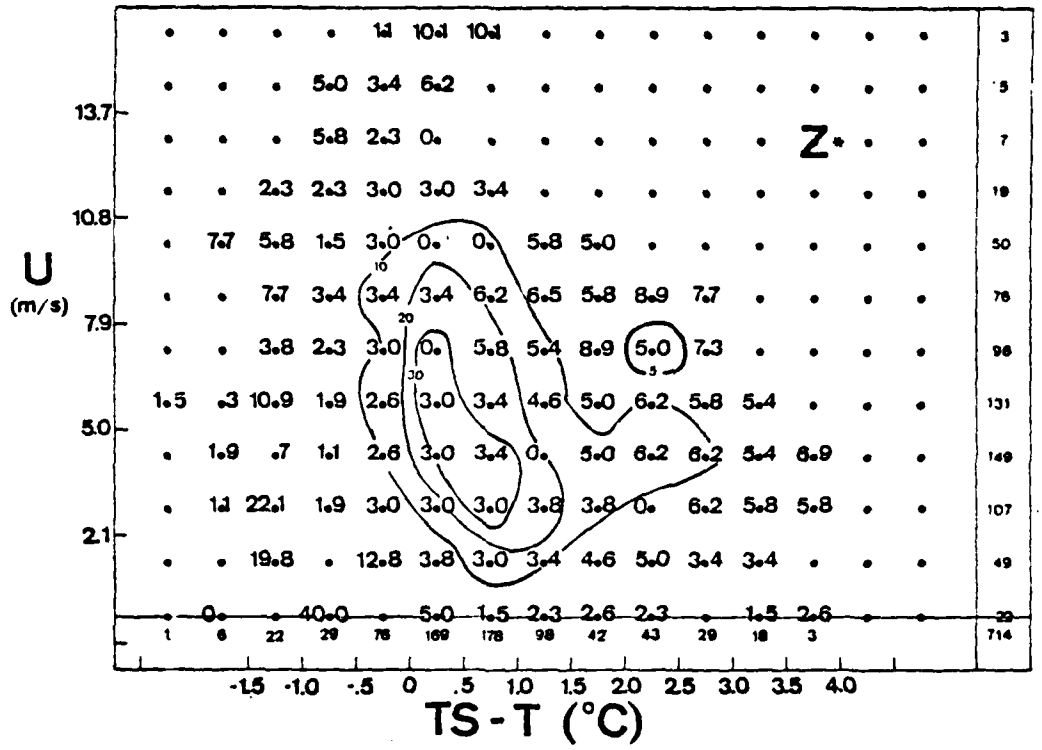

Figure 7. Conditional mean (plotted numbers) of Z* for joint-frequency distribution (delineated with solid labelled isolines) of wind speed, (U) and air-sea temperature difference, (Ts-T). Integers along the right and bottom edges are sums of occurrences in respective rows or columns. The total sum is 714 but may be less if the compared variables are truncated when out of range.

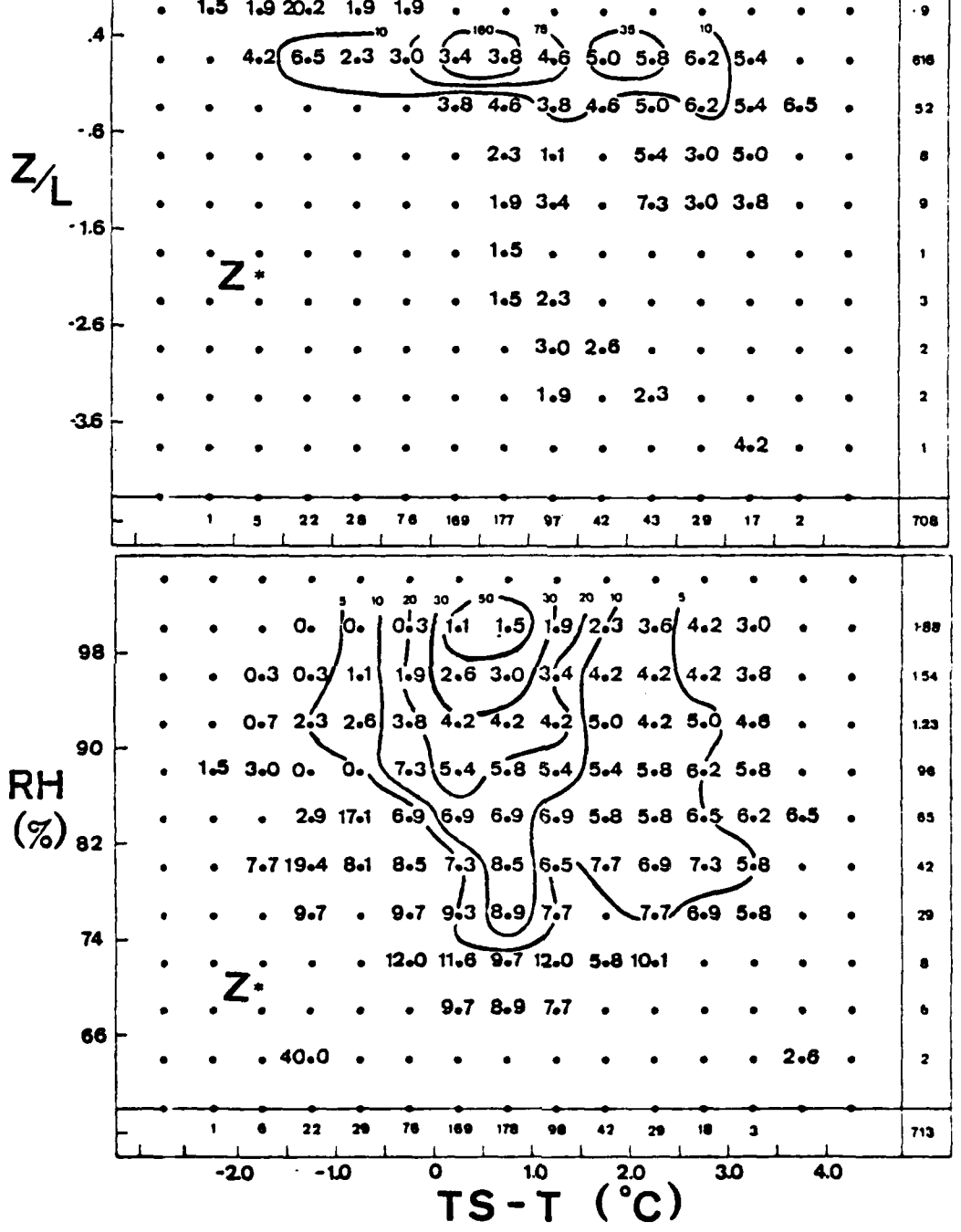

Figure 8 (top). JDF of Z/L and Figure 9 (bottom) JDF of RH and Ts-T to CMF of Z*.

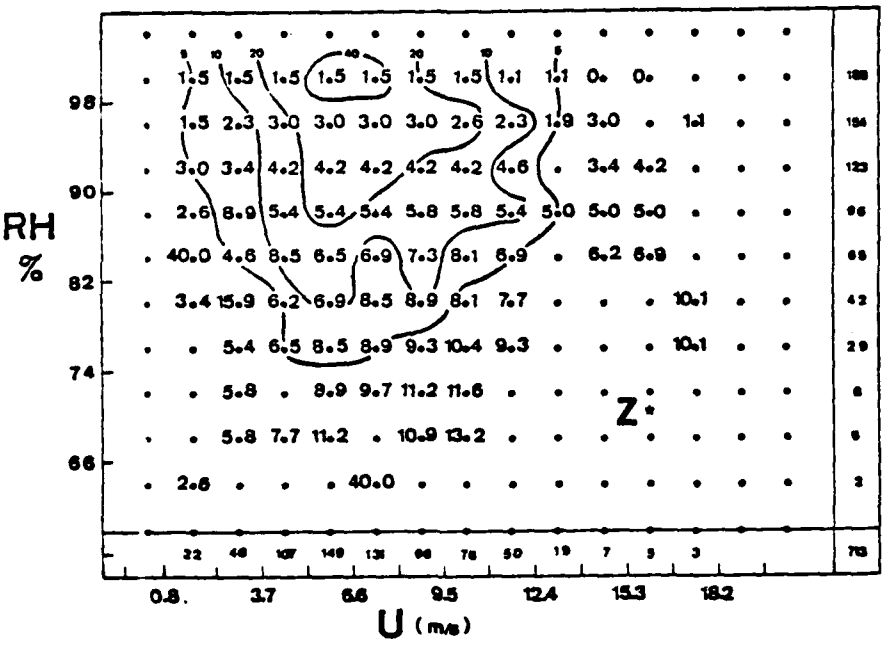

Figure 10. JDF of wind speed and relative humidity to CMF of Z*.

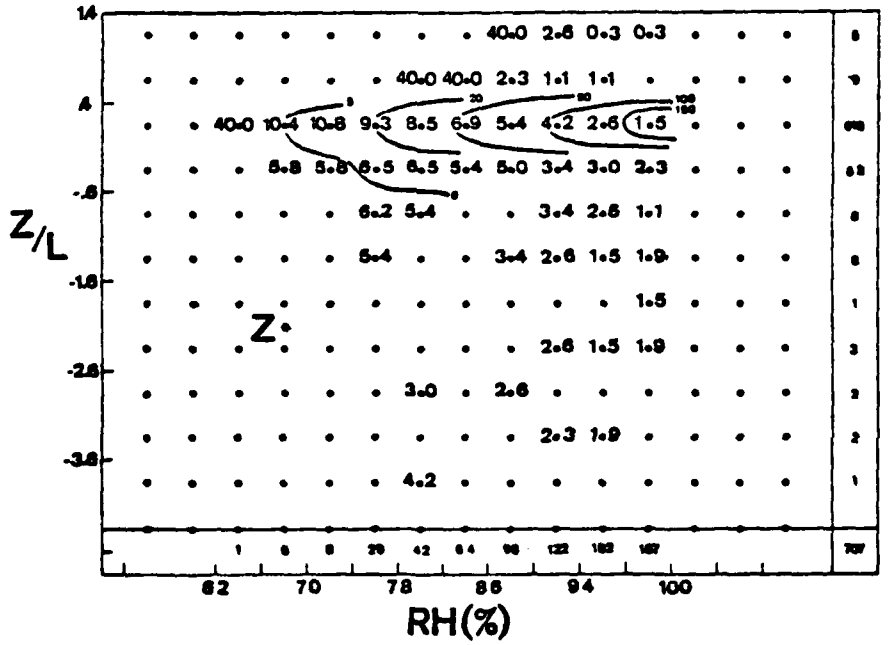

Figure 11. JDF of relative humidity and stability to CMF of Z*.

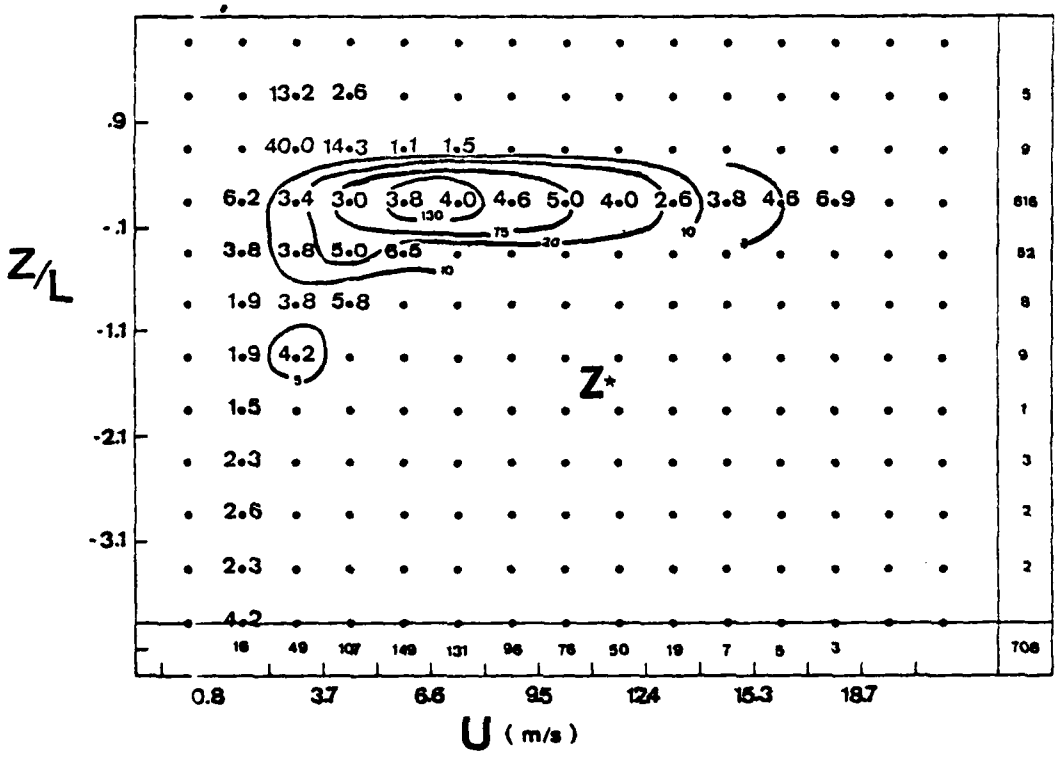

Figure 12. JDF wind speed and stability to CMF of Z*.

(JDF). Similarly, a conditional mean function (CMF), defined as the average values of Z* for all observation times when the two independent variables had values within the joint intervals, was defined for each joint class interval. A subjective analysis of the JDF's and the CMF's was performed to distinguish relationships as being from computational artifacts or from accidental occurrences.

a. Air-Sea Temperature Difference (Ts-T): (Figures 7, 8 and 9)

The air temperature averaged 0.5°C colder than the sea surface temperature. Z*(Ts) calculations were largely influenced by the observing ship's location in the JASIN area (Fig. 6). Air temperature variations were primarily influenced by migratory weather systems. The most notable positive deviation of Z* occurred when Ts-T was less than zero (-.5°C), with low relative humidity (RH<85%) and stable atmospheric conditions (Z/L> 0). However, under these conditions duct strength was extremely sensitive to humidity and stability changes. If RH increased Sigma(RH) or Z/L decreased Sigma (Z/L) then the evaporation duct virtually vanished. Generally, Ts-T had little effect on Z* when RH>90%. As Ts-T approached zero or became positive, more positive Z* deviations occurred for a wider range of RH e.g. (50-90%). The poorest ducting conditions occurred when T exceeded Ts more than 0.5°C and RH was in the high 90%'s. In near-neutral conditions, as Ts-T increased Z* tended to increase fractionally. Generally then, Ts-T was more of a determinant than stability, except in the special situation of warm, moist air over cooler water.

b. Relative Humidity: (Figures 9, 10 and 11)

Average humidity was 90% and ranged from 49% to 100%. Significant changes in humidity were directly due to the passage of large-scale weather systems. As relative humidity dropped to 80%, marked increases in Z* occurred. The largest Z* values occurred when dry (RH<80%) and warm air overlay cool water (Ts-T <-.5°C). For the relative humidity range (50-90%), larger than average Z* values occurred when the air was 1.0°C cooler than the sea surface. Lowest ducts occurred in warm, moist meteorological conditions (RH:85-100%, Ts-T:-2 to 0).

c. Wind Speed (U): (Figures 7, 10 and 12)

Wind was most influential on Z* values in low wind situations. In light winds, changes in atmospheric stability (Z/L) drastically changed the duct. As seen in Figure 12, a change in Z/L by Sigma (Z/L) changed Z* from 3 to 40 meters for winds near 5 m/s. In moist air (RH>90%), Z* was low regardless of wind speed. In dryer air (RH<85%) wind caused increased Z* as U increased from 5 to 12 m/s.

d. Stability (Z/L): (Figures 8, 11 and 12)

Average stability was near-neutral. The greatest deviations of Z* occurred when Ts-T<0 (warm air) and light wind (U<5m/s). Otherwise changes in Z/L, hence changes in Z*, were small as winds increased or colder air was advected over relatively warmer water (Ts-T>0).

Figure 13 illustrates the interrelationships that the combination of selected parameters had on Z*. The ranges of Z* are

depicted for the primary and secondary extremes encountered in the joint probability density distribution. With the exception of the dependent parametric interrelationship of stability (Z/L) and air-sea temperature (Ts-T), all parameters caused large values of Z*. The primary extreme range was a reflection of the special situation in which large values of Z* were generated due to atmospheric conditions where winds were light and warm, dry, stable air overlay relatively cooler waters. A more significant indication of atmospheric influence was the secondary range. This range reflected more accurately the effects due to characteristic changes in atmospheric variables with synoptic conditions of a summer regime.

The most influential meteorological factors were air-sea temperature and relative humidity, followed closely by the interrelationship of wind speed to air-sea temperature. Because the secondary range of wind speed to relative humidity was small, this indicated that large positive Z* deviations were influenced most significantly by air-sea temperature. Stability only became a significant factor in light winds. Table IV summarizes the relationship of duct strength to atmospheric parameters.

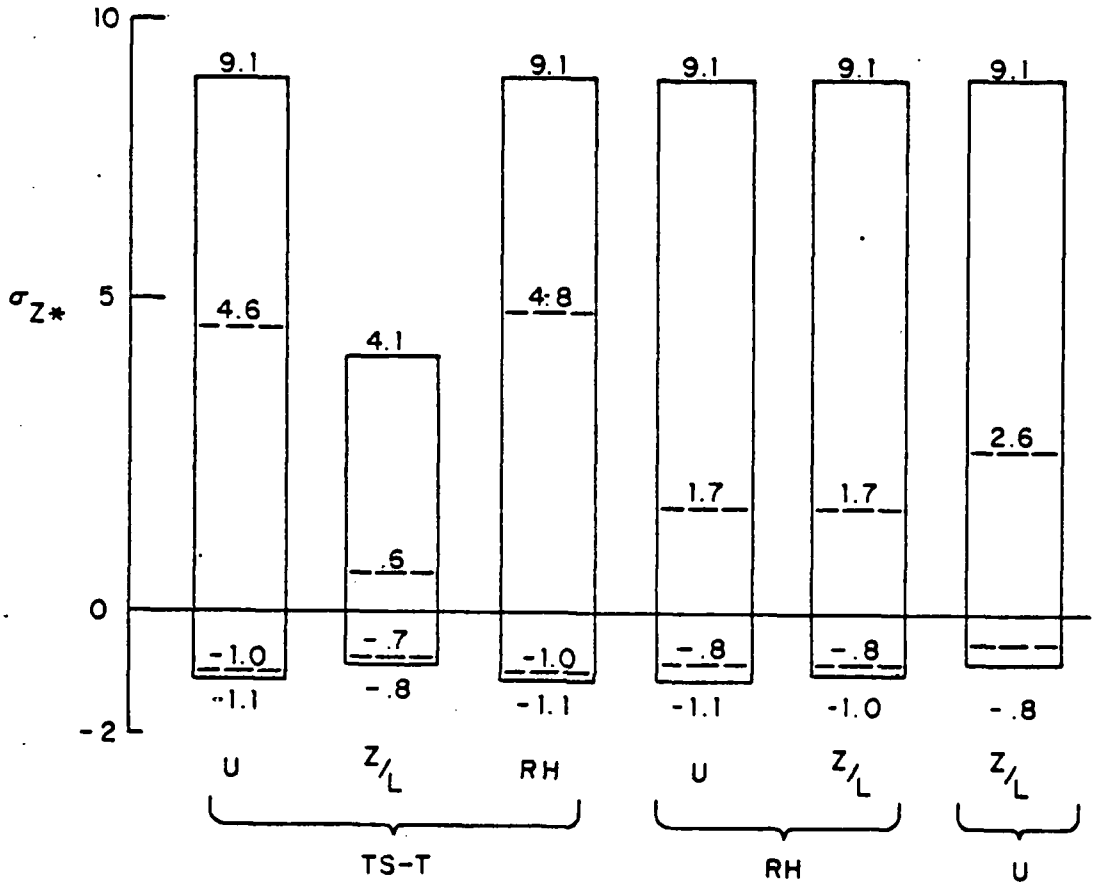

Figure 13. Parametric Interrelationship to Duct Height

TABLE IV

DUCT STRENGTH VS. ATMOSPHERIC PARAMETERS

Z*	RH (%)	U (m/s)	Ts-T (°C)	Z/L
STRONGEST	< 80	< 5	< -.5	> 0
STRONG	< 85	5-12	> 0	
WEAK	85-100		-2 to 0	> 0
WEAK	> 90		> 0	

5. Z* OCCURRENCE AND DURATION

Histograms of duct occurrence and duration of duct heights are shown in Figure 14. This figure indicates the occurrence of strong evaporation ducts during the summer is small and short-lived. Duct heights of 6m or less occurred 78% of the time. Rarely did significant ducts occur for more than several hours. Figure 5 shows the changing weather conditions throughout the summer and the effect on duct height. Rarely did one weather pattern dominate or persist. Consequently, the occurrence of strong ducting was irregular. It was most closely associated with atmospheric conditions that caused either cold, dry air or warm, dry air to move over the area. Incursions of relatively cold, dry air, usually from the northwest (Figures 21-23, 28-33 and 40-43), caused rapid formation of evaporation ducts (9-12m) which rarely lasted longer than 9-12 hours. Dry air did not last long over the area before it was modified. Incursions of warm dry air were evident and produced brief (3-6 hrs) but strong evaporation ducts (>8m). Conditions less favorable for the formation of ducts were associated with cyclonic southwesterly flow of warm, moist air (Figure 20).

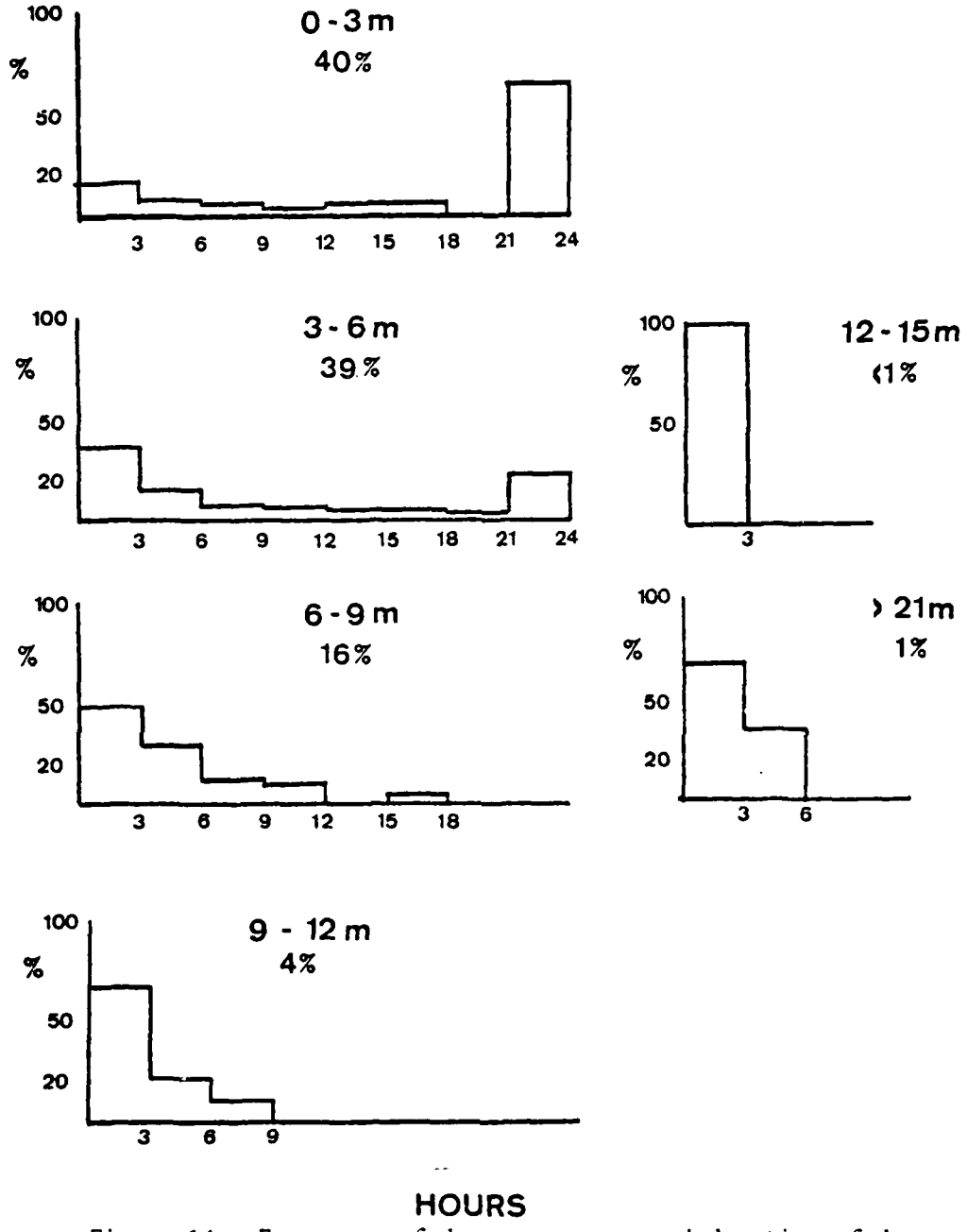

Figure 14. Frequency of duct occurence and duration of duct heights.

Figure 15 and 16 compare the distribution frequency of Z*. Of the three locations, JASIN indicates a higher percentage of low duct heights, Ocean Station INDIA shows its mode (group that occurs most frequently) in the 6-9 m range, the highest of the three. Additionally, INDIA had a greater percentage of Z* in the 9-18m range. Ocean Station ALFA located off the east coast of Greenland and in an oceanic region of confluence where the cold Greenland current meets the cool Irminger current, indicated a mode of 3-6m and a generally higher percentage of Z* greater than JASIN but less than INDIA.

This difference between the evaporation duct climatology in the three areas appears to have been due to (1) the proximity of ALFA to the Greenland landmass and the associated, extremely cold water and (2) INDIA's location in the deeper and warmer water of the North Atlantic current. Interpretation of visual and infrared satellite imagery indicates (Figures 28-33) the flow of cold, dry air off Greenland, coupled with cold sea surface temperatures, causes higher Z* values at ALFA due to the large difference in surface humidity and atmospheric humidity. As the dry air mass moves across the North Atlantic atmospheric humidity changes are relatively small as it approaches both the JASIN and INDIA locations. The key difference between the two locations is Ts. The warmer water at INDIA causes higher surface humidity, thus a larger difference in atmospheric and surface humidity resulting in the occurrence of stronger ducts. JASIN, because the air mass has become more moist since leaving ALFA, but enters an area of relatively warmer water, experiences the smallest

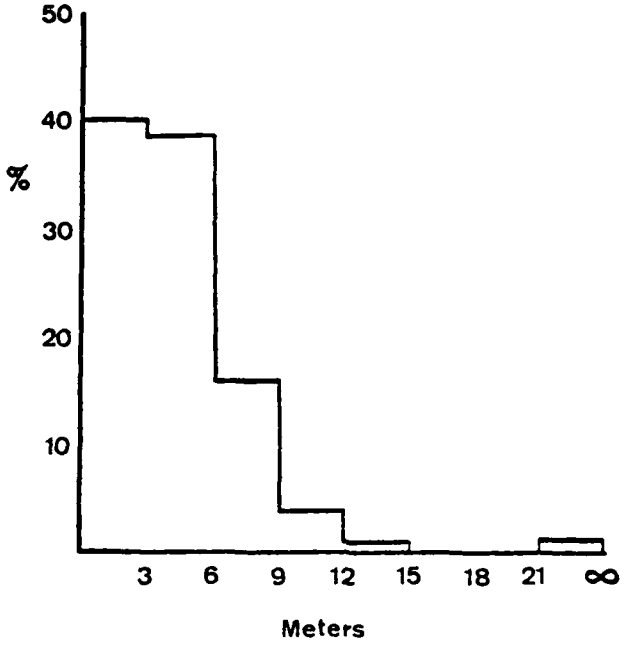

JASIN AREA

Figure 15. Frequency of Z* occurrence (13 Jul - 6 Sep 1978)

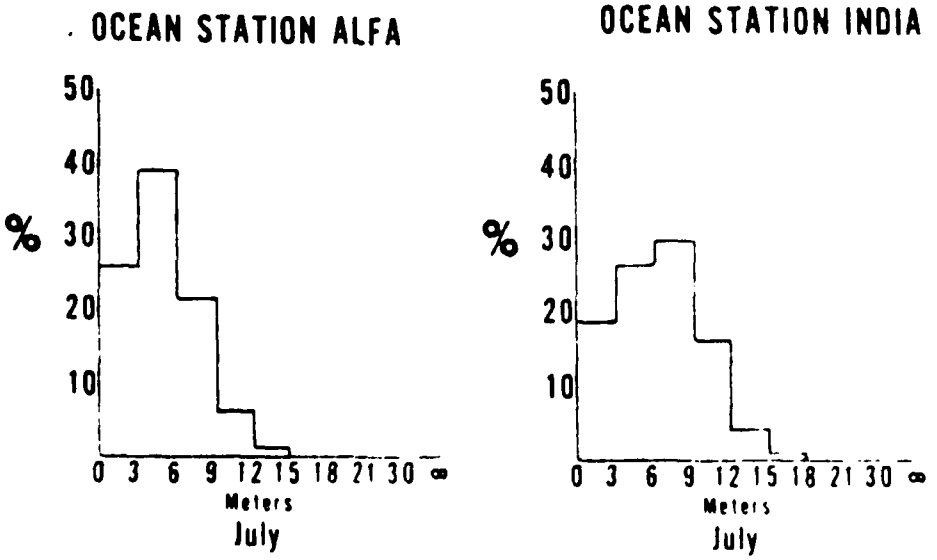

Figure 16. Frequency of Z* occurrence (climatology) at North Atlantic Ocean Stations nearest JASIN.

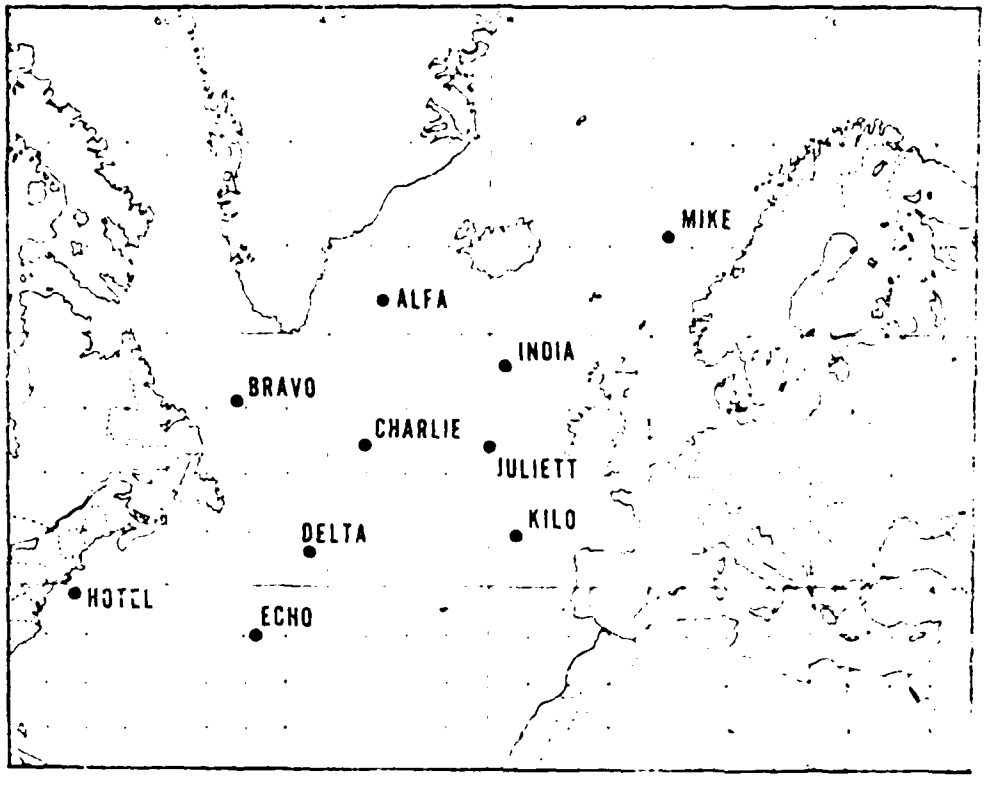

Figure 17. Ocean Stations in the North Atlantic: ALFA (62N, 33W) and INDIA (58N, 19W).

difference in atmospheric and surface humidities, therefore the weakest ducts of the three locations.

B. HORIZONTAL NATURE OF THE EVAPORATION DUCT

The three periods (7-8, 23-25 August and 30 August - 1 September) examined corresponded to times when ships were positioned at all corners of the JASIN triangle. The objectives of analysis for these periods were to:

1. Determine the horizontal homogeneity of the evaporation duct.
2. Determine which meteorological factors enhanced or degraded areal ducting.

The analysis procedure for this was to:

1. Compare computed Z* values at different ship positions and concomitant meteorological parameters to assess similarity.
2. Analyze synoptic meteorological conditions utilizing satellite imagery (visual/infrared), ship observations and synoptic weather maps.
3. Analyze the temporal variations or consistency of horizontally homogeneous conditions.
4. Relate the above fields to the spatial nature of the evaporation duct.

Area homogeneity was determined by comparing Z*, Ts-T, RH and U for ships positioned at each corner of the triangle. Azimuthal sectors were defined as the legs of the triangle (NW sector: NW-S, NE sector: NE-S, E sector: NE-NW). Using the South (S) position as the reference, differences were determined relative to Northwest (NW) and Northeast (NE) locations (NW and NE sectors, respectively). Similarly, using the Northwest observer as reference, differences were determined relative to the Northeast location (East sector). Differences between locations (ships) relative to sectors are tabulated in Tables V through VII.

1. Z* Range in Homogeneous Atmosphere

A necessary step to interpret the results of the tabulated differences is the performance of an error analysis to determine the possible range of computed Z* which could occur in a homogeneous atmospheric situation due to measurement inaccuracies. An assessment was required to ascertain the maximum deviation allowable in Z* for the three-ship system under nearly homogeneous atmospheric conditions. Additionally, a sensitivity analysis of Z* values was performed for each inherent measurement uncertainty.

Previous studies on bulk measurements [Davidson et al, 1978] have concluded that representative inaccuracies in bulk parameter measurements are:

RH = 3%
Ts-T = 0.5°
U = 10%

Five observation times were chosen to perform the error analysis. These corresponded to times when air temperature, relative humidity and wind speed were nearly similar for all ships stationed on the triangle. Benchmark Z* values were computed from each of these representative homogeneous atmospheric situations. Atmospheric conditions at 1500 GMT August 23, 24 and 0600 GMT 25 August were similar at all three ship locations. Mean values of bulk parameters were used to compute a Z* at each corner of the triangle assuming no measurement inaccuracies. A similar analysis was performed on data taken at 0600 and 1500 GMT 31 August. The following gives the results of the two periods:

CASE I

Ts = 12 °C T = 11.8 °C RH = 90% U = 8.1 m/s

SHIP	Z(m)	Z/L	Z*(m)
ENDURER	4	-.0055	4.44
MURRAY	6	-.0082	4.32
METEOR	11	-.0139	4.17

CASE II

Ts = 12.5 °C T = 11.5°C RH = 75% U = 10 m/s

SHIP	Z(m)	Z/L	Z*(m)
ENDURER	4	-.015	10.4
MURRAY	6	-.023	10.1
METEOR	11	-.045	9.7

The Z* values computed in each of the above cases represented reference Z* values for each measurement height, Z (e.g. 4, 6, 11m) in a spatially homogeneous, mixed layer. Measurement uncertainties listed below were introduced into the Z* calculations and the maximum error computed. Percentage values for both cases reflect the change in Z* due only to the measurement errors of each individual parameter.

	CASE I	CASE II	MEASUREMENT ERROR(rms)
U	7%	3%	10%
RH	25%	8%	3%
Ts	14%	2%	.5 °C

The cumulative error in the worst case situation, where measurement uncertainties were between two ships in a horizontally homogeneous atmosphere, produced the following difference in Z* values:

Z* (m)	Z* Diff (Max-Min)
4	2.7
10	2.9

Therefore, it was concluded that if the atmosphere were homogeneous and the only uncertainties were in measurements of T, Ts, RH and U, then the greatest difference in Z* that any two ships would have experienced was 2.9 m.

2. Case Studies of Horizontal Homogeneity

Three periods were examined, in view of the error analysis, when ships were stationed at the corners of the JASIN triangle (approximately 200 km apart). Simultaneous meteorological observations, taken at three-hour intervals, and their respective Z* values were compared. In each case, an average or better than average evaporation duct existed. Extensive periods of below average ducting were not considered.

The examination included consideration of the general synoptic conditions, differences in local meteorological conditions between ships (and the factors which most influenced Z*), the extent of the duct over the entire triangle (areal homogeneity) and between corners (sector homogeneity). The maximum Z* difference (2.9m) between ships (due to measurement errors as previously described) was the criterion for duct homogeneity. Therefore, if the maximum difference in Z* between all three ships was less than or equal to 2.9m, areal homogeneity was assumed to exist. Similarly, if the criterion was valid between corners of the triangle, sector homogeneity was assumed to exist.

a. Case I

(1) Period. 7 Aug (0000 GMT) - 8 Aug (2100 GMT)

(2) Observer Positions on Triangle.

Northwest (NW) - ENDURER
Northeast (NE) - MURRAY
South (S) - METEOR

(3) Synoptic Conditions - Blocked. A ridge persisted over the area as it intensified and moved slowly east (Figure 19). Northerly surface winds were moderate in the eastern region and lighter in the west. Low level instability prevailed as cold air was advected over warmer water. However, convection was inhibited by warm air aloft as an occlusion moved slowly over the area (Figures 25-27).

(4) Results of Tabulated Differences - (Table V). Observations at NW and NE were more humid than S. Winds were stronger at NE than NW and S. Air-sea temperature differences were greatest at S. The duct heights on the average were 2m higher in the south than the two northern positions (i.e. 6.9m vs. 4.9m).

(5) Areal Homogeneity. Similar evaporation duct strengths occurred simultaneously at the three stations 30% of the time with the most sustained conditions lasting 12 hours. Figure 18 illustrates by sectors the percentage of homogeneous ducts and the longest duration experienced. Northerly flow coincided with similarity between the two northern positions while the greatest disparity occurred between southern and western positions. The most persistent horizontal homogeneity occurred between NW and NE where humidities and air-sea temperature differences were most similar. Poorest conditions existed

TABLE V

TABULAR DIFFERENCE BETWEEN SHIPS BY SECTOR

DTG	REF		Z* (m)			TS-T (DEG C)			RH (%)			U (m/s)		
	S	W	NW	E	NE	NW	E	NE	NW	E	NE	NW	E	NE
78080700	6.3/	7.4	1.1	-.7	.4	-.7	-.2	-.9	-14.0	11.3	-2.7	-2.2	3.5	1.3
78080703	6.9/	3.2	-3.7	3.2	-.5	-.5	-.6	-1.1	3.4	-1.2	2.2	-4.7	7.0	2.3
78080706	9.3/	5.0	-4.3	.9	-3.4	.3	0.0	.3	19.7	-.2	19.5	-1.2	3.0	1.8
78080709	9.5/	5.5	-4.0	-.9	-4.8	.4	-.5	-.1	19.9	1.0	20.9	-.2	.5	.3
78080712	8.4/	2.3	-6.1	2.3	-3.9	1.2	-1.1	.1	21.6	-6.2	15.4	-5.2	5.5	.3
78080715	6.9/	3.8	-3.1	1.6	-1.5	.9	-1.2	-.3	7.8	-.3	7.5	-3.2	5.0	1.8
78080718	7.5/	5.1	-2.4	-.4	-2.8	-.1	-.2	-.3	5.6	9.9	15.5	-2.1	4.0	1.9
78080721	6.9/	2.7	-4.0	2.6	-1.4	.6	-.7	-.1	18.5	-8.7	9.8	-2.1	4.5	2.4
78080800	6.6/	2.9	-3.8	1.7	-2.0	-.6	.4	-.2	-1.3	9.0	7.7	-5.2	5.0	-.2
78080803	4.9/	4.1	-.8	3.1	2.3	-1.6	1.0	-.6	-16.1	.0	-16.1	-5.7	5.0	-.7
78080806	8.1/	2.5	-5.5	4.7	-.9	-.4	.4	0.0	15.5	-7.9	7.6	-4.1	5.5	1.4
78080809	8.1/	5.1	-2.9	.3	-2.7	-1.7	2.0	.3	-.3	12.1	11.7	-3.7	3.0	-.7
78080812	7.1/	4.2	-2.9	.3	-2.6	-1.0	1.4	.4	6.3	10.4	16.7	-2.6	3.0	.4
78080815	6.8/	4.9	-2.0	1.0	-1.0	-.4	.9	.5	1.9	13.3	15.2	-2.1	5.0	2.9
78080818	6.5/	6.4	-.1	-1.6	-1.7	-1.8	1.4	-.4	-8.3	18.3	10.0	-2.1	2.5	.4
78080821	8.1/	5.8	-2.3	-1.0	-3.3	-1.2	1.2	0.0	8.4	5.8	14.2	-1.7	1.0	-.7
MEAN	7.4	4.4	-2.9	1.1	-1.9	-.4	.3	-.2	5.5	4.2	9.7	-3.0	3.9	.9
STANDARD DEVIATION	1.2	1.5	1.9	1.8	1.8	.9	1.0	.4	11.8	8.2	9.2	1.6	1.7	1.2
VARIANCE	1.4	2.2	3.5	3.2	3.1	.8	.9	.2	138.9	67.0	85.4	2.6	3.0	1.4

between NW and S due primarily to the dissimilarity in Ts-T and RH and the consequent difference in air-sea humidity (Figures 44-47).

b. Case II

(1) Period: 22 August (1500 GMT) - 25 August (1500 GMT)

(2) Observer Positions on Triangle:

Northwest (NW) - ENDURER
Northeast (NE) - HECLA
South (S) - METEOR

(3) Synoptic Conditions - Moist Anticyclonic. An advancing cold front passed over the area the afternoon of 23 August (Figures 21, 28, 31). Cold, dry northwesterly air immediately followed the frontal passage and prevailed through 24 August (Figures 22,32, 33). Humidity gradually increased from the west over the area by 25 August as a warm front approached (Figures 23, 34, 35).

(4) Results of Tabulated Differences -(Table VI). Generally, the greatest differences experienced were between NW and NE stations due to the west to east movement of the air mass over the area. Winds and humidity were similar at all observing stations. Air-sea differences were least at the NE position where water was the coldest, hence weakest ducts were generated. Duct heights ranged 1.1-12.2m and averaged 5m over the area.

(5) Areal Homogeneity. The area experienced homogeneous ducting 44% of the time with the longest duration 9 hours. Homogeneity was nearly equal for all sectors with the northeast experiencing slightly stronger ducting and lasting for 24 hours following frontal passage (Figure 18). The greatest Z* difference across the front was

TABLE V!

TABULAR DIFFERENCE BETWEEN SHIPS BY SECTOR

DTG	REF		Z* (m)			TS-T (DEG C)			RH (%)			U (m/s)		
	S	N	NW	E	NE	NW	E	NE	NW	E	NE	NW	E	NE
78082215	3.5/	3.9	.4	-.3	.1	.4	-.3	.1	1.2	-5.6	-4.4	-1.0	1.7	.7
78082218	3.3/	3.9	.6	1.7	2.3	.3	0.0	.3	.0	-10.9	-10.9	-1.8	0.0	-1.8
78082221	5.4/	9.3	3.9	-5.7	-1.8	.1	.7	.8	-9.9	9.0	-1.0	-.8	0.0	-.8
78082300	8.6/	8.5	-.0	-6.2	-6.2	.7	-.6	.1	3.0	12.4	15.4	-.8	-1.5	-2.3
78082303	4.2/	8.6	4.4	1.9	6.3	.3	.7	1.0	-10.2	-8.2	-18.3	.7	-2.0	-1.3
78082306	6.8/	5.6	-1.3	2.1	.8	.3	1.1	1.4	5.6	-11.7	-6.1	.2	.5	.7
78082309	6.3/	6.4	.2	-3.5	-3.3	.1	.5	.6	1.3	2.3	3.5	.2	-.5	-.3
78082312	3.5/	6.6	3.1	-3.8	-.7	.1	.5	.6	-6.6	2.2	-4.4	3.2	-1.5	1.7
78082315	4.4/	5.9	1.6	-1.4	.1	-.4	.5	.1	-4.3	-.3	-4.6	.8	1.0	1.8
78082318	3.9/	5.1	1.2	-.5	.8	-.1	.6	.5	-3.4	-5.4	-8.8	-2.3	3.5	1.2
78082321	5.2/	6.3	1.1	-4.1	-3.0	.3	.7	1.0	-1.2	3.5	2.3	-.8	1.5	.7
78082400	5.9/	5.9	.0	-2.6	-2.6	.4	-.2	.2	2.1	3.3	5.4	.7	-2.5	-1.8
78082403	6.2/	4.2	-2.0	.4	-1.6	.1	0.0	.1	8.6	-5.7	2.9	-.8	2.0	1.2
78082406	7.0/	4.5	-2.5	-.2	-2.7	.1	.6	.7	7.9	-5.4	2.3	-3.9	3.5	-.4
78082409	5.2/	8.1	3.1	-4.2	-1.1	.3	.7	1.0	-5.6	4.5	-1.0	-.8	3.0	2.2
78082412	4.3/	12.2	7.9	-8.0	-.1	-.1	1.1	1.0	-17.0	13.7	-3.3	-.8	0.0	-.8
78082415	4.9/	10.2	5.4	-4.2	1.2	.1	1.0	1.1	-12.4	5.8	-6.6	-2.3	3.0	.7
78082418	5.5/	9.0	3.5	-1.3	2.2	.4	.6	1.0	-7.9	-1.0	-8.9	.3	2.0	2.3
78082421	7.0/	7.2	.2	.8	1.0	.3	.5	.8	1.0	-5.7	-4.7	-.2	2.5	2.3
78082500	5.1/	5.1	.1	5.0	5.1	.7	.3	1.0	2.1	-13.4	-11.3	-.2	1.0	.8
78082503	7.2/	4.1	-3.0	-2.2	-5.2	.3	.1	.4	10.9	-.0	10.9	1.3	2.0	3.3
78082506	4.5/	4.3	-.3	-.4	-.7	-.1	.1	0.0	.0	-3.5	-3.5	-2.7	3.0	.3
78082509	6.3/	2.3	-4.0	-.7	-4.7	.2	1.4	1.6	12.6	-8.8	3.7	-3.2	4.0	.8
78082512	4.6/	2.6	-2.0	.2	-1.8	.8	.8	1.6	7.8	-8.8	-1.1	-.6	1.0	.4
78082515	4.2/	1.1	-3.1	-.6	-3.7	-.2	1.2	1.0	9.3	-9.0	.2	-1.1	1.5	.4
MEAN	5.3	6.1	.7	-1.5	-.8	.2	.5	.7	-.2	-1.9	-2.1	-.7	1.1	.5
STANDARD DEVIATION	1.3	2.6	2.9	3.0	3.0	.3	.5	.5	7.7	7.4	7.2	1.5	1.8	1.4
VARIANCE	1.8	7.0	8.4	8.7	8.8	.1	.2	.2	59.3	55.4	52.0	2.3	3.3	2.0

3.8m i.e. 6.6m (NW) vs. 2.8m (NE) Horizontally homogeneous ducting lasted for nearly 15 hours following frontal passage before another impulse of dry air entered the western area. It took 15 hours for the dry air to move across the JASIN area and strengthen the duct in the east (Figures 48-53).

c. Case III

(1) Period. 30 August (0000 GMT) - 1 September (2100 GMT)

(2) Observer Positions on Triangle.

NORTHWEST (NW) - ENDURER
NORTHEAST (NE) - HECLA
SOUTH (S) - METEOR

(3) Synoptic Conditions - Mobile Westerly. A weak depression moved over the region (Figure 19). The JASIN area was in a warm sector on 30 August as a cold front passed early on 31 August. A warm front approached from west late on 1 September (Figures 40-43.2).

(4) Results of Tabulated Difference - (Table VII). The average duct height was 6m. The most intense ducts occurred on 31 August after the cold front passed. They occurred in the west and south where sea surface temperatures were highest and air-sea temperature differences were greatest. On the average, relative humidity was lower to the northeast than the western and southern region which were largely under the influence of warm sector of the low.

(5) Areal Homogeneity. Due to the high mobility of the weather systems, areal horizontal homogeneous ducting occurred only 29% of the time with a maximum duration of 9 hours during very low ducts. Sector homogeneity was poorest between the northeast and northwest

TABLE VII

TABULAR DIFFERENCE BETWEEN SHIPS BY SECTOR

DTG	REF		Z* (m)			TS-T (DEG C)			RH (%)			U (m/s)		
	S	W	NW	E	NE	NW	E	NE	NW	E	NE	NW	E	NE
78083000	4.7/	2.8	-1.9	5.1	3.2	.3	.5	.8	10.4	-49.9	-39.5	2.2	-3.5	-1.3
78083003	3.5/	3.9	.4	-1.2	-.8	.2	1.8	2.0	2.4	-33.7	-31.4	2.2	-5.7	-3.5
78083006	2.3/	1.3	-1.0	4.1	3.1	-.3	2.5	2.2	2.3	-26.2	-23.9	2.2	-2.5	-.3
78083009	2.1/	1.5	-.6	8.5	7.9	.4	-.2	.2	3.4	-35.1	-31.7	2.7	-1.7	1.0
78083012	1.8/	1.9	.1	3.2	3.3	.7	.9	1.2	5.6	-8.5	-3.0	.8	4.4	5.2
78083015	1.7/	1.8	.1	.3	.5	.3	-.5	-.2	6.6	-3.5	3.1	.8	-1.9	-1.1
78083018	3.2/	.8	-2.4	-.2	-2.6	.1	-.1	0.0	8.9	0.0	8.9	-.7	-.5	-1.2
78083021	1.3/	1.8	.6	-1.0	-.4	.9	-.8	.1	3.4	-1.2	2.2	-4.5	3.7	-.8
78083100	.4/	8.8	8.3	-6.1	2.3	.8	-.6	.2	-18.4	16.0	-2.4	-2.5	-1.0	-3.5
78083103	2.5/	11.7	9.2	-7.9	1.3	.7	-.9	-.2	-28.0	22.0	-6.0	.5	-3.1	-2.6
78083106	10.3/	9.9	-.3	-1.6	-1.9	.3	-.2	.1	2.9	-2.1	.8	-.5	1.4	.9
78083109	8.5/	12.7	4.2	-2.8	1.3	-.6	-.5	-1.1	-11.9	4.5	-7.4	1.4	-.9	.5
78083112	13.2/	8.6	-4.6	2.8	-1.8	.5	-1.1	-.6	16.6	-11.4	5.2	-1.5	.7	-.8
78083115	11.0/	9.7	-1.2	-.6	-1.8	1.0	-1.2	-.2	5.4	-1.4	4.1	-.6	-1.1	-1.7
78083118	8.9/	9.3	.5	-4.5	-4.0	.4	-.2	.2	-2.7	15.7	13.1	-1.6	4.4	2.8
78083121	11.8/	8.6	-3.3	.8	-2.5	0.0	-.1	-.1	11.7	-4.5	7.1	-1.6	.8	-.8
78090100	7.5/	8.5	1.0	2.9	4.0	-.4	.1	-.3	-1.0	-14.8	-15.8	3.4	-2.7	.7
78090103	6.5/	5.2	-1.3	4.6	3.3	-.2	-.2	-.4	4.6	-20.3	-15.7	1.4	-3.0	-1.6
78090106	9.0/	5.9	-3.2	1.4	-1.8	.2	-.3	-.1	10.8	-7.9	2.9	-.7	-1.9	-2.6
78090109	8.7/	5.4	-3.4	3.2	-.2	.4	-.6	-.2	10.9	-10.9	.0	-2.7	1.5	-1.2
78090112	7.7/	4.5	-3.2	.8	-2.3	0.0	-.4	-.4	10.0	-4.6	5.4	-1.6	.1	-1.5
78090115	7.1/	6.7	-.4	-1.6	-2.0	.1	-.1	0.0	2.1	2.6	4.7	-.7	-.4	-1.1
78090118	6.4/	4.2	-2.2	3.0	.8	.2	-.9	-.7	7.7	-10.0	-2.3	-1.3	3.0	1.7
78090121	5.9/	2.1	-3.8	4.6	.8	.8	-1.0	-.2	14.7	-17.3	-2.6	-.8	3.3	2.5
MEAN	6.1	5.7	-.3	.7	.4	.3	-.2	.1	3.3	-8.4	-5.2	-.2	-.3	-.4
STANDARD DEVIATION	3.7	3.6	3.4	3.8	2.8	.4	.9	.8	10.2	16.6	14.0	1.9	2.7	2.0
VARIANCE	13.5	13.0	11.6	14.2	7.8	.2	.7	.6	104.2	275.1	196.2	3.7	7.2	4.2

positions and best between south and northeast (Figure 18). The maximum difference in Z* across the cold front was 9.5m i.e. 11.7m (NW) vs. 2.2m(S). The strongest duct heights associated with any weather system were generated on 31 August following the cold front. Though outside the limits of horizontal homogeneity criterion, 2.9m, duct heights of 8.6-13.4m occurred at all stations for 12 hours before weakening in the east (Figures 54-59).

3. Summary of Horizontal Variation of Z*

The periods of the three cases studied were chosen because higher than normal ducts occurred for reasonably long periods. The horizontal nature of significant ducting in the region could be assessed. Each case was unique in that strong ducting was the result of differing synoptic meteorological conditions.

The strongest ducts occurred as mobile westerly depressions moved through the area; however, horizontal homogeneity was poorest. Air-sea temperature differences and relative humidity were the most important parameters affecting duct strength. Larger Z* values were experienced at the NW and S locations because these locations had higher values of Ts than the NE location. Since Ts gradients did exist between observation positions, sector horizontal homogeneity appeared to be influenced by the direction from which the air mass entered the area. The NW and NE positions, which experienced the largest Ts gradient, had more homogeneous ducting with northerly flow than westerly flow. The gradient between S and NE was small and resulted in consistently homogeneous conditions in all three cases.

Case I illustrated the effect wind plays on Z* values. Both NE and NW had high relative humidity, but NW had a greater air-sea temperature difference, resulting in a larger moisture flux. However the stronger winds in the eastern region compensated for the lower moisture flux producing nearly similar duct heights. A comparison of the S and NE stations, which had similar winds and air-sea temperature differences, showed significantly different duct heights. The important parameters in this case were relative humidity and sea surface temperature which produced larger surface moisture fluxes.

Case II exhibits the effects due to incursions of cold, dry air with moderate to fresh winds. Satellite pictures (Figures 50, 51) indicated low level instability under windy and drying conditions. However, significant afternoon heating sharply reversed the air-sea temperature difference causing the ducts to strengthen. Despite the afternoon variation, this case had the most consistent horizontally homogeneous ducting, occurring 44% of the time, as well as the most equal sector homogeneity of the three cases. The strongest ducts were toward the northwest where the air was the driest. The strong zonal flow inhibited the driest from reaching the southern region where relative humidity varied little and air-sea temperature differences were small.

Case III illustrates the effect of rapidly moving depressions on the formation and duration of ducts. The strongest areal ducts formed with the passage of a cold front but lasted only a short period before the next upstream weather system weakened the duct in the western region. The occurrence of ducts in the NE lagged the

occurrence of similar ducts at the NW position by six hours.

A composite of the frequency of occurrence of areal and sector homogeneous ducts and maximum duration is depicted in Figure 18. It was concluded that areal homogeneity was a probable occurrence only 35% of the time for the three periods studied, with a maximum likely duration of 12 hours. The NE sector appeared to maintain the best horizontal homogeneous conditions. The sector also appeared to exhibit good homogeneity but of short duration. The NW sector exhibited the least homogeneous conditions but when homogeneity occurred, it lasted up to 24 hours.

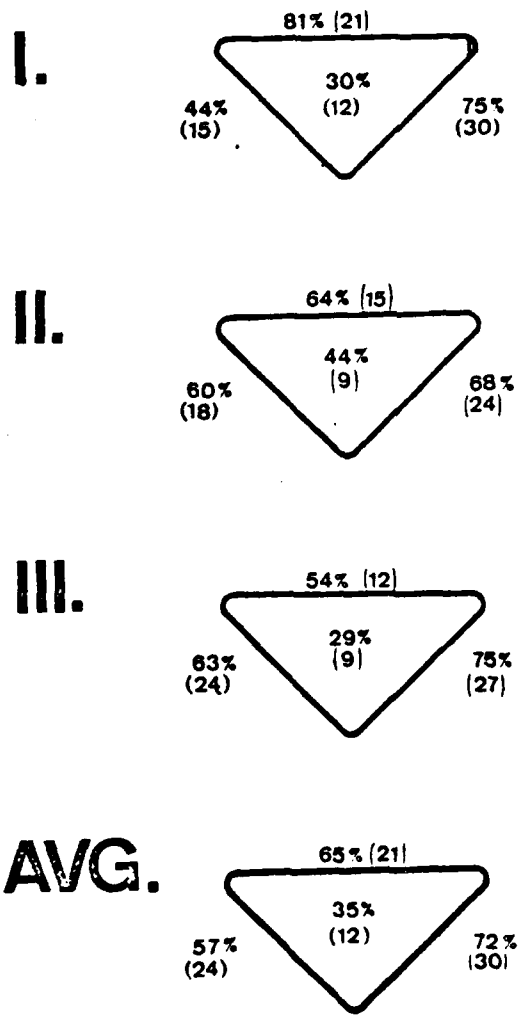

Figure 18. Percentage of areal and sector horizontal homogeneity of ducting and maximum duration for three cases and the average.

VII. SUMMARY AND CONCLUSIONS

Unique temporal and spatial descriptions of evaporation duct features in the Northeast Atlantic were described from observational data taken from four ships spaced in a fixed array. Evaporation duct heights were determined from accurately measured bulk surface data utilizing Monin-Obukhov scaling in flux-profile relationships. Discernible synoptic features from surface pressure fields and DMSP satellite pictures were air mass histories, trajectories and horizontal variations (frontal zones). Synoptic scale spatial variations of the sea surface temperature were also available and were as important in the spatial variation as the atmosphere.

Evaporation duct features established for this data set were:

1. The mean Z* values were less than those reported in available climatologies based on weather ships' observations (4.2m versus 7.0m).

2. Z* values at or above 8-10 meters occur frequently in conjunction with outbreaks of cold, dry air from the north or northwest and have durations of 9 to 12 hours.

3. Air-sea temperature differences and relative humidity were the important surface layer parameters in establishing tactically significant values and the former was the most important.

4. If horizontal homogeneity were defined as representatively uniform Z* values over 200 km distances, such conditions occurred only 35% of the times when significant duct heights existed, and for durations of up to 12 hours.

Conclusions relative to synoptic scale features most closely associated with these near-surface features are:

1. The primary synoptic influence on the duct height is the air-mass trajectory (due to its role in determining the moisture content) and the air-surface temperature difference. North and northwest

trajectories have the highest associated Z* values.

2. The primary feature influencing horizontal homogeneity over distances of 200km is the sea surface temperature, and its influence depends on the air mass trajectory.

3. Light wind conditions modify the above specified synoptic feature-surface duct feature relationships. The modifications occur over smaller temporal and spatial scales than those of the prevailing features.

A concluding assessment is that tactically significant features of the evaporation duct in the study area and for the study period can be established from synoptic scale descriptions. Further exploitation of available data should emphasize satellite imagery which could delineate surface temperature and air mass characteristics.

A recommendation for further efforts is that all available surface data from the JASIN project be used in order to extend and substantiate feature descriptions and relationships identified in this study. Since the start of this study, additional surface layer data from buoys and other participating ships have been compiled by the organizing institutions and made available on computer tapes. These data would increase the observations used by two orders of magnitude, thereby improving the descriptions of both the temporal and spatial features.

APPENDIX A.

TABLE A-I

Julian (year) Day and Date

Date	Day	Date	Day	Date	Day
July 12	193	Aug. 1	213	Sept. 1	244
13	194	2	214	2	245
14	195	3	215	3	246
15	196	4	216	4	247
16	197	5	217	5	248
17	198	6	218	6	249
18	199	7	219	7	250
19	200	8	220	8	251
20	201	9	221	9	252
21	202	10	222	10	253
22	203	11	223	11	254
23	204	12	224	12	255
24	205	13	225	13	256
25	206	14	226	14	257
26	207	15	227	15	258
28	209	16	228	16	259
29	210	17	229	17	260
30	211	18	230		
31	212	19	231		
		20	232		
		21	233		
		22	234		
		23	235		
		24	236		
		25	237		
		26	238		
		27	239		
		28	240		
		29	241		
		30	242		
		31	243		

Figure 19. **DAILY WEATHER MAPS**

(12GMT) 3 - 17 JULY 1978

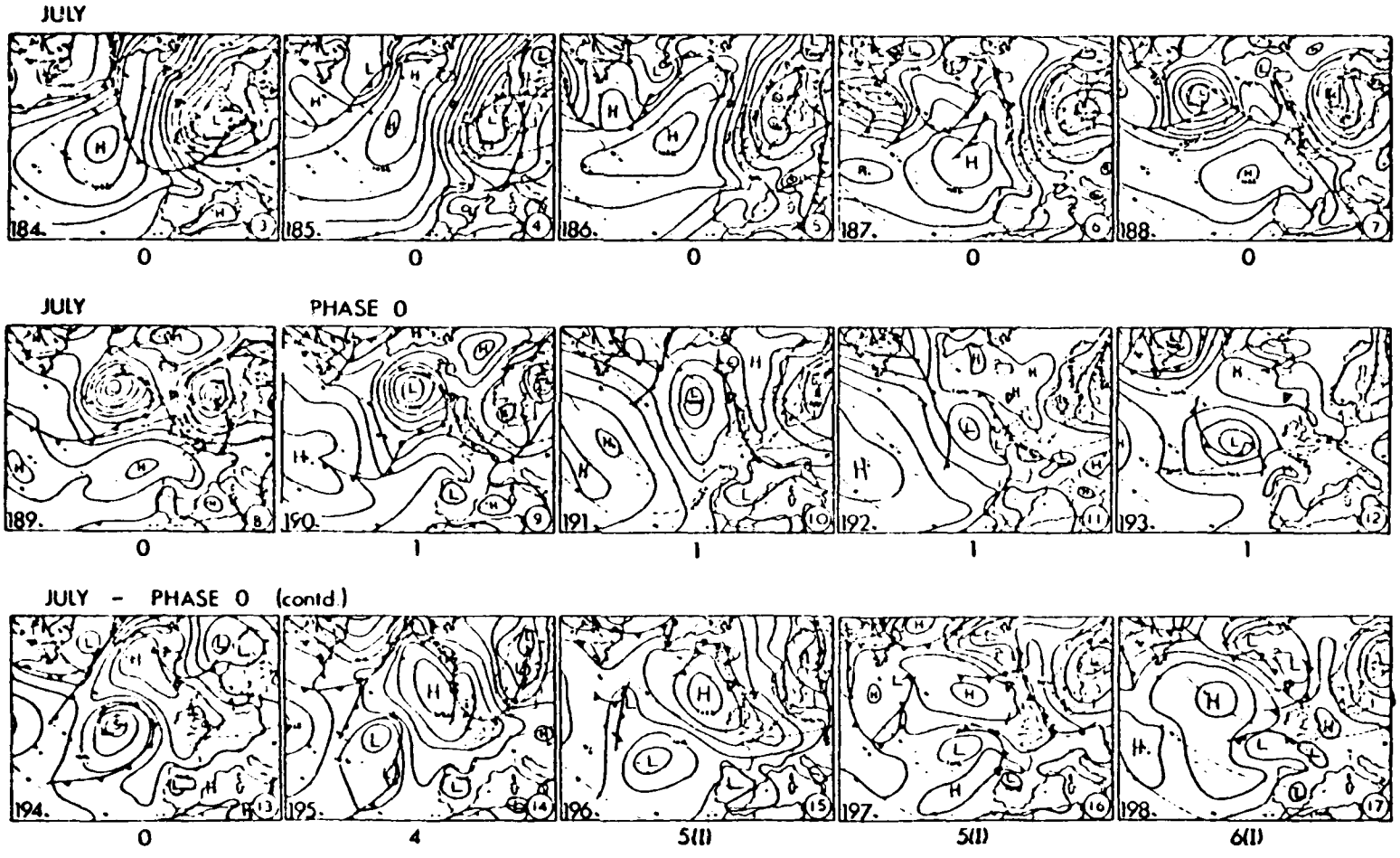

Figure 19. (contd.) DAILY WEATHER MAPS

(12GMT) 18 JULY -- 1 AUGUST 1978

JULY - PHASE 0 (contd.)

6(I) 6(I) 6RA(I) 7(I) 8 I

JULY - PHASE 1

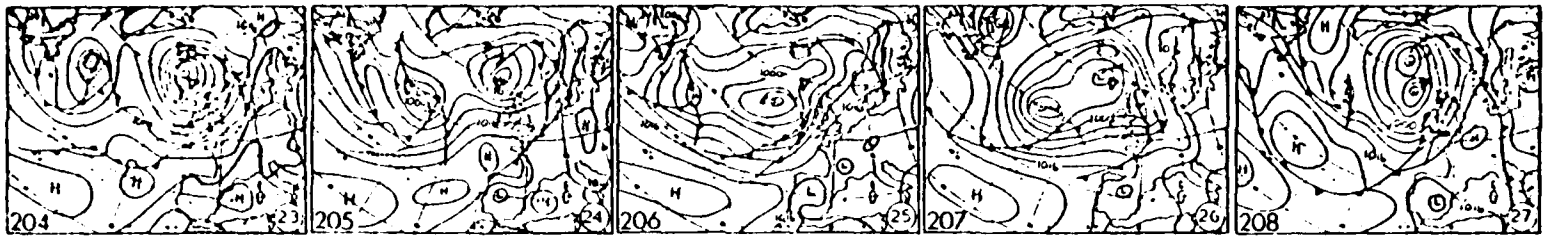

5 4A 4R 4A 5R

JULY - PHASE 1 (contd.)

AUGUST

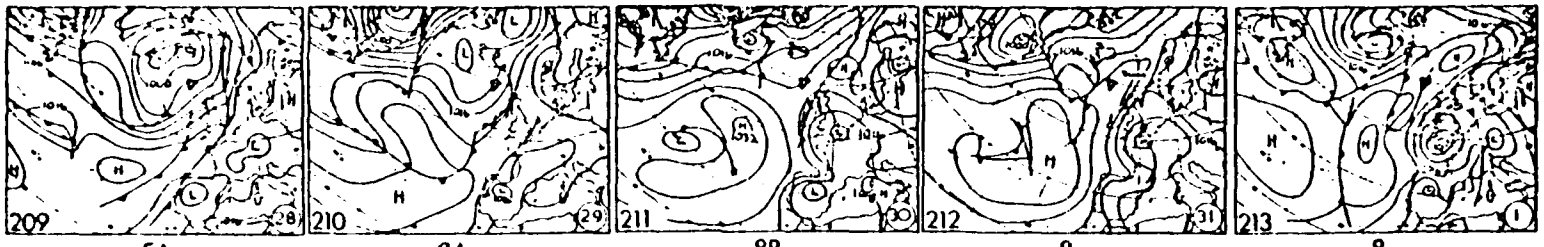

5A 8A 8R 8 8

Figure 19. (contd.) DAILY WEATHER MAPS

(12GMT) 2 - 16 AUGUST 1978

AUGUST - PHASE 1 (contd.)

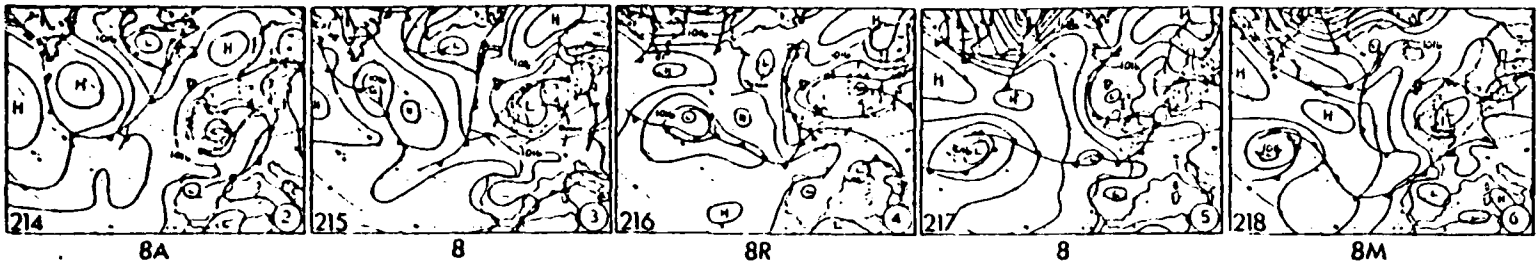

8A 8 8R 8 8M

AUGUST - PHASE 1 (contd.)

8RAM 8AM 8IA 5M 3M

AUGUST - PHASE 1 (contd.)

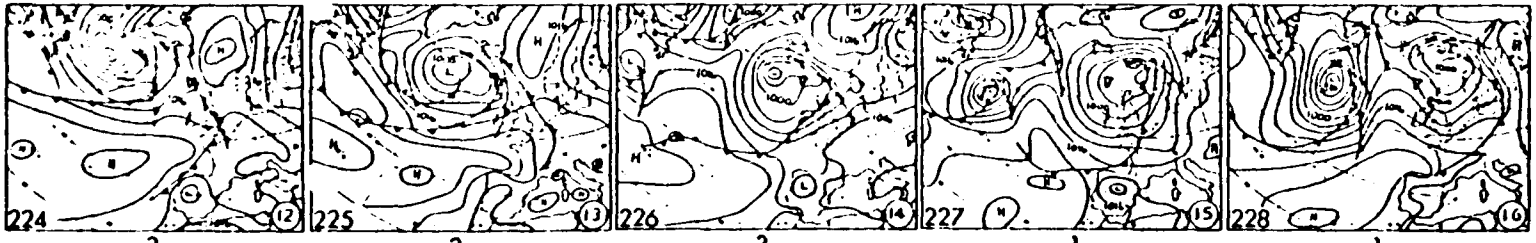

3 3 3 1 1

Figure 19. **(contd.) DAILY WEATHER MAPS**

(12 GMT) 17 - 31 AUGUST 1978

AUGUST - PHASE 2

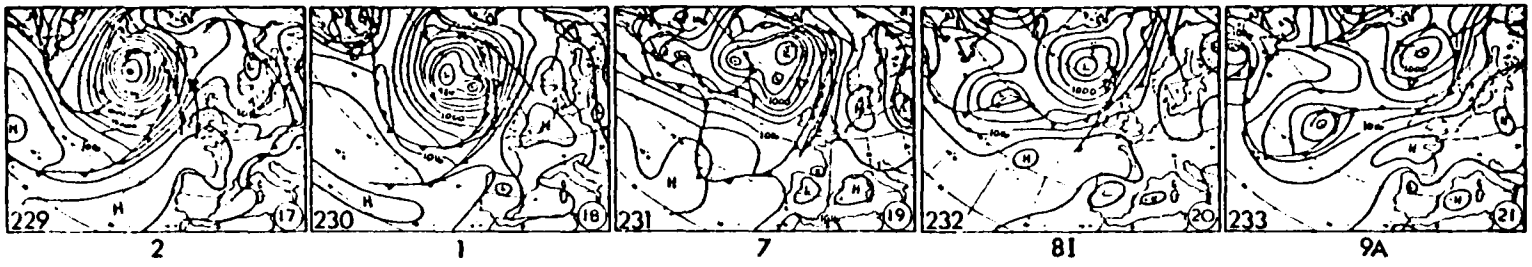

2 1 7 81 9A

AUGUST - PHASE 2 (contd.)

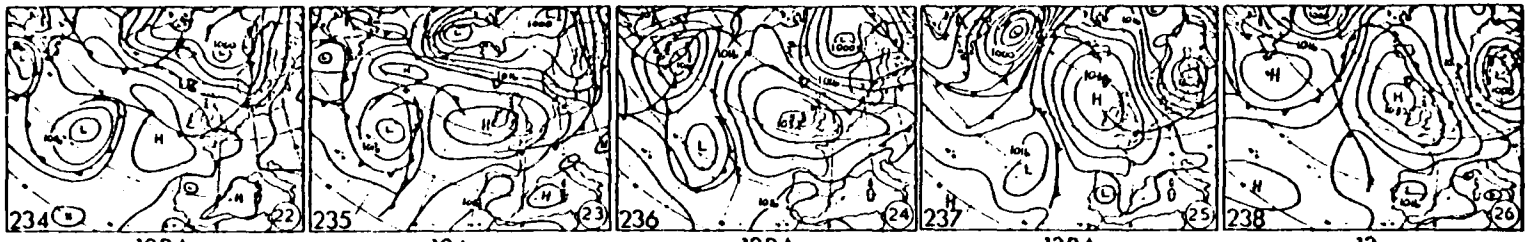

10RA 10A 12RA 13RA 13

AUGUST - PHASE 2 (contd.)

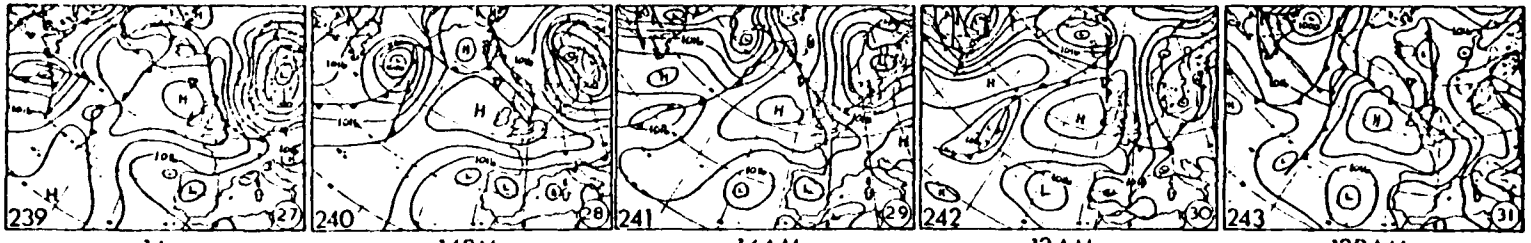

14 14RM 14AM 12AM 12RAM

Figure 19. **(contd.) DAILY WEATHER MAPS** (12GMT) 1 - 15 SEPTEMBER 1978

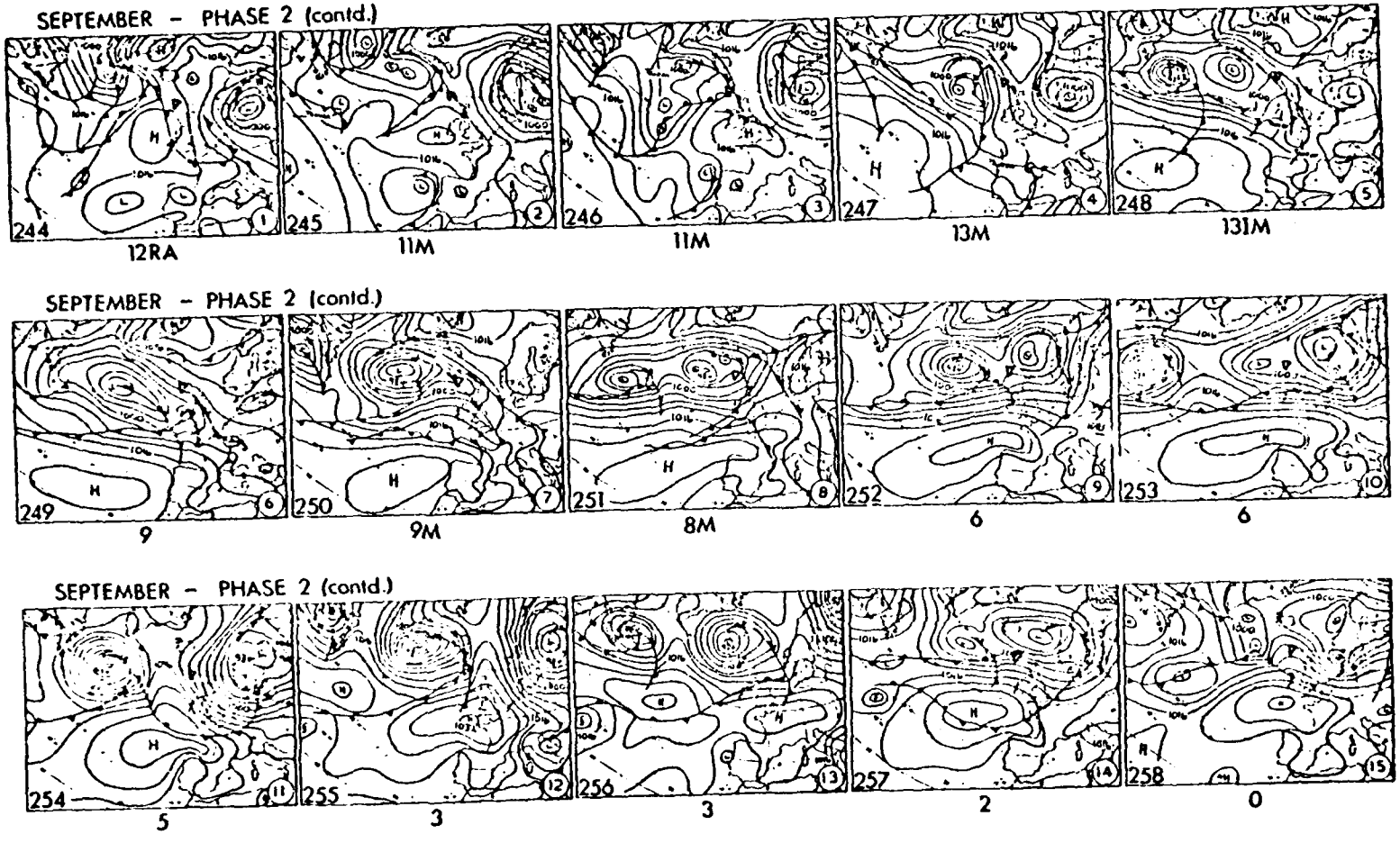

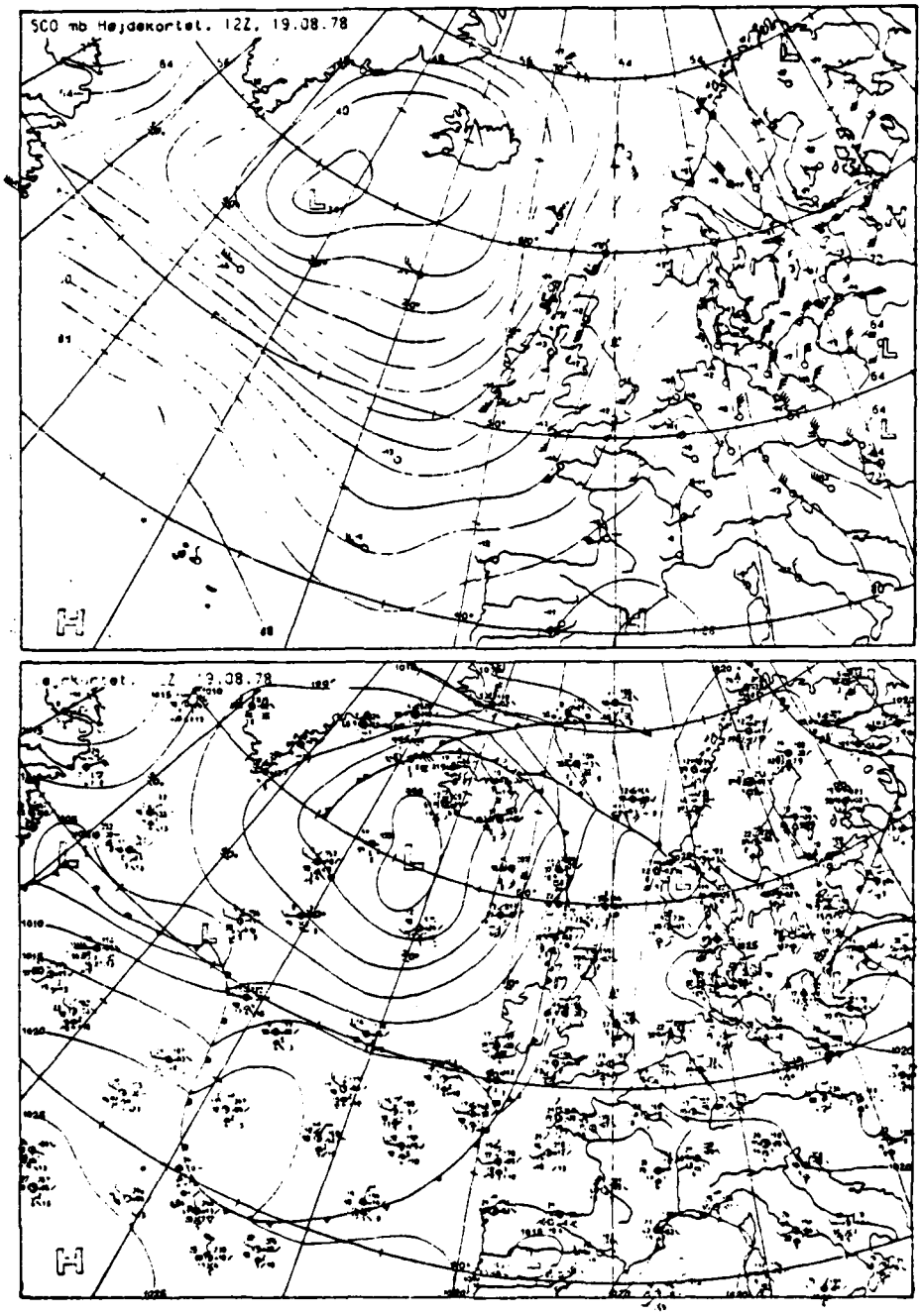

Figure 20, 500 mb (Top) and SFC Pressure Maps (Bottom), 1200 GMT 19 Aug 78.

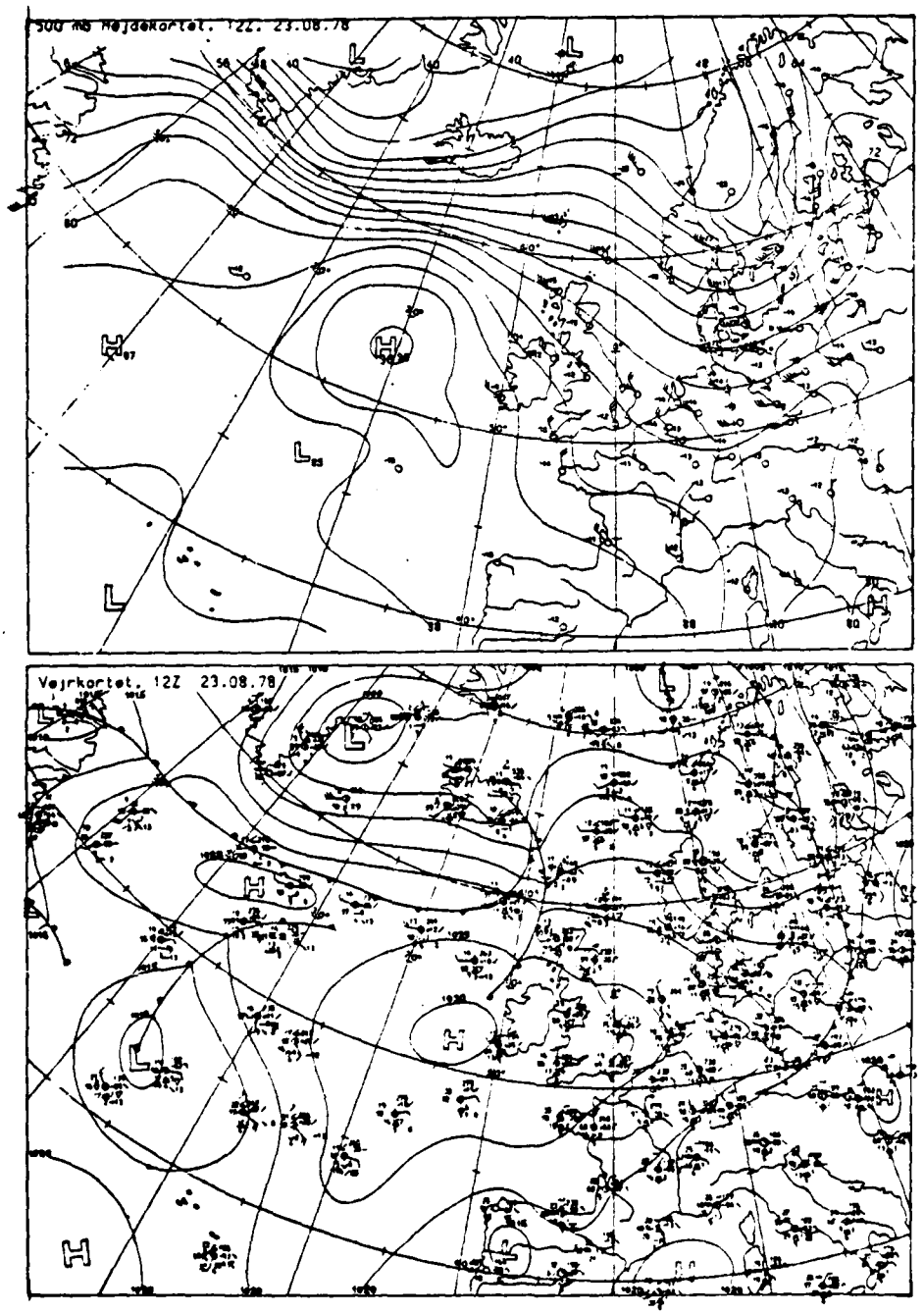

Figure 21. 500 mb (Top) and SFC Pressure (Bottom) Maps, 1200 GMT, 23 Aug 78.

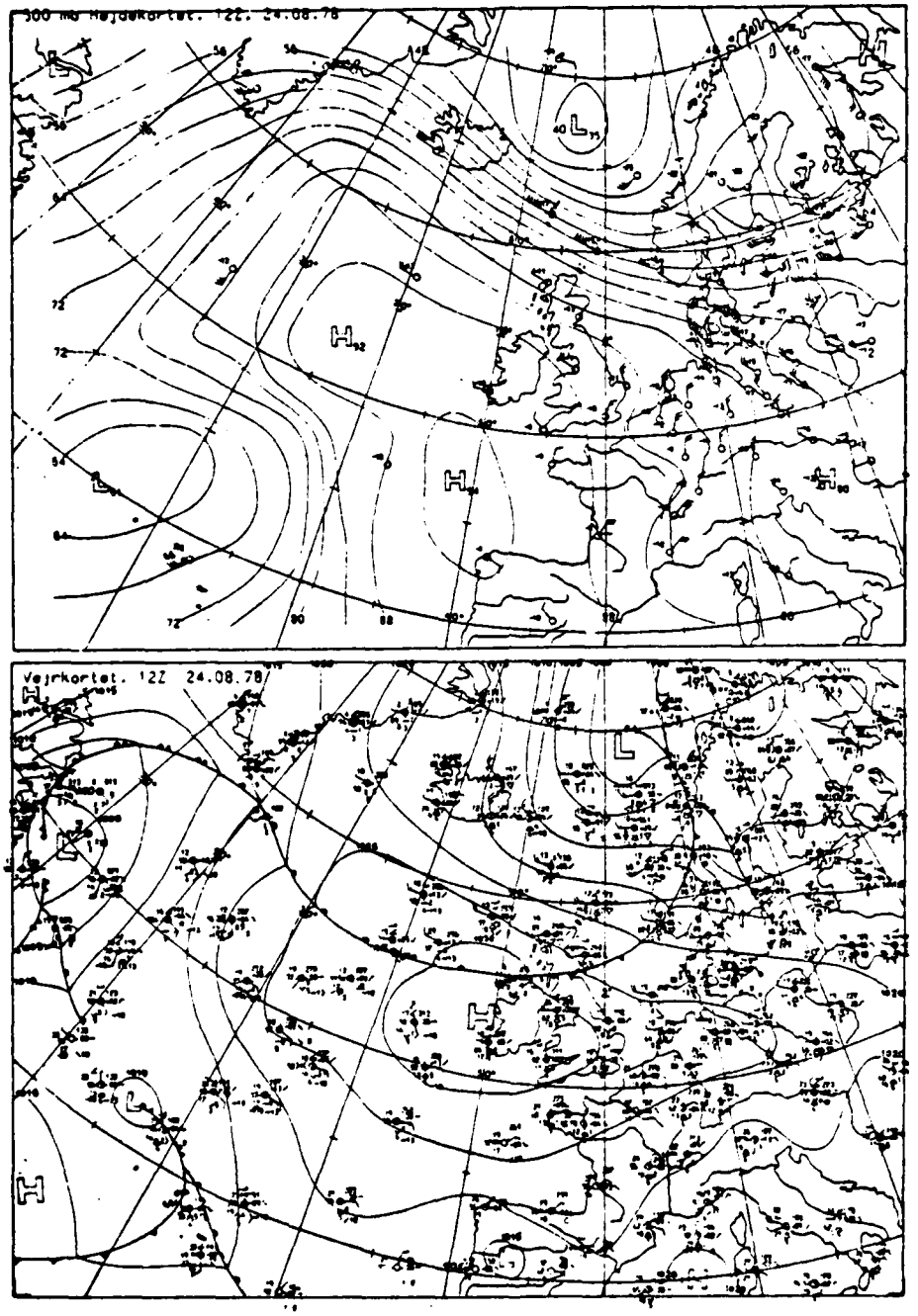

Figure 22. 500 mb (Top) and SFC Pressure (Bottom) Maps, 1200 GMT, 24 Aug 78.

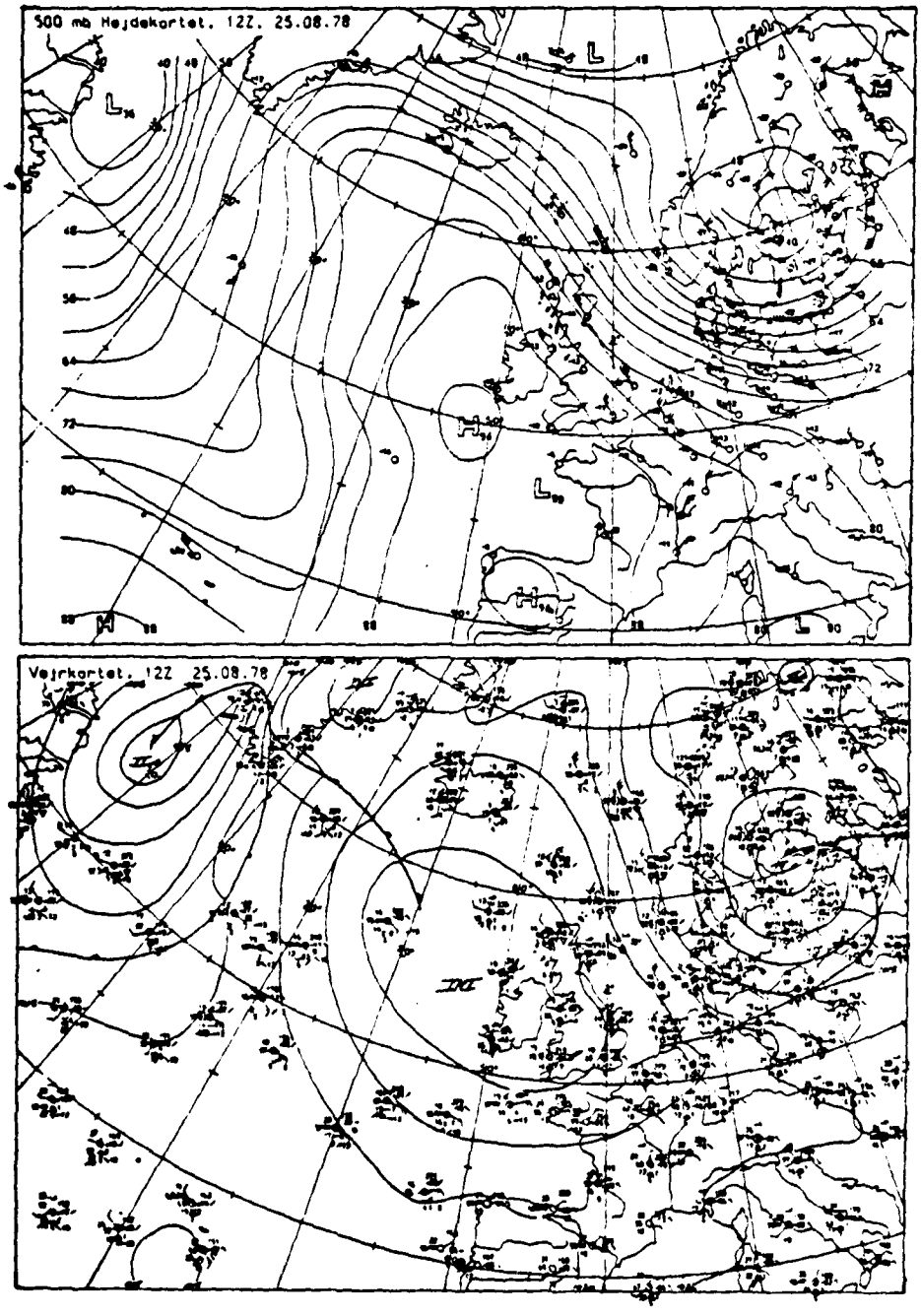

Figure 23. 500 mb (Top) and SFC Pressure (Bottom) Maps, 1200 GMT, 25 Aug 78.

APPENDIX B

Defense Meteorological Satellite Program (DMSP) imagery (visual and infrared) of the Northeast Atlantic and high-resolution imagery of the JASIN area corresponding to periods of significant ducting.

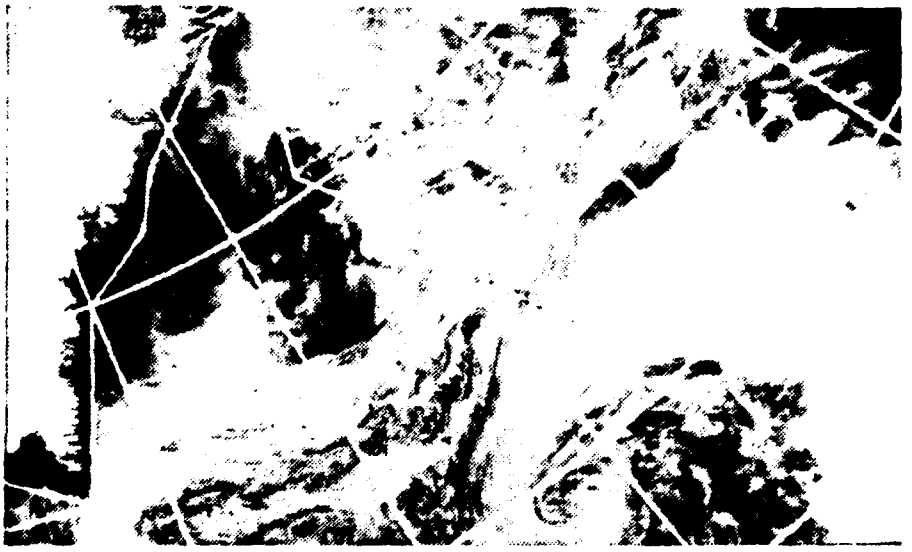

Figure 24. DMSP visual imagery, 25 July, 1212 GMT.

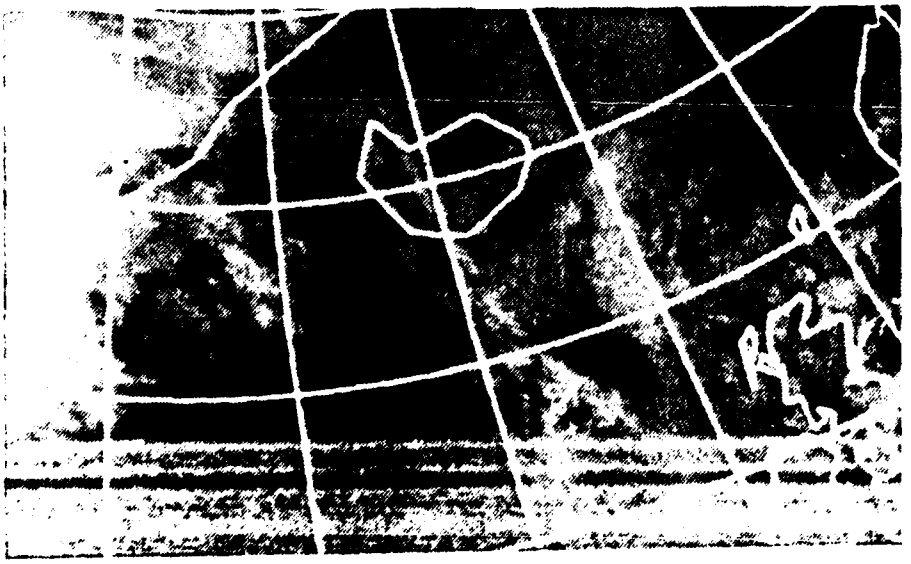

Figure 25. DMSP infrared imagery, 7 August, 1032 GMT.

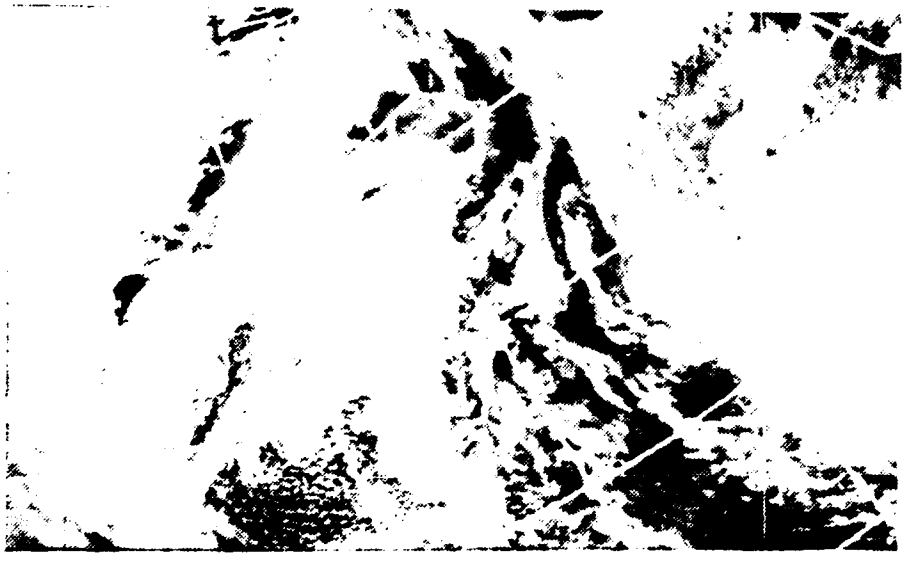

Figure 26. DMSP visual imagery, 8 August, 1145 GMT.

Figure 27. DMSP infrared imagery, 8 August, 1145 GMT.

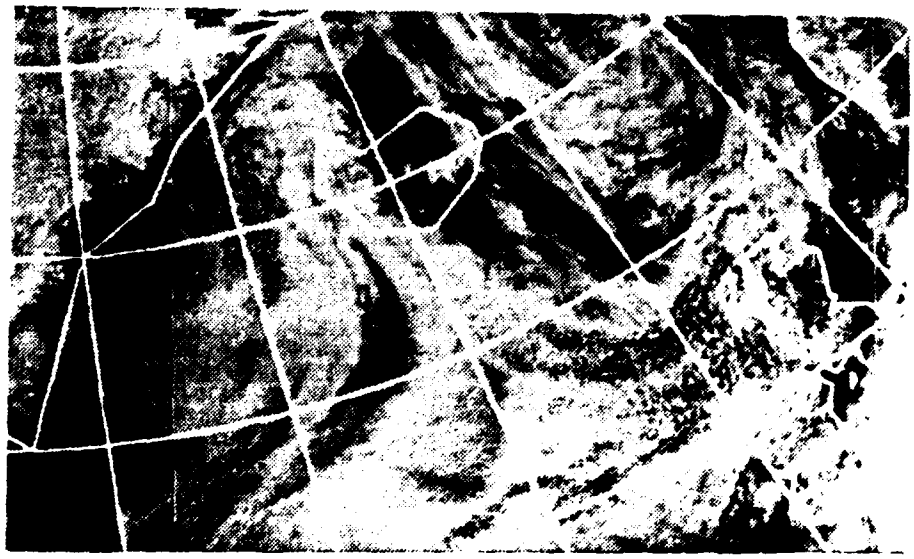

Figure 28. DMSP visual imagery, 22 August, 1110 GMT.

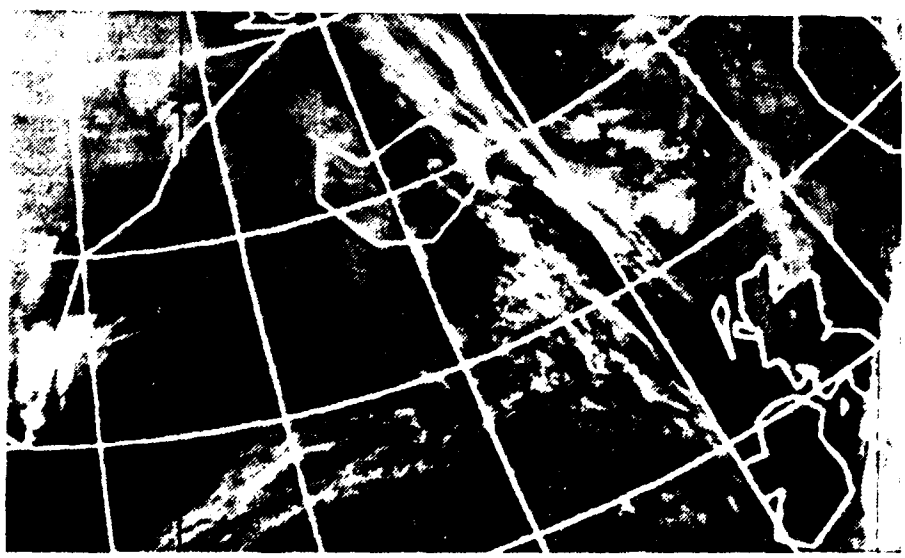

Figure 29. DMSP infrared imagery, 22 August, 1110 GMT.

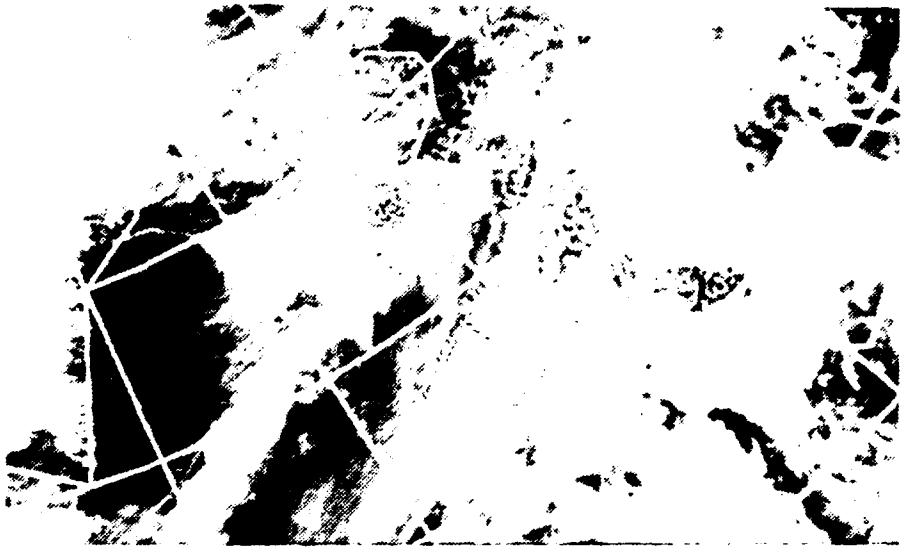

Figure 30. DMSP visual imagery, 23 August, 1221 GMT.

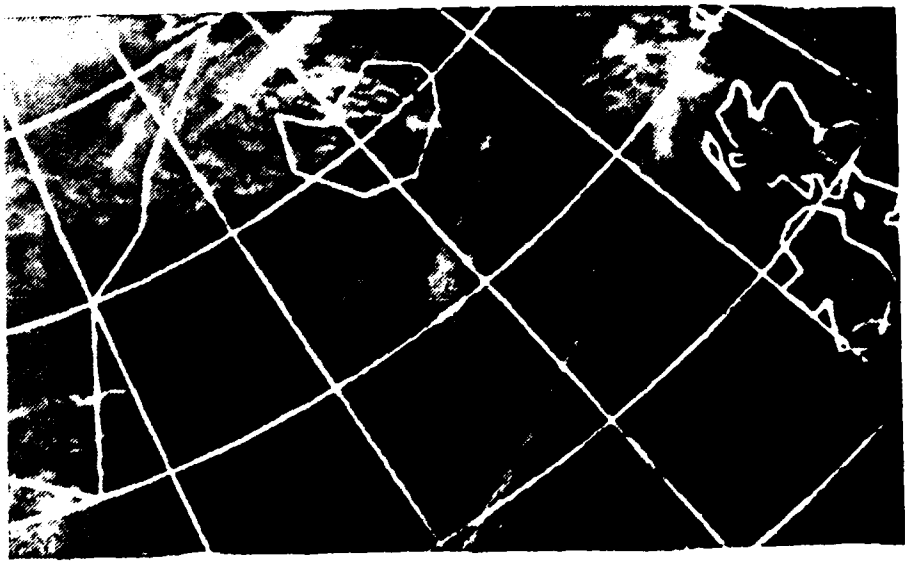

Figure 31. DMSP infrared imagery, 23 August, 1221 GMT.

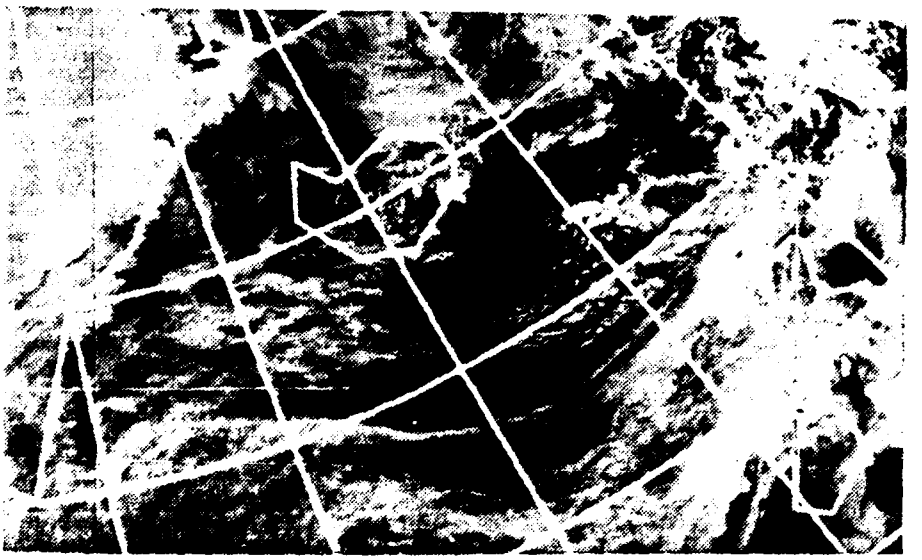

Figure 32. DMSP visual imagery, 24 August, 1138 GMT.

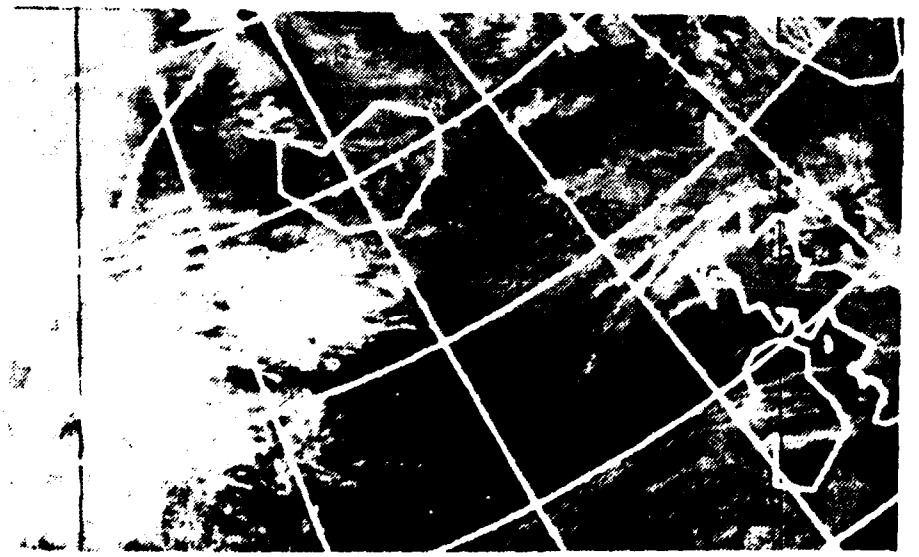

Figure 33. DMSP infrared imagery, 24 August, 1138 GMT.

Figure 34. DMSP visual imagery, 25 August, 1054 GMT.

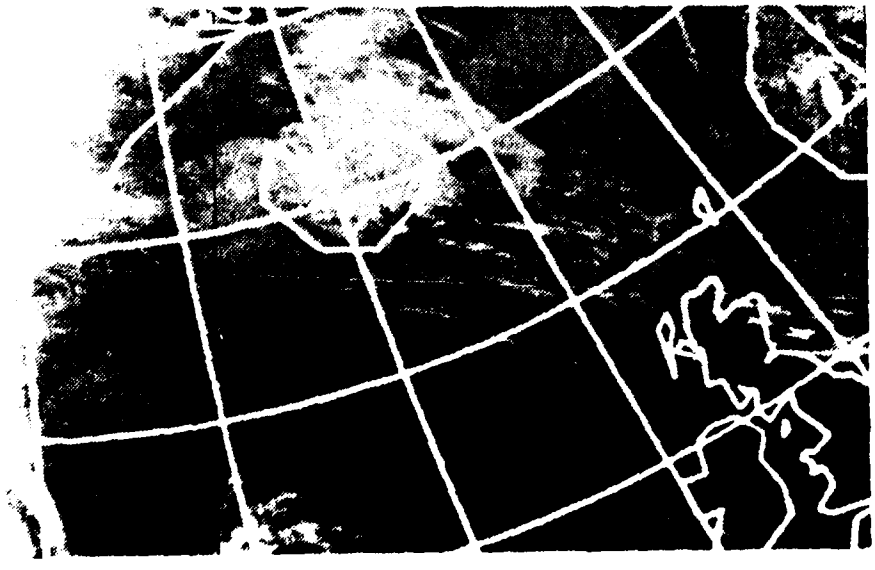

Figure 35. DMSP infrared imagery, 25 August, 1054 GMT.

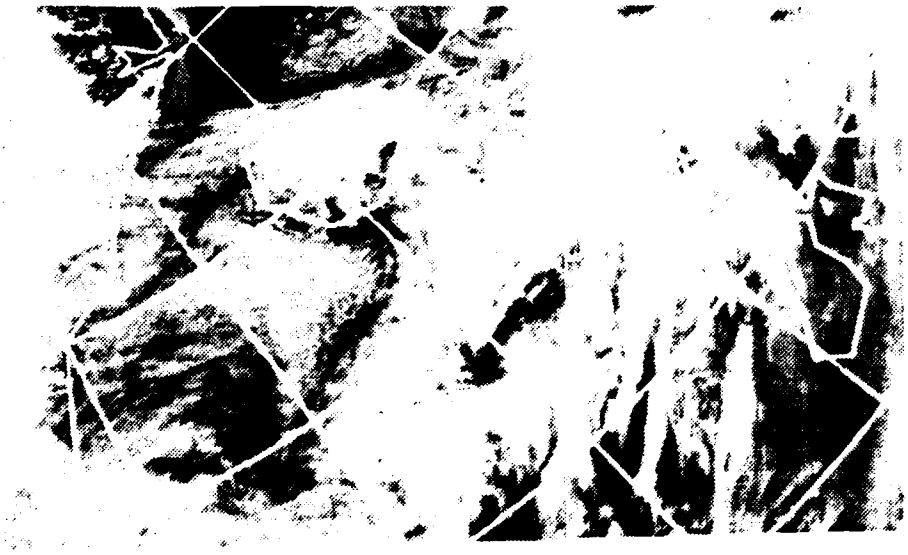

Figure 36. DMSP visual imagery, 28 August, 1233 GMT.

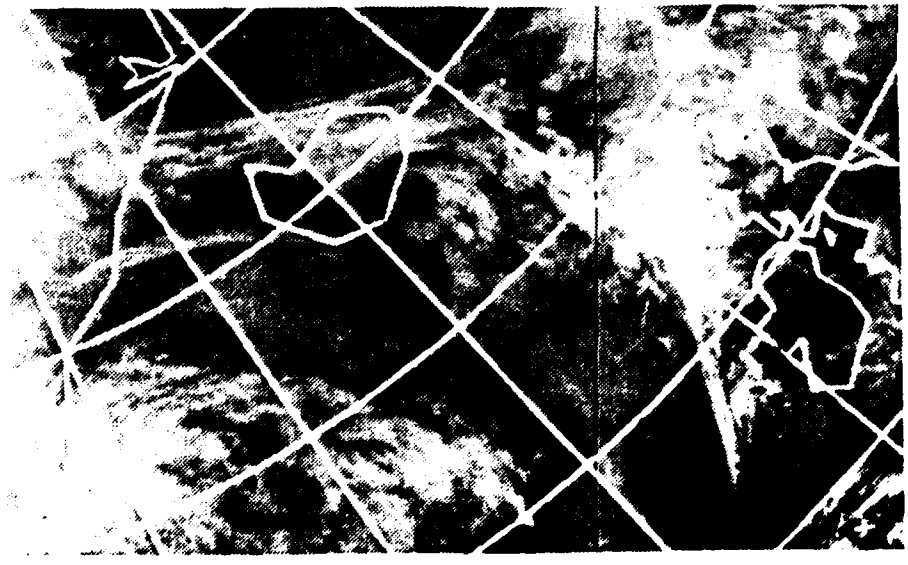

Figure 37. DMSP infrared imagery, 28 August, 1233 GMT.

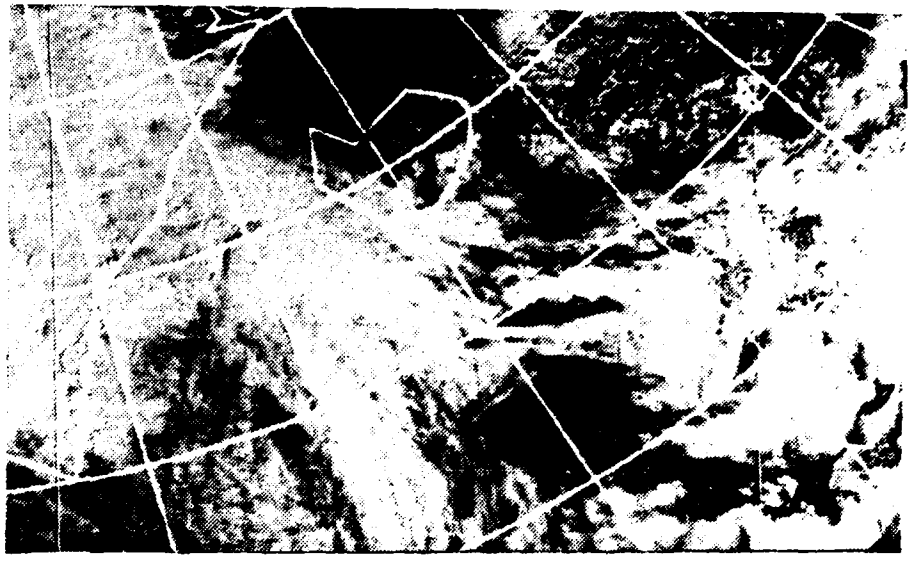

Figure 38. DMSP visual imagery, 29 August, 1150 GMT.

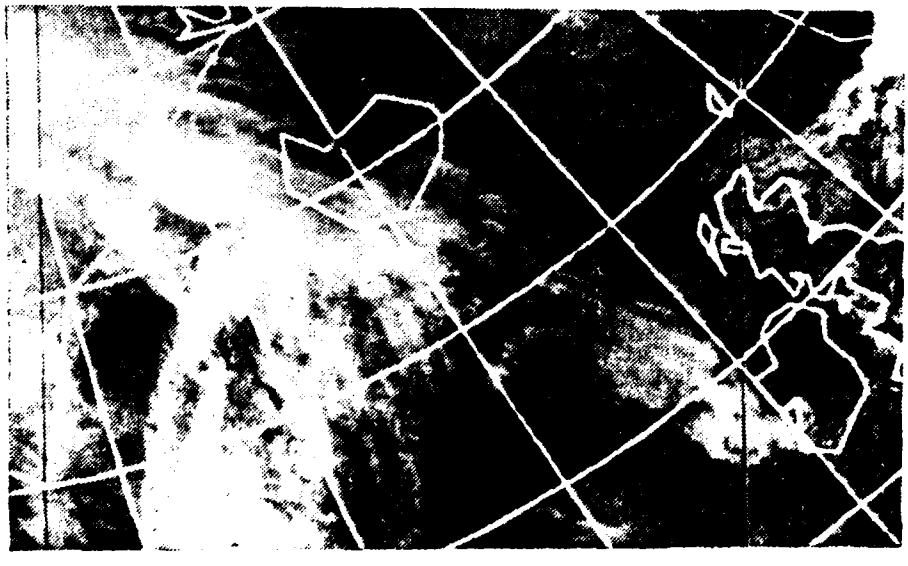

Figure 39. DMSP infrared imagery, 29 August, 1150 GMT.

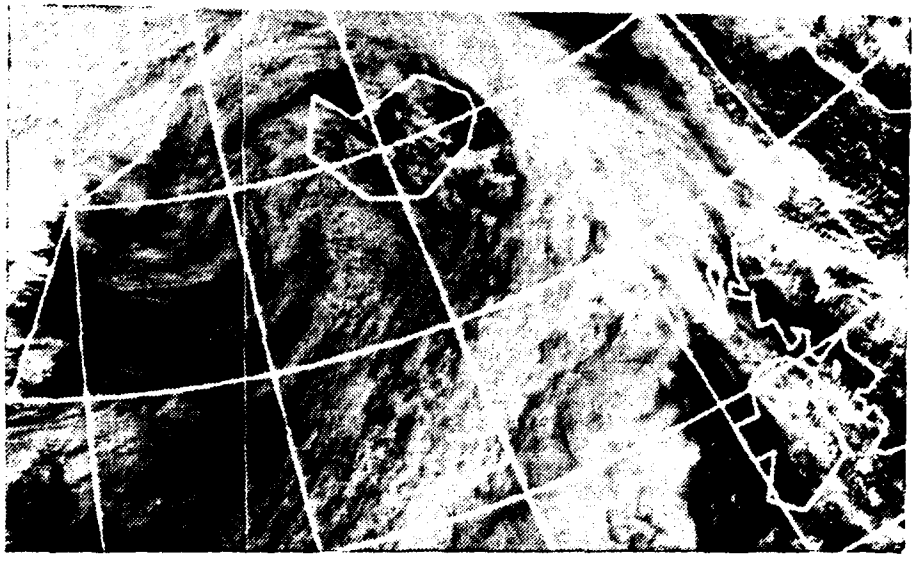

Figure 40. DMSP visual imagery, 30 August, 1107 GMT.

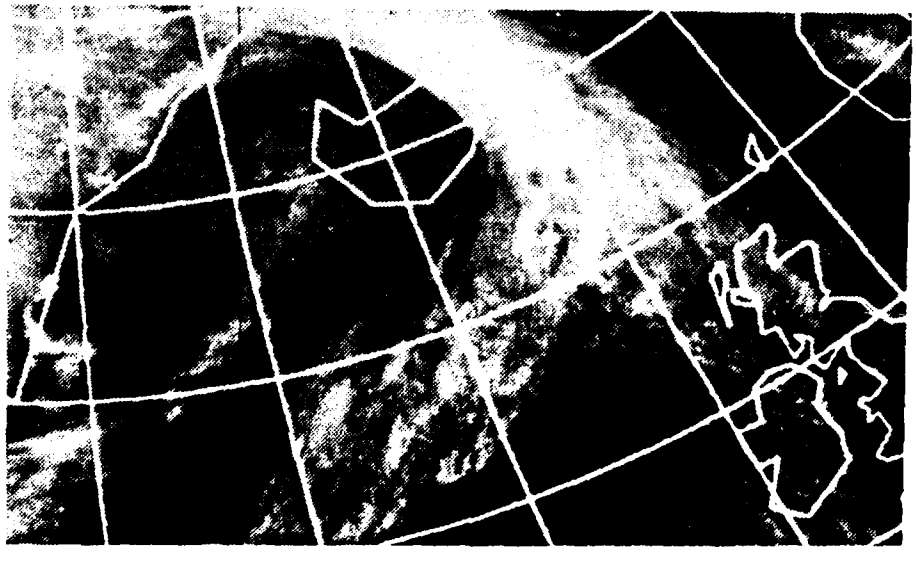

Figure 41. DMSP infrared imagery, 30 August, 1107 GMT.

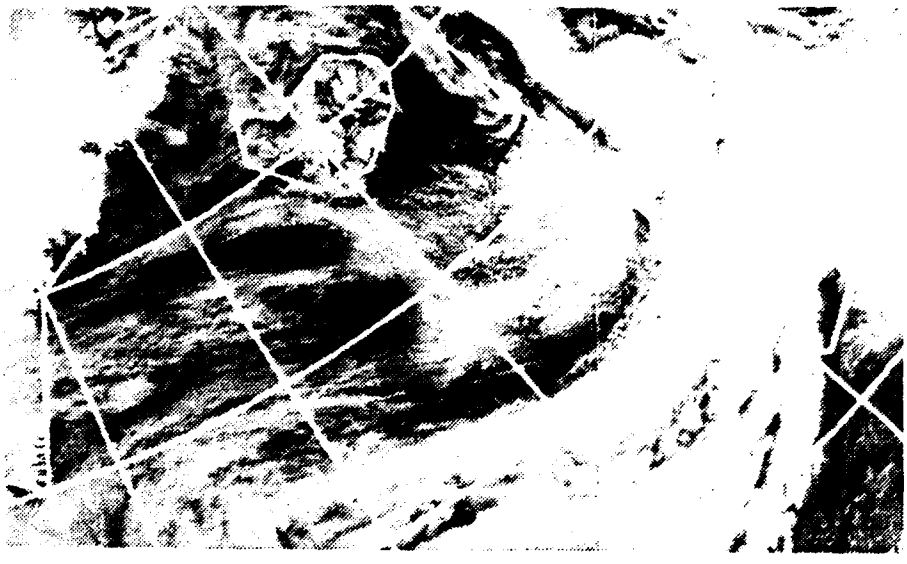

Figure 42. DMSP visual imagery, 31 August, 1218 GMT.

Figure 43. DMSP infrared imagery, 31 August, 1218 GMT.

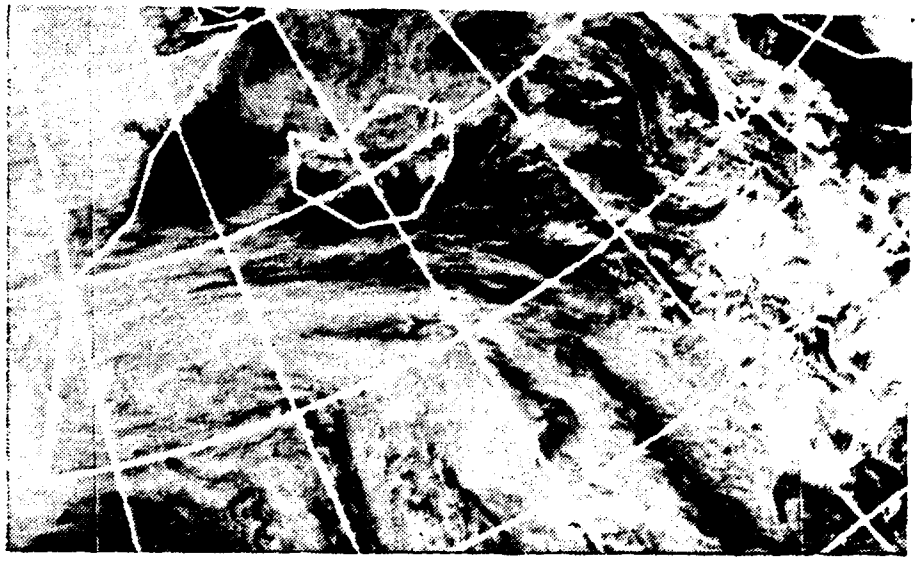

Figure 43.1 DMSP visual imagery, 1 Sept, 1135 GMT.

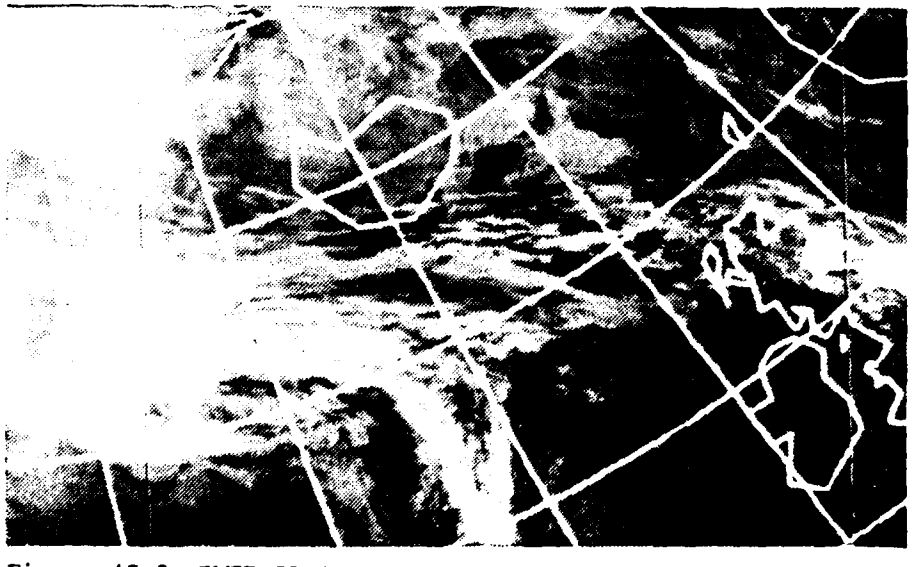

Figure 43.2 DMSP IR imagery, 1 Sept, 1135 GMT.

7 AUG (1200 GMT)

SHIP	Z/L	Z*	U*	T*	q*	U	TS-T	RH
ENDURER	-1.5	2.3	.08	-.13	-.073	2.0	2.9	100
METEOR	-.139	8.4	.27	-.06	-.108	7.2	1.7	78
MURRAY	-.062	4.5	.30	-.07	-.056	7.5	1.8	94

Figure 44. High-resolution DMSP visual imagery and surface data.

7 AUG (1200 GMT)

SHIP	Z/L	Z*	U*	T*	q*	U	TS-T	RH
ENDURER	-1.5	2.3	.08	-.13	-.073	2.0	2.9	100
METEOR	-.139	8.4	.27	-.06	-.108	7.2	1.7	78
MURRAY	-.062	4.5	.30	-.07	-.056	7.5	1.8	94

Figure 45. High-resolution DMSP IR imagery and surface data.

8 AUG (1200 GMT)

SHIP	Z/L	Z*	U*	T*	q*	U	TS-T	RH
ENDURER	-.063	4.2	.07	-.05	-.103	2.0	1.3	82
METEOR	-.506	7.1	.17	-.08	-.132	4.6	2.3	76
MURRAY	-.232	4.5	.19	-.10	-.079	5.0	2.7	92

Figure 46. High-resolution DMSP visual imagery and surface data.

8 AUG (1200 GMT)

SHIP	Z/L	Z*	U*	T*	q*	U	TS-T	RH
ENDURER	-.063	4.2	.07	-.05	-.103	2.0	1.3	82
METEOR	-.506	7.1	.17	-.08	-.132	4.6	2.3	76
MURRAY	-.232	4.5	.19	-.10	-.079	5.0	2.7	92

Figure 47. High-resolution DMSP IR imagery and surface data.

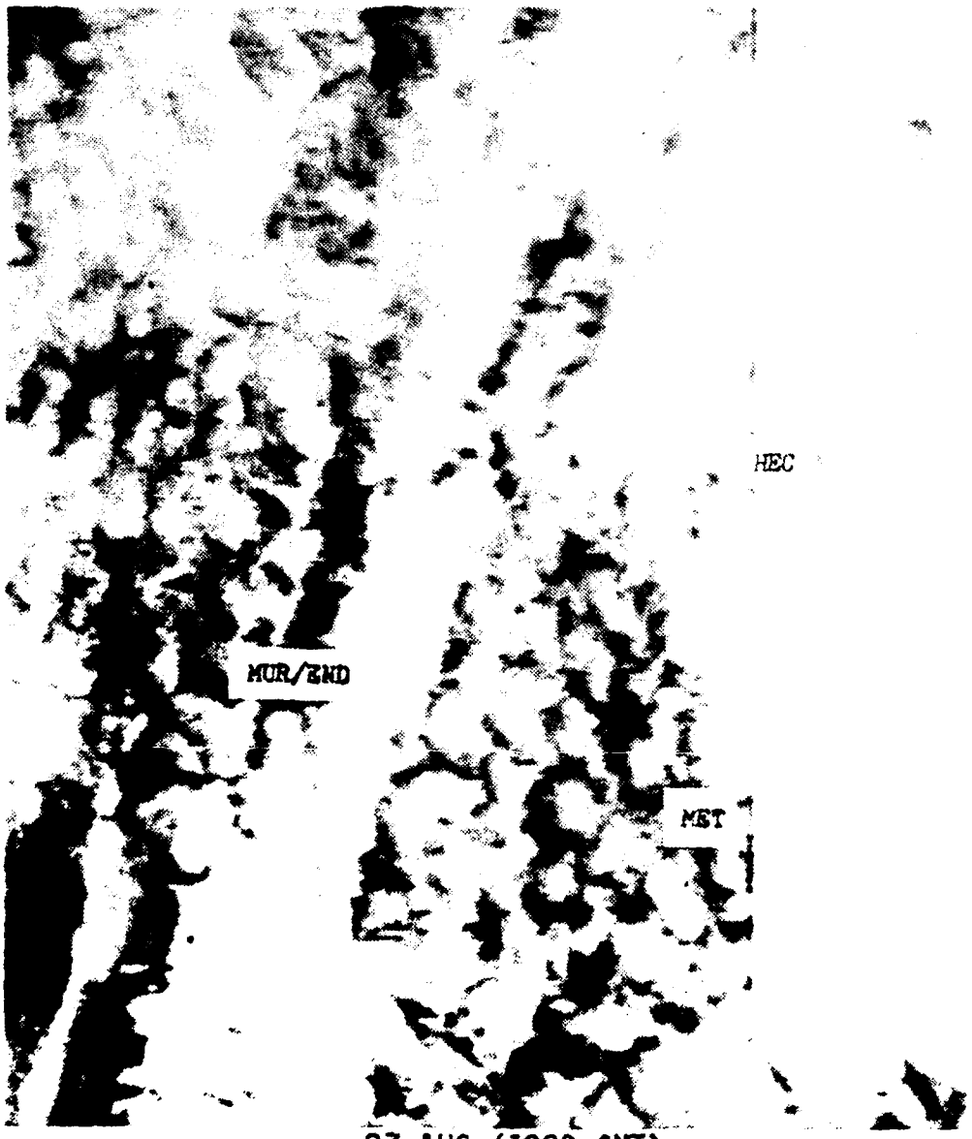

23 AUG (1200 GMT)

SHIP	Z/L	Z*	U*	T*	q*	U	TS-T	RH
MURRAY	-.049	5.0	.21	-.02	-.051	5.5	.6	88
ENDURER	-.004	6.6	.62	-.02	-.059	14.0	.5	86
METEOR	-.012	3.5	.41	-.01	-.030	10.8	.4	93
HECLA	-.021	2.8	.48	.04	-.016	12.5	-1.0	89

Figure 48. High-resolution DMSP visual imagery and surface data.

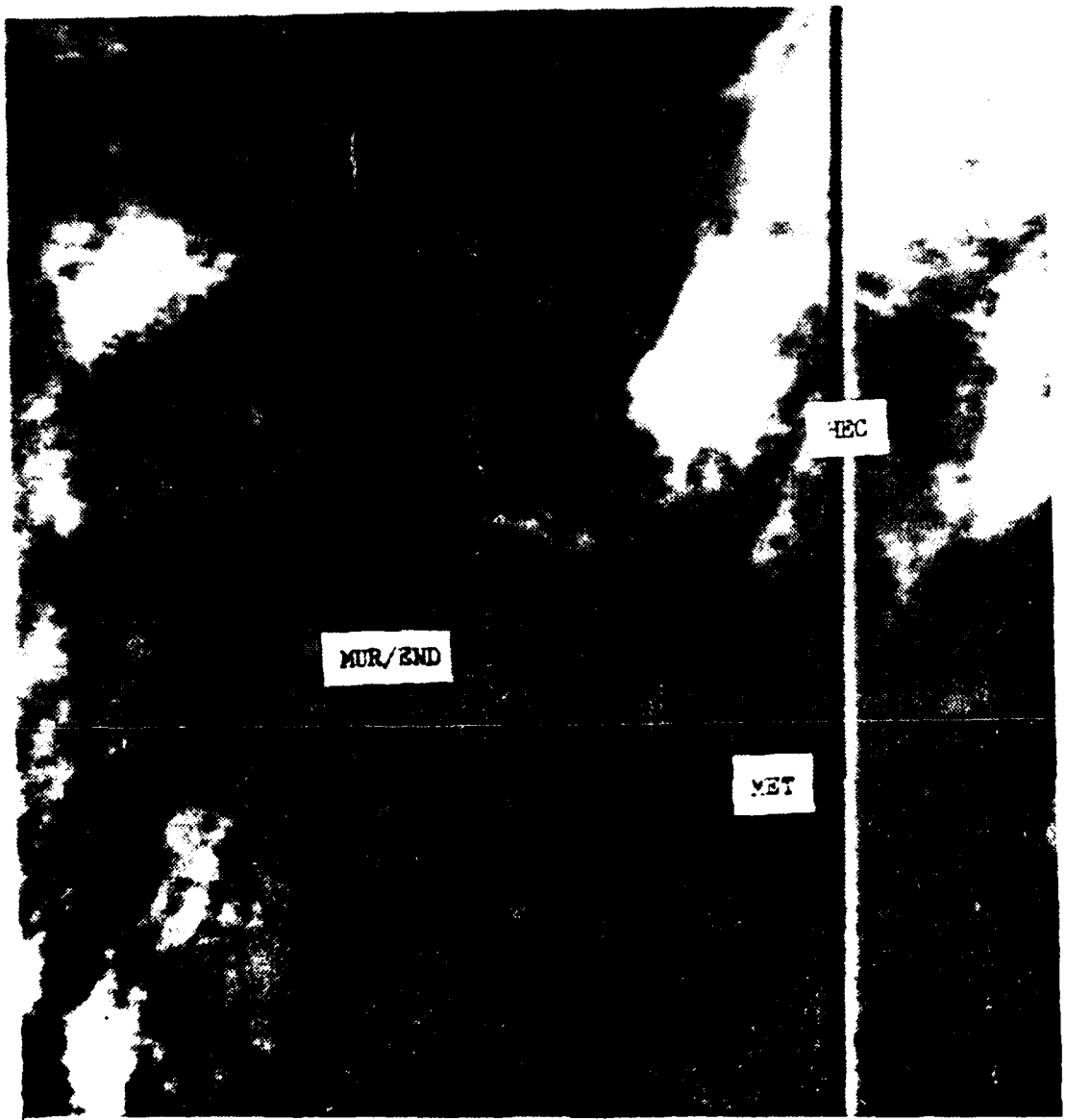

23 AUG (1200 GMT)

SHIP	Z/L	Z*	U*	T*	q*	U	TS-T	RH
MURRAY	-.049	5.0	.21	-.02	-.051	5.5	.6	88
ENDURER	-.004	6.6	.62	-.02	-.059	14.0	.5	86
METEOR	-.012	3.5	.41	-.01	-.030	10.8	.4	93
HECLA	-.021	2.8	.48	.04	-.016	12.5	-1.0	89

Figure 10. High-resolution DMSP IR imagery and surface data.

24 AUG (1200 GMT)

SHIP	Z/L	Z*	U*	T*	q*	U	TS-T	RH
MURRAY	-.008	8.1	.36	.00	-.070	9.0	.1	80
ENDURER	-.010	12.2	.45	.01	-.099	10.5	-.3	71
METEOR	-.009	4.3	.43	.02	-.032	11.3	-.4	88
HECLA	-.043	4.2	.39	.05	-.022	10.5	-1.4	84

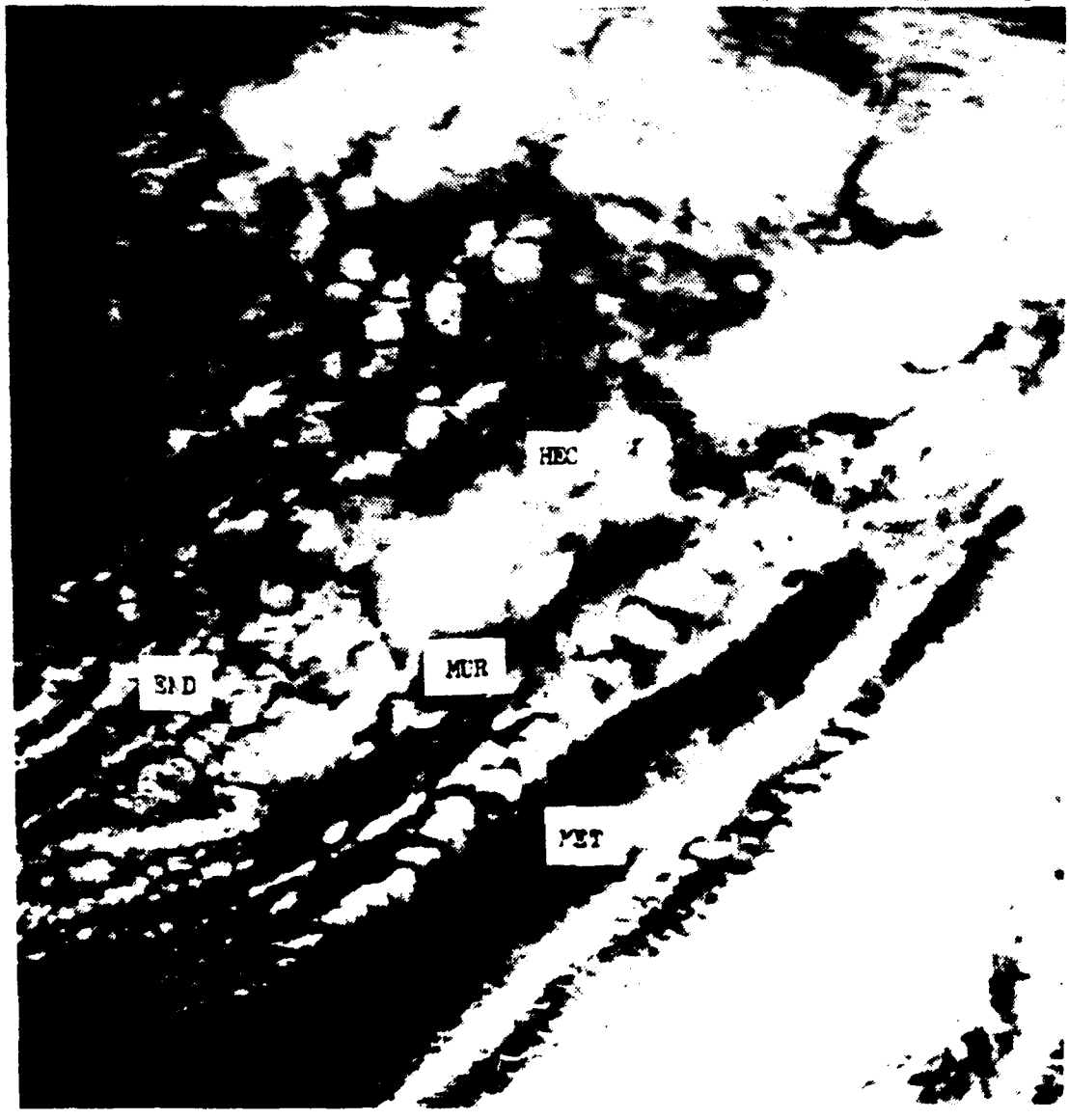

Figure 50. High-resolution DMSP visual imagery and surface data.

24 AUG (1200 GMT)

SHIP	Z/L	Z*	U*	T*	q*	U	TS-T	RH
MURRAY	-.008	8.1	.36	.00	-.070	9.0	.1	80
ENDURER	-.010	12.2	.45	.01	-.099	10.5	-.3	71
METEOR	-.009	4.3	.43	.02	-.032	11.3	-.4	88
HECLA	-.043	4.2	.39	.05	-.022	10.5	-1.4	84

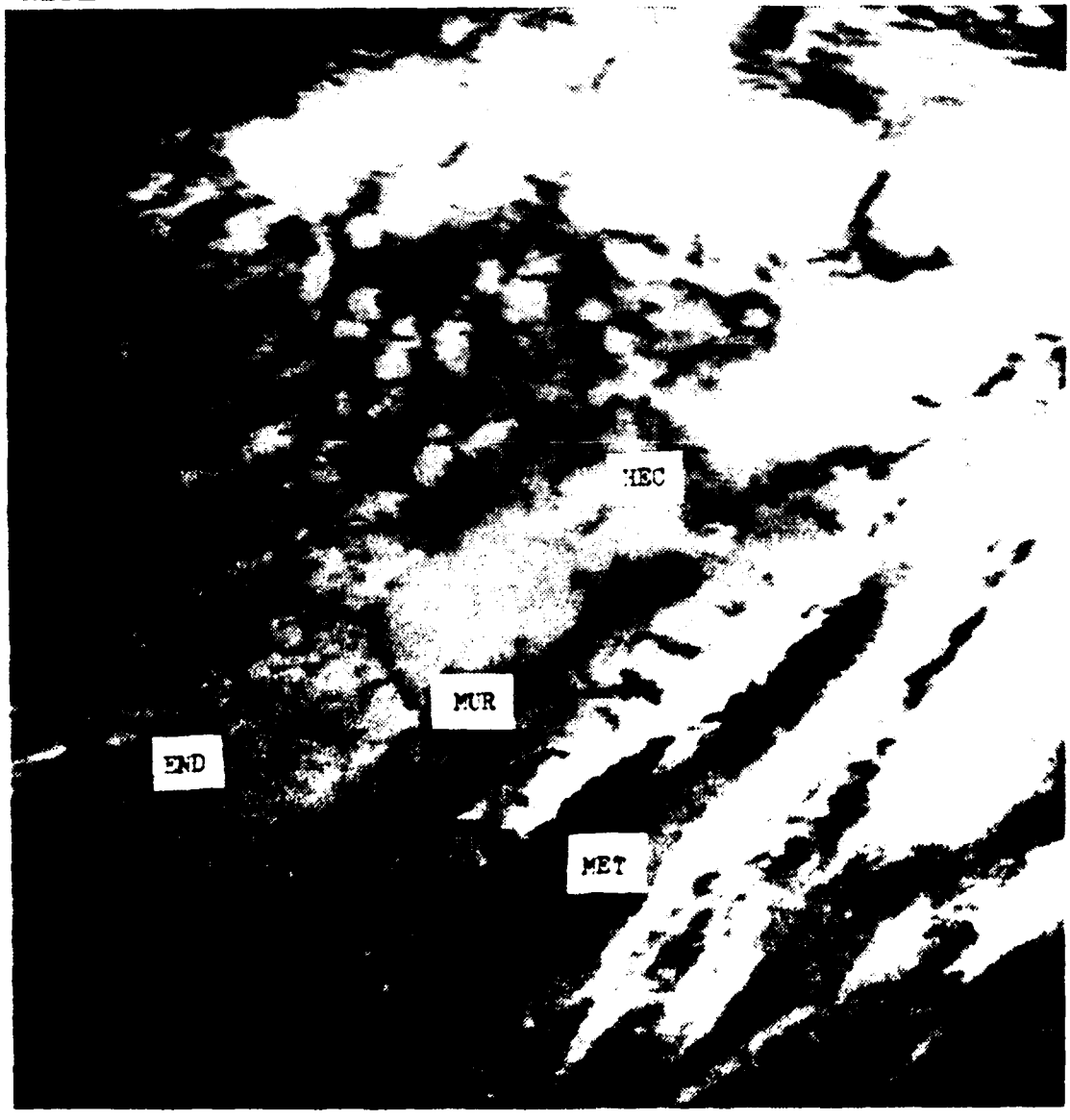

Figure 51. High-resolution DMSP IR imagery and surface data.

25 AUG (1200 GMT)

SHIP	Z/L	Z*	U*	T*	q*	U	TS-T	RH
MURRAY	-.072	5.4	.16	-.02	-.058	4.5	.5	86
ENDURER	-.058	2.6	.17	-.03	-.031	4.5	.8	96
METEOR	-.011	4.6	.18	.00	-.037	5.1	.0	89
HECLA	_.024	2.8	.17	.05	-.007	5.5	-1.6	88

Figure 52. High-resolution DMSP visual imagery and surface data.

25 AUG (1200 GMT)

SHIP	Z/L	Z*	U*	T*	q*	U	TS-T	RH
MURRAY	-.072	5.4	.16	-.02	-.058	4.5	.5	86
ENDURER	-.058	2.6	.17	-.03	-.031	4.5	.8	96
METEOR	-.011	4.6	.18	.00	-.037	5.1	.0	89
HECLA	-.024	2.8	.17	.05	-.007	5.5	-1.6	88

Figure 53. High-resolution DMSP IR imagery and surface data.

30 AUG (1200 GMT)

SHIP	Z/L	Z*	U*	T*	q*	U	TS-T	RH
ENDURER	-.025	1.9	.29	-.04	-.023	7.0	1.0	100
METEOR	-.019	2.1	.14	.00	-.017	4.1	.1	95
HECLA	-.041	5.1	.44	-.05	-.055	11.4	1.5	91

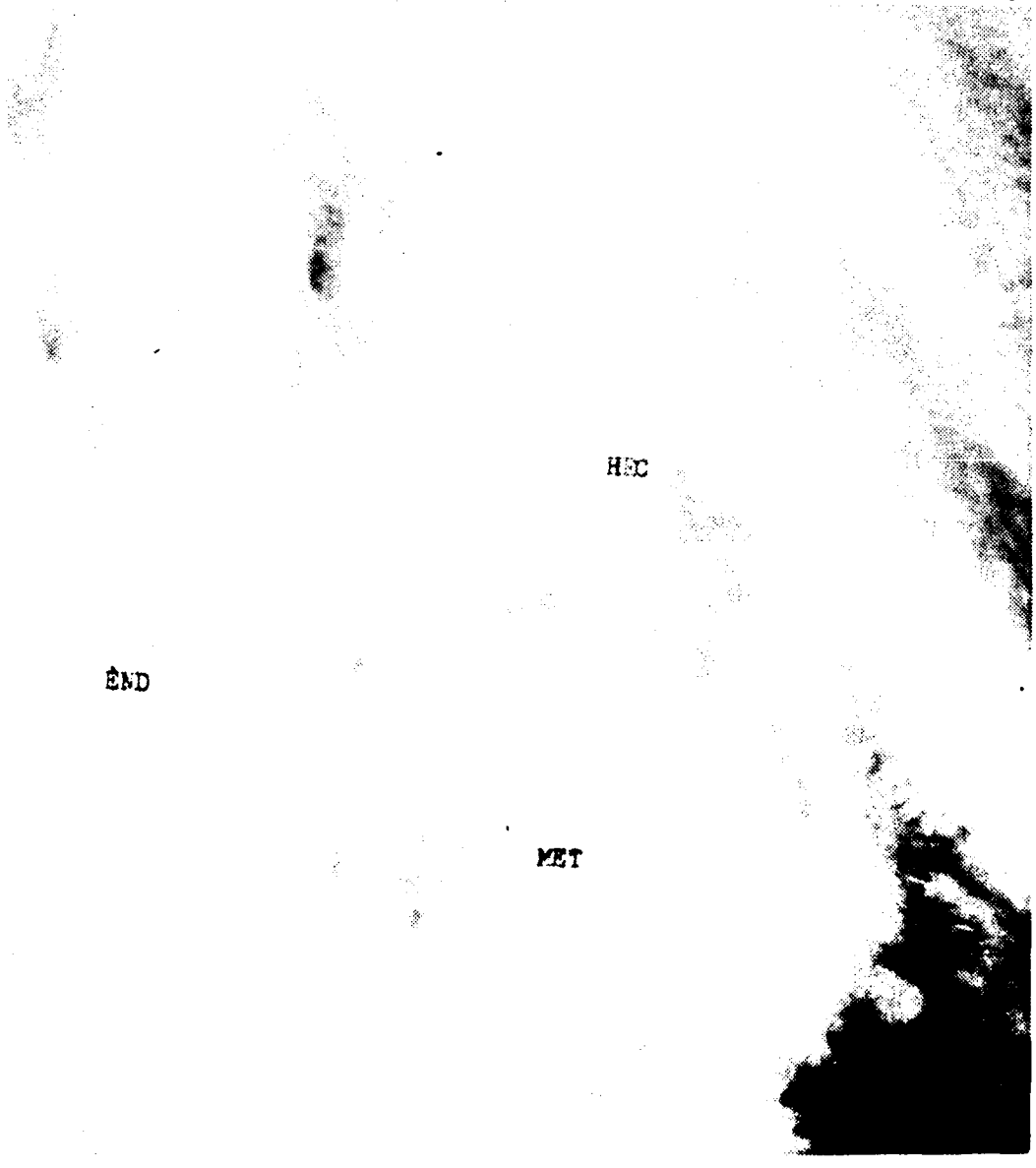

Figure 54. High-resolution DMSP visual imagery and surface data.

30 AUG (1200 GMT)

SHIP	Z/L	Z*	U*	T*	q*	U	TS-T	RH
ENDURER	-.025	1.9	.29	-.04	-.023	7.0	1.0	100
METEOR	-.019	2.1	.14	.00	-.017	4.1	.1	95
HECLA	-.041	5.1	.44	-.05	-.055	11.4	1.5	91

Figure 55. High-resolution DMSP IR imagery and surface data.

AD-A096 363 NAVAL POSTGRADUATE SCHOOL MONTEREY CA F/G 4/2
EVAPORATION DUCT OCCURRENCES IN THE NORTHEAST ATLANTIC DURING L--ETC(U)
SEP 80 T E CALLAHAM

UNCLASSIFIED NL

2 OF 2
AD A096363

END
4-81

31 AUG (1200GMT)

SHIP	Z/L	Z*	U*	T*	q*	U	TS-T	RH
ENDURER	-.023	8.6	.36	-.05	-.092	8.5	1.2	80
METEOR	-.034	13.4	.41	-.02	-.132	10.8	.7	64
HECLA	-.019	11.3	.35	.00	-.101	9.2	.1	69

Figure 56. High-resolution DMSP visual imagery and surface data.

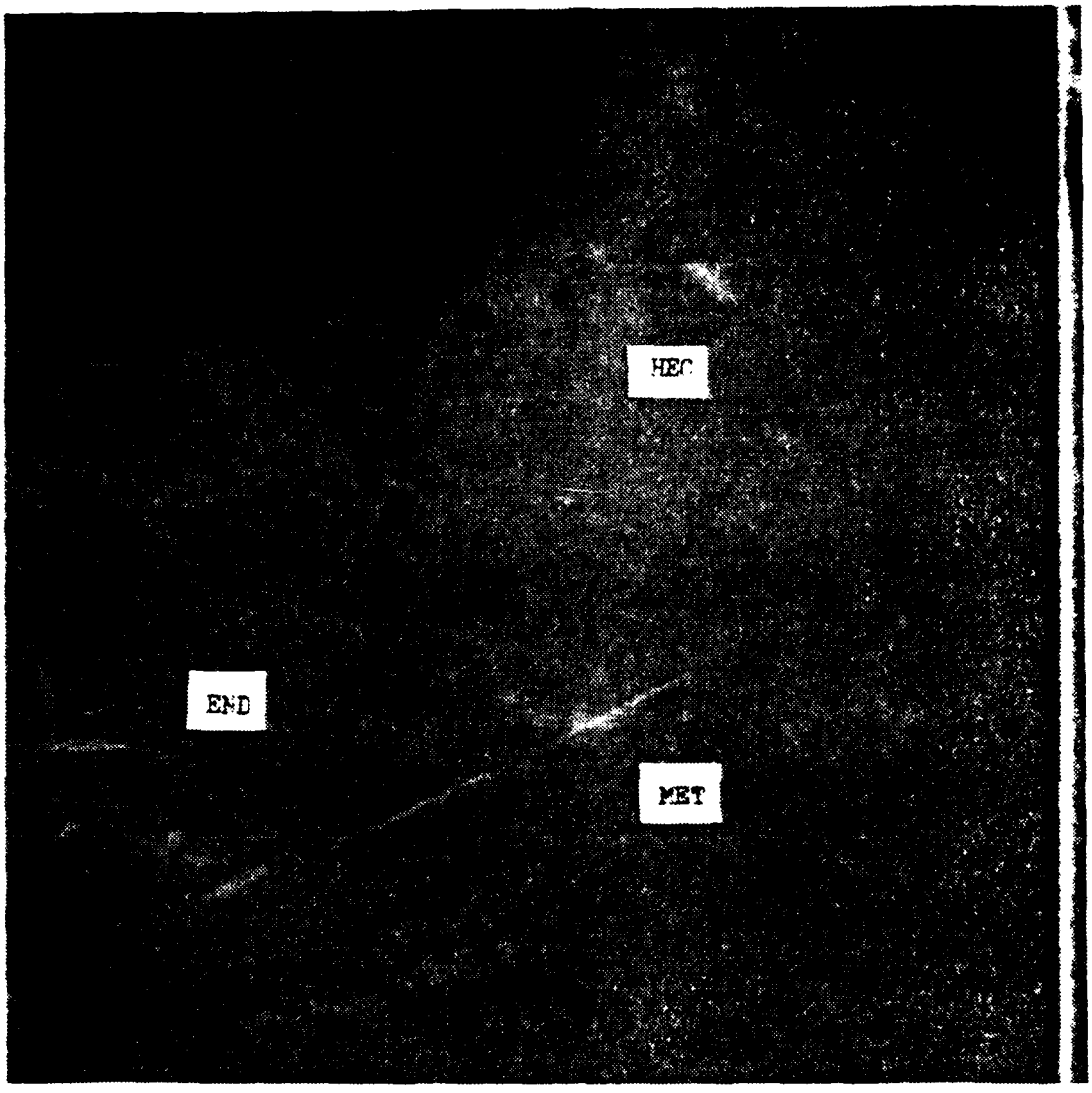

31 AUG (1200GMT)

SHIP	Z/L	Z*	U*	T*	q*	U	TS-T	RH
ENDURER	-.023	8.6	.36	-.05	-.092	8.5	1.2	80
METEOR	-.034	13.4	.41	-.02	-.132	10.8	.7	64
HECLA	-.019	11.3	.35	.00	-.101	9.2	.1	69

Figure 57. High-resolution DMSP IR imagery and surface data.

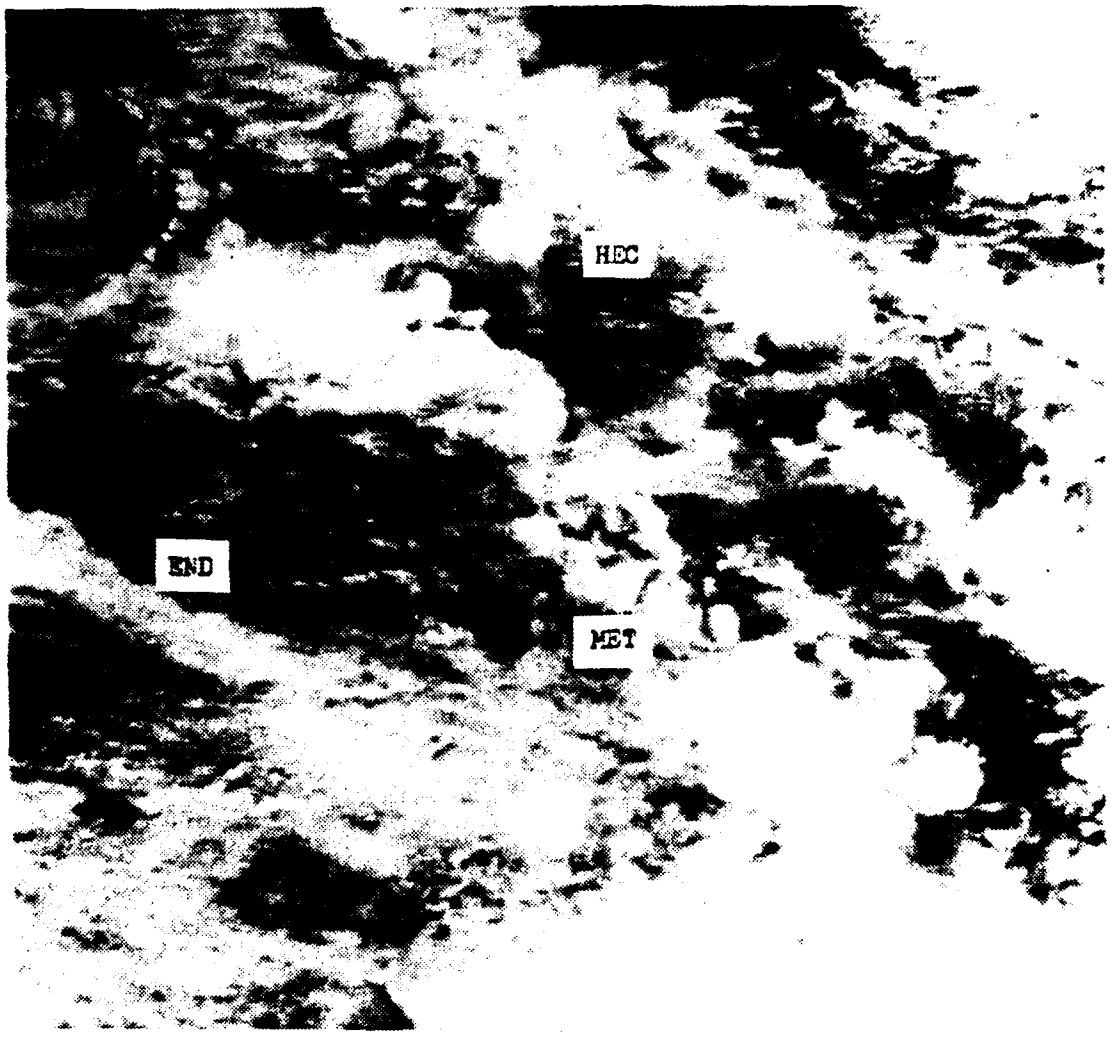

1 SEPT (1200 GMT)

SHIP	Z/L	Z*	U*	T*	q*	U	TS-T	RH
ENDURER	-.029	4.5	.24	-.03	-.048	6.0	.7	91
METEOR	-.048	7.8	.31	-.02	-.077	8.2	.7	81
HECLA	-.043	5.4	.22	-.01	-.050	6.1	.3	86

Figure 58. High-resolution DMSP visual imagery and surface data.

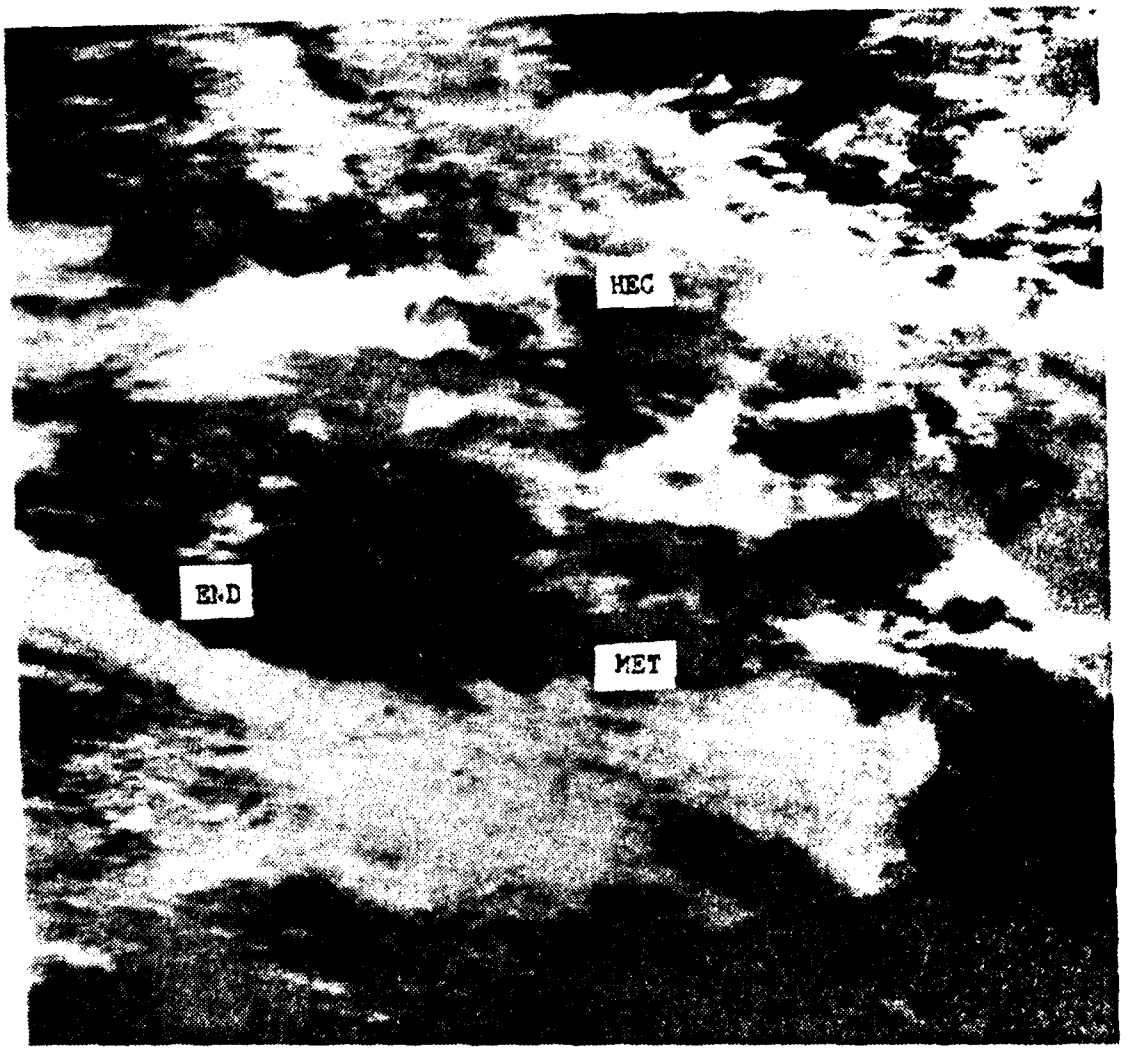

1 SEPT (1200 GMT)

SHIP	Z/L	Z*	U*	T*	q*	U	TS-T	RH
ENDURER	-.029	4.5	.24	-.03	-.048	6.0	.7	91
METEOR	-.048	7.8	.31	-.02	-.077	8.2	.7	81
HECLA	-.043	5.4	.22	-.01	-.050	6.1	.3	86

Figure 59. High-resolution DMSP IR imagery and surface data.

LIST OF REFERENCES

Batchelor, G. K., 1953: The Theory of Homogeneous Turbulence, Cambridge University Press, Cambridge, England.

Battan, L. J., 1959: Radar Meteorology, The University of Chicago Press.

Businger, J. A., 1973: Workshop on Micrometeorology, AMS Publication (Science Press, Ephrata, Pa.), 76-77.

Businger, J. A., Wyngaard, J. C., Izumi, Y. and Bradley, E. F., 1971: Atmospheric Science, 28, 181.

Davidson, K. L., Houlihan, T. M., Fairall, C. W., and Schacher, G. E., 1978: Boundary Layer Meteorology, 15, 507-523.

Fairall, C. W., Davidson, K. L., Schacher, G. E. and Houlihan, T. M., 1978: Evaporation Duct Height Measurements in the Mid-Atlantic, NPS61-78-05, Naval Postgraduate School, Monterey.

Guymer, T. H. and Taylor, P. K., 1978: Preliminary Assessment of Shipboard Meteorological Program, JASIN News, No. 14, 3-8.

Hitney, H. V., 1975: Propagation Modeling in the Evaporation Duct, NELC TR 7947, Naval Electronics Laboratory Center, San Diego.

Holland, J. Z., 1968: An Application of Some Statistical Techniques to the Study of Eddy Structure, TID-24585, U. S. Atomic Energy Commission, Washington, D. C.

Jeske, H., 1971: The State of Radar Range Prediction Over Sea. Tropospheric Radio Wave Propagation - Part III, NATO-AGARD.

Katzin, M., Bauchman, R. W., and Binnian, W., 1947: 3- and 9- Centimeter Propagation in Low Ocean Ducts, Proc. IEEE, 35, 891-905.

Kerr, E. C., 1951: Propagation of Short Radio Waves, McGraw-Hill Book Company.

Kondo, J., 1975: Boundary Layer Meteorology, 9, 91.

Liu, W. T. and Katsaros, K. B., 1978: Preliminary Analysis of the Sea Surface Temperature Variations During JASIN '78.

Macklin, S. A. and Guymer, T. H., 1980: Interplatform Comparisons of JASIN WMO Observations, JASIN News, No. 15, 5-9.

Sweet, W., 1979: Monthly Climatology for Evaporation Duct Occurrence in the North Atlantic Ocean, NEPRF TR 79-01, Naval Environmental Prediction Research Facility, Monterey.

INITIAL DISTRIBUTION LIST

		No. Copies
1.	Defense Technical Information Center Cameron Station Alexandria, Virginia 22314	2
2.	Library, Code 0142 Naval Postgraduate School Monterey, California 93940	2
3.	Commander Naval Oceanography Command NSTL Station, Mississippi 39529	1
4.	Commanding Officer Fleet Numerical Oceanography Center Monterey, California 93940	1
5.	Officer-in-Charge Naval Environmental Prediction Research Facility Monterey, California 93940	1
6.	Prof. G. J. Haltiner, Code 63Ha Naval Postgraduate School Monterey, California 93940	1
7.	Prof. C.N.K. Mooers, Code 68Mr Naval Postgraduate School Monterey, California 93940	1
8.	Prof. R. L. Elsberry, Code 63Es Naval Postgraduate School Monterey, California 93940	1
9.	Department of Meteorology Library, Code 63 Naval Postgraduate School Monterey, California 93940	1
10.	Prof. R. L. Haney, Code 63Hy Naval Postgraduate School Monterey, California 93940	1

11. LCDR T. E. Callaham, Code N341 — 2
Naval Oceanography Command
NSTL Station, Mississippi 39529

12. Dean of Research, Code 012 — 1
Naval Postgraduate School
Monterey, California 93940

13. Dr. C. W. Fairall — 1
BDM Corporation, 1340 Munras St.
Monterey, California 93940

14. Professor J. Dyer, Code 61Dy — 1
Naval Postgraduate School
Monterey, California 93940

15. Assoc. Professor K. L. Davidson, Code 63Ds — 10
Naval Postgraduate School
Monterey, California 93940

16. Professor G. E. Schacher, Code 61Sq — 1
Naval Postgraduate School
Monterey, California 93940

17. Dr. A. Goroch — 1
Naval Environmental Prediction Research Facility
Monterey, California 93940

18. Dr. A. Weinstein — 1
Director of Research
Naval Environmental Prediction Research Facility
Monterey, California 93940

19. Dr. Kristina Katsaros — 1
Atmospheric Sciences Dept.
University of Washington
Seattle, Washington 98195

20. Dr. C. A. Friehe — 1
Deputy Manager for Research, RAF
National Center for Atmospheric Research
P. O. Box 3000
Boulder, Colorado 80307

21. Dr. J. C. Wyngaard — 1
CIRES
University of Colorado/NOAA
Boulder, Colorado 80309

22. Dr. Hans Panofsky — 1
Department of Meteorology
Penn State University
State College, Pennsylvania 16801

23. CDR K. Van Sickle — 1
Code Air-370
Naval Air Systems Command
Washington, D. C. 20360

24. Dr. A. Shlanta — 1
Code 3173
Naval Weapons Center
China Lake, California 93555

25. Dr. Barry Katz — 1
Code R42
Naval Surface Weapons Center
White Oak Laboratory
Silver Spring, Maryland 20362

26. Dr. J. H. Richter — 1
Code 532
Naval Oceans Systems Center
San Diego, California 92152

27. Dr. Lothar Ruhnke — 1
Code 8320
Naval Research Laboratory
Washington, D. C. 20375

28. Officer-in-Charge — 1
Naval Oceanography Command Detachment
FPO New York 09571

29. CDR Rudolph Dahl — 1
5421 Glenwood Road
Bethesda, Maryland 20034